2011

CONSTRAINED VOLUME PACKING OF DEPLOYABLE WINGS FOR UNMANNED AIRCRAFT

Turner John Harris
University of Kentucky, turn.j.harris@gmail.com

ABSTRACT OF THESIS

CONSTRAINED VOLUME PACKING OF DEPLOYABLE WINGS FOR UNMANNED AIRCRAFT

UAVs are becoming an accepted tool for sensing. The benefits of deployable wings allow smaller transportation enclosures such as soldier back packs up to large rocket launched extraterrestrial UAVs. The packing of soft inflatable wings and Hybrid inflatable with rigid section wings is being studied at the University of Kentucky. Rigid wings are volume limited while inflatable wings are mass limited. The expected optimal wing design is a hybrid approach. Previous wing designs have been packed into different configurations in an attempt to determine the optimal stowed configurations. A comparison of rigid, hybrid, and inflatable wings will be presented. Also a method for simulating optimally packed wings with respect to geometric constraints will be presented. A code has been written to study soft wing packing and verified the soft wing packing results. This code can be used during initial wing design to help predict wing size and packing configurations. In this thesis, an over view of the packing configurations as well as packing observations will be covered such , packing inefficiencies, wing mounting limits, long term storage, and scaling of packing

KEYWORDS: Packing, Inflatable Wings, Long Term Storage, Unmanned Aerial Vehicle, Wing Length Estimation

Turner Harris

March 9, 2011

CONSTRAINED VOLUME PACKING OF DEPLOYABLE WINGS FOR UNMANNED AIRCRAFT

By

Turner John Harris

Dr. Suzanne Weaver Smith
Director of Thesis

Dr. James McDonough
Director of Graduate Studies

March 2, 2011

RULSE FOR THE USE OF THESES

Unpublished theses submitted for the Master's degree and deposited in the University of Kentucky Library are as a rule open for inspection, but are to be used only with due regard to the rights of the authors. Bibliographical references may be noted, but quotations or summaries of parts may be published only with the permission of the author, and with the usual scholarly acknowledgments.

Extensive copying or publication of the thesis in whole or in part also requires the consent of the Dean of the Graduate School of the University of Kentucky.

A library that borrows this thesis for use by its patrons is expected to secure the signature of each user.

Name Date

_____

_____

_____

_____

_____

_____

_____

_____

THESES

Turner John Harris

College of Engineering

University of Kentucky

2011

CONSTRAINED VOLUME PACKING OF DEPLOYABLE WINGS FOR UNMANNED AIRCRAFT

THESIS

A thesis submitted in partial fulfillment of the requirements for the degree of Master of Science in the College of Engineering at the University of Kentucky

The views expressed are those of the author and do not reflect the official policy or position of the Department of Defense or the U.S. Government

By

Turner John Harris

Lexington, Kentucky

Director: Dr. Suzanne Weaver Smith, Donald and Gertrude Lester Professor of Mechanical Engineering

Lexington, Kentucky

2011

Acknowledgements

This thesis would not have been possible without the loving encouragement of my parents. Their support throughout my education was immeasurable. My wife also urged my completion to the end of writing. I must thank my thesis advisor, Dr. Suzanne Weaver Smith for the opportunity to enter the Masters program under her guidance. Dr. Jamey Jacob at the Oklahoma State University, Joep Breuer, and ILC Dover provided deployable wings for this research.

The University of Kentucky Athletics program brought me to Kentucky on a NCAA Rifle scholarship. At UK, I participated in BIG BLUE V which perked my interest in aerospace and opened many doors for me. The University of Kentucky Mechanical Engineering department allowed me to be a teaching assistant while completing graduate courses. My thesis work was guided and funded by the DARPA Rapid Eye SBIR through NextGen Aeronautics in conjunction with Boeing, L3, and Swift.

My thesis committee Dr. Ting-Wen and Dr. T. Michael Seigler taught several courses that I thoroughly enjoyed. Abu-Farha Fadi's Phase I wing material tensile testing data set the base line for the long-term Phase II testing. Dr. Burak Basaran helped with the long-term Phase II.

Lastly, I'd like to thank all my friends in the RGAN 010 lab. The lively learning environment was a great resource for ideas and answers. Thank you for the support.

Table of Contents

List of tables

List of figures

List of files

Genetic Algorithm Files

runGaCode.m ..... 4 KB

gaCode.m ..... 2 KB

gatool1.m ..... 3 KB

create_permutationsH.m ..... 2 KB

crossover_permutationH.m ..... 2 KB

Packing Simulation Files

adjHingeRigidWingPackVolFunc.m ..... 2 KB

closenessFunc.m ..... 1 KB

closenessFunc2.m ..... 1 KB

colorPlotFunc.m ..... 5 KB

confinmentAreaFunc.m ..... 3 KB

cross2Func.m ..... 1 KB

inpoly.m ..... 7 KB

PackingCodeQuickLaunchAngleQuicker.m ..... 25 KB

pePlotPointsFunc.m ..... 3 KB

pointOnLineSegmentFunc.m ..... 3 KB

quadrentSlopeFunc.m ..... 4 KB

rot2dFunc.m ..... 1 KB

RunRandomPacking5Oct.m ..... 16 KB

RunRigidWingPackingVolTEN.m ..... 2 KB

slopeFunc.m ..... 1 KB

thicknessCheckFunc.m ..... 3 KB

traceOptPlotTextFunc.m ..... 1 KB

validStartPointFunc.m ..... 1 KB

Phase I and Phase II Tensile Testing Files

LongTermTensileCod.m ..... 5 KB

LongTermDataReadInAMBII.m ..... 4 KB

importfileTJ.m ..... 1 KB

FadiDataReadIn.m ..... 2 KB

Text Input Files

box.txt ..... 1 KB

boxPE.txt ..... 1 KB

bodyIntubeQuater.txt ..... 1 KB

orange.txt ..... 1 KB

orangeLeftWall.txt ..... 1 KB

Chapter 1

1.1 Introduction

Packable wings have been used for aircraft for most of aviation history. In every era that recognizes the importance of air superiority, the desire for more aircraft is a natural one. Folding wings as seen on aircraft carriers or other forms of packing are continually of interest. With rigid-wing aircraft, options for packing are limited to hinged or removable sections.

Now, as new concepts and new designs for unmanned aircraft, also known as unmanned aerial vehicles (UAVs), are emerging, new packing strategies are needed as well. There are a wide variety of new concepts including inflatable and hybrid rigid/inflatable wings. This class of wings is studied extensively at the University of Kentucky, so these wings are available and consequently the focus of this thesis.

1.2 Motivation

The motivation for this thesis is to understand and develop methods to estimate packed wing size for a specified enclosure. There are two design strategies that could be adopted when considering UAV packable wings. First, when using a design optimization program, the design process balances aerodynamic variables such as flight duration, aircraft velocity, and weight, which would determine an optimized wing length for the aerodynamically optimized wing. Then, a separate design iteration process could determine the smallest packed volume for this wing length.

The second strategy to optimize a UAV with packable wings would be to include packing variables as part of the main optimization process. This would include packing shape and volume limitations, thus integrating them in the optimum deployed wing length.

In other words, there are two different design approaches. One starts with a known volume and shape limitation which determines an optimum length. The other approach starts from an aerodynamic optimized length and determines a minimized volume. These two design approaches will produce two different designs.

Additional packing observations are noted throughout the research of this thesis. Often packing considerations may strongly influence the optimal design. A Mars exploration mission will have similar packing requirements as a munitions-packed UAV. Both missions require a UAV to be stored for long periods of time. Traveling to Mars takes seven months. The munitions-launched UAV would be stored and packed in a depot, ready until a conflict necessitated use. A backpack UAV may be packed a few hours before mission commencement. These three missions may each have a different priority for packing, again altering the optimal design.

Figure 1.1 NASA's ARES Mars aircraft [1]

Wing packing strategies were compared in an attempt to determine optimum packing configuration trends. Lab experiments were conducted with folded wings made with different materials and designs; measurements were taken. These measurements confirmed that inflatable wings generally pack down to 2-10% of their deployed volume, hybrid wings pack less efficiently and rigid wings pack the least efficiently.

1.3 Goals and Objectives

This thesis includes a packing study of inflatable wings to compare packed percentages for inflatable wings as well as for hybrid and rigid wings. Additionally, this thesis classifies and compares various wing designs based on their packing mode and packing efficiency. A method to classify packing characteristics of deployable wings, as well as a database of packing measurements, is covered in this thesis.

Deployable UAVs packed in advance for future missions must be reliable. UAV missions were the packed UAV is stored for long periods impose additional constraints. An example of a mission requiring long storage times is DARPA's Rapid Eye [2]. This thesis also presents a long term packing study of wing materials to understand design considerations for long duration packed UAVs.

1.4 Thesis Overview

In this thesis, Chapter 2 presents prior UAV and packing literature. Chapter 3 introduces physical wing packing of inflatable and hybrid inflatable/rigid wings, along with a mathematical model for a rigid wing with hinge. Chapter 4 explains how a simulation can predict inflatable wing length inside an enclosure. Chapter 5 develops better methods to organize a wing packing configuration resulting in more efficient packs. Chapter 6 simulates wing packing with analyst-guided choices for maximizing packed configurations in constrained spaces. Chapter 7 describes a long term packing experiment of flexible wing materials. Chapter 8 summarizes this thesis and suggests future work.

Chapter 2

2.1 Literature Review – Theses and Dissertations

In the literature, Andrew Simpson's Dissertation researched inflatable wings with "bumpy" airfoil for low speed flight with Reynolds's numbers ranging from 25,000-100,000. The bumps were caused by the construction of the inflatable wings. Simpson used smoke-wire to visualize flow across an airfoil in a wind tunnel. He found that an ideal smooth airfoil showed flow separation near the leading edge and never reattached [3]. The "bumpy" or rough surface airfoil showed attached flow over a larger portion of the wing. It was concluded that the rough surface tripped the air flow, thus showing a benefit to inflatable wings at low Reynolds's numbers.

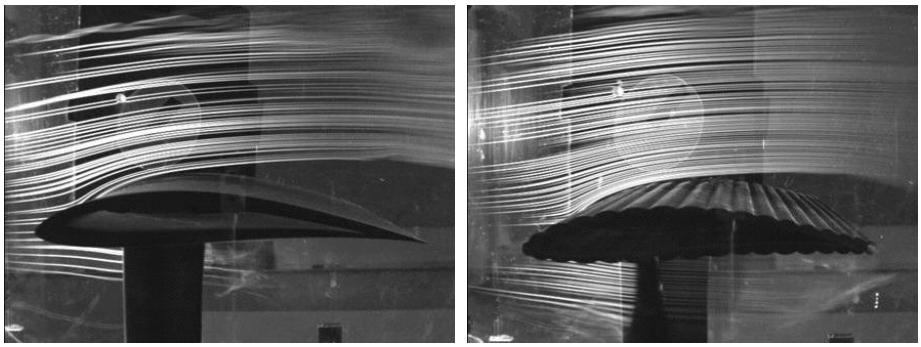

Figure 2.1 Re= 25,000, 0^{o} angle of attack. Ideal airfoil (left), rough airfoil (right) [3]

Inflatable wings that pack well do not have control surfaces such as ailerons. These UAVs use tail control or use external force to warp the wing. Wing warping tests both static and dynamic were conducted with no damage to the wings. Also, rapid wing deployment tests show that inflatable wings are resilient [4]. The inflatable wings survived snap back testing in which an inflatable wing was mounted like a cantilever beam and a 50 pound sandbag was dropped onto the wing. The wing deflected more than 45 degrees, snapped back above horizontal with no damage [4].

Over 300 inflatable winged flight tests have been conducted at the University of Kentucky [3]. The inflatable wing technology is durable and can be used to provide impact cushion support for UAV components. ILC Dover and the University of Kentucky jointly designed the Technology Demonstrator with inflatable wings and vertical tail to protect the pusher propulsion system in the event of a crash.

Figure 2.2 ILC Dover and University of Kentucky's technology demonstrator [3]

2.2 Inflatable Wings with Enclosures

Packable wings have been used for aircraft for most of aviation history. Steven Landon's thesis provides a comprehensive history of deployable aircraft [5]. Andrew Simpson's Dissertation also covered UAV history [3]. In 1956, the Goodyear Inflatoplane was an inflatable aircraft system designed to be dropped to downed pilots. The plane consisted of rigid landing gear connected to the engine with inflatable fuselage tail and wings. The packed aircraft fit into a single enclosure that was parachute dropped to the pilot [6]. Aircraft carriers with limited

flight deck area benefit from folding wing tipped fighter planes. These fighter planes have two packing constraints. One constraint is the limited carrier flight deck area. The other enclosure constraint, boxed shape, occurs below deck when ceiling height as well as parking area space is limited. Another example of enclosure restrictions is launch tube mission based UAV. ILC Dover built the Apteron, a small unmanned aerial vehicle that was severely restricted by the launch tube enclosure requirements. In 2001s NASA Dreydon I2000 UAV demonstrated rapid deployment inflatable wing that used the wing as an outer enclosure shown in Figure 2.3. The two restrictive enclosures are simulated in Chapters 4-6.

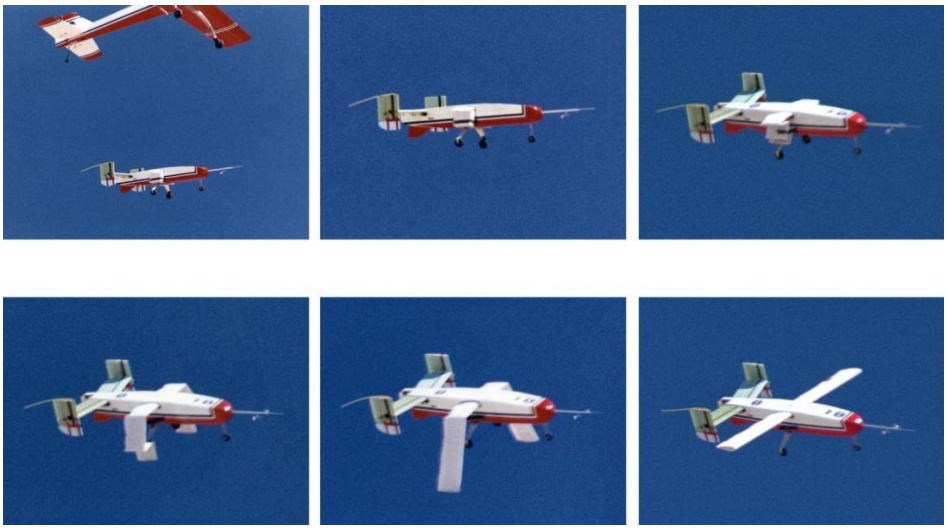

Figure 2.3 NASA Dryden UAV wing deployment, 2001

2.3 BIG BLUE

In 2003, the University of Kentucky's BIG BLUE, BB, project demonstrated inflatable wing technology by successfully deploying and curing inflatable/rigidizable wings at high altitude. The wings were packed into boxes to shade the UV-reactive resin from the Sunlight until deployment [7]. The box was designed to fit the wing for this technology development mission rather than the wing fitting into a constrained space.

Later BBV conducted many low altitude test flights with new ILC Dover orange wings, referred to as F5 wings. That year's pilots were amateur students and many hard landings occurred. The landings often broke landing gear, propellers, fuselage, and tail sections, but never the inflatable wings. The finial balloon launch selection process considered offshore launch and using the inflatable wings to float the UAV after splash down. These same wings reached a temperature of -70^{o}C during assent to 89,000 feet and survived to be used for additional BB related projects. The resilience of inflatable wings has been confirmed elsewhere [8].

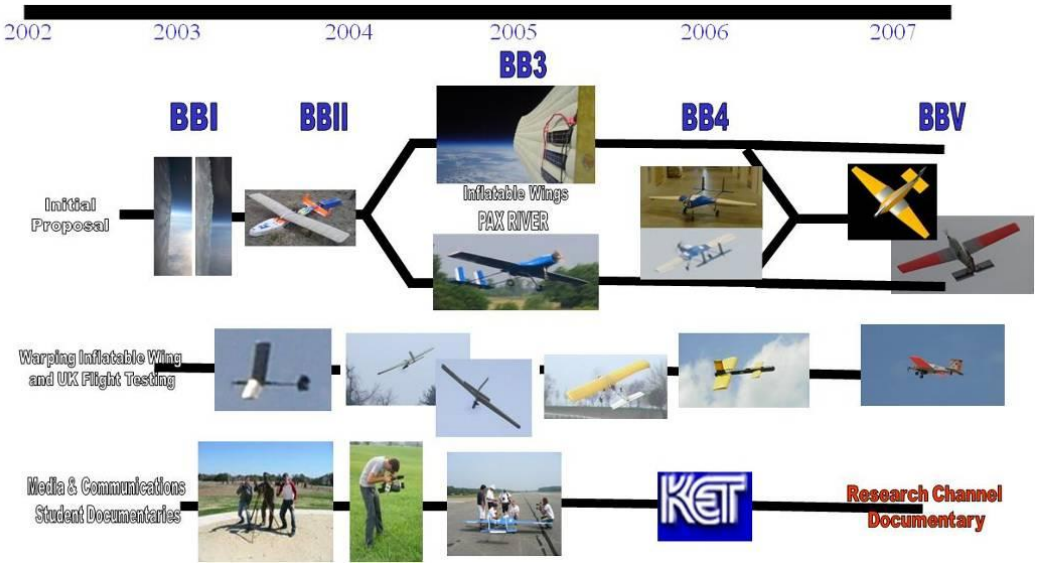

Figure 2.4 BIG BLUE timeline [7]

The BB series of wings, shown in Figure 2.5 BBIII vectran wings (left), BBIV yellow wings (center), BBV orange wings (right) were used throughout this thesis for packing studies and for sizing of rigid wing simulations.

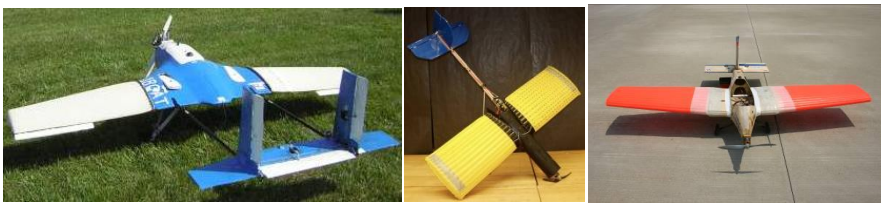

Figure 2.5 BBIII vectran wings (left), BBIV yellow wings (center), BBV orange wings (right) [7]

2.4 Multi Role Designs

Inflatable wings should be used for multiple uses if possible. This improves packing because one object can accomplish two jobs. The wings could be used as protective packing material in solder backpacks. The wings may protect sensitive communications equipment, autonomous ground station, or the UAV itself.

NASA conducted a study to improve packing for space missions by using clothing as packing material [9]. Alternatively, because inflatable wing packs so well and conforms to complex shapes, they could be used to fill unused space between fuselage and containment enclosure [10]. Additional multipurpose uses include, ground sleeping pad for soldier, impact landing cushion similar to Mars rover air bags, flotation device, rain shelter or poncho, signaling device, water collection, etc. The soft materials should not just be waste, but should be useful. Multi-role inflatable wings reduce the need to pack additional items. A similar concept, transformation, fit this role [11]. The V-22 Osprey tilt rotor aircraft starts as a vertical takeoff similar to a helicopter and transforms into a prop driven aircraft.

In some cases inflatable wings can be packed so tightly they take on a specific shape and represent a solid object that's completely non-flexible. This is similar to parachutes that are packed in a compression bag with laces [12]. This solid property could be utilized for additional multi role applications.

2.5 Packing Design Considerations

The primary benefit to inflatable wings is their ability to pack into small odd shaped enclosures. Many sources have stated that inflatable wing pack "tens of time smaller" without having exact data [13]. The design space needs to be expanded for inflatable wing technology so that the wings are incorporated into new UAV systems. A mission system is Tube launched UAVs that eject from their tube enclosure. Many have long fuselages and use a scissor rotating rigid wing. The long fuselage adds weight. These deployable UAVs are significantly affected by mission packing constraints. The special case tube enclosure with wing packing configurations will be simulated and presented. The plane of deployment also matters. Out of plane deployment wing designs are limited by volume. In plane deployment is shape limited such as scissor deployment [5].

Packed duration for inflatable wings has caused concern for wings that must deploy reliably. BIG BLUE I used UV hardening resin to hold the airfoil shape of the wing with no internal pressure. The high altitude experiment resulted in asymmetric wings. A possible reason is the wings were packed for one week for shipment to the finial mission [7]. The z-packed wings could have squeezed resin out of the inflatable wing. There is little data on long term storage of packed deployable wings in particular the textile fabrics. Long duration tests are difficult and need to be conducted for inflatable wings technology to mature. This thesis provides a chapter on long term packing with some unexpected findings.

Chapter 3

3.1 Empirical Packing Study

Little information with respect to packing is available to the designers of deployable-winged UAVs. An empirical packing study was conducted with all wings that have passed through the UK Dynamic Structures and Controls laboratory during the last two years. Wings from the Advanced Technology Research Center laboratory room at Oklahoma State University were also packed and measured for this study. The wing types varied from inflatable to hybrids of rigid parts and flexible fabrics to purely rigid wings with a mid-span hinge. The resulting data shows several trends.

This study is a significant contribution to understanding the packaging of UAVs with deployable wings because it compares 23 wing designs and their packing properties to demonstrate the design space. There were 67 packing configurations total. For inflatable wings packed volumes of 2-10% of deployed volumes are thought to be achievable, but few data points are available. In order to understand the packing potential of various classes of deployable wings, a comparative study was undertaken.

The data for the study was generated by first measuring a deployed wing's boxed volume as seen in Figure 3.1. Here a tapered inflatable wing is seen. The span, root chord, and maximum thickness define the enclosed boxed volume. A selection of wings is shown in Figure 3.3 and in Table 3.1.

Table 3.1 A selection of measured wings for the Empirical Packing Study

Label	Wing Description	Class	Deployed Vol [in^3]
H7	Rapid Eye Telescoping Red (3 ribs)	telescoping	1006.2
H23	OSU black telei wing 4 ribs	Rigid Ribs, flexible skin	1284.9
F5	Orange Wing BIGBLUE V (BBV003L)	Only flexible inflatable	2331.0
F9	Vectran no wing root, with bladder	Only flexible inflatable	2142
F13	Air Bag, Curved Wing, Joep	Only flexible inflatable	8443.05
F18	Air Bag, Rectangle Wing, Joep	Only flexible inflatable	5622.75
F27	Yellow Wing	Only flexible inflatable	979.5

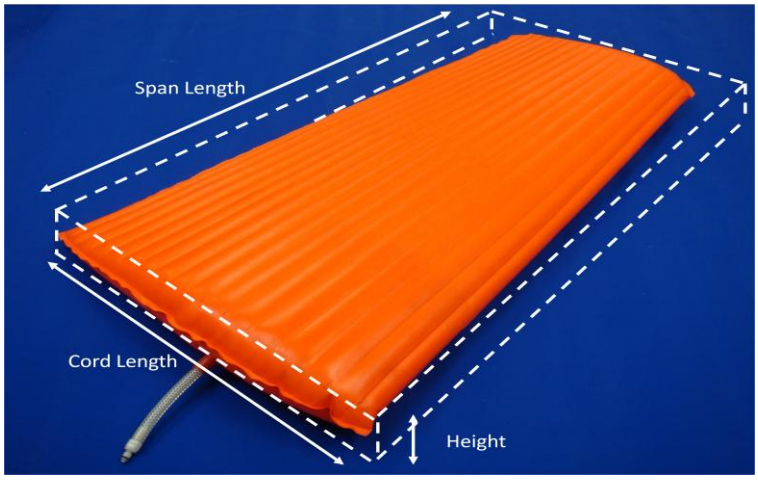

Figure 3.1 Deployed boxed volume measurements

Next the wing was folded, rolled, or otherwise packed into different configurations and the packed boxed volume was measured shown in Figure 3.2. The same wing is z-folded here. The tape measure and calipers seen here were acting as weights to hold the folded shape and were used to measure the packed boxed volume.

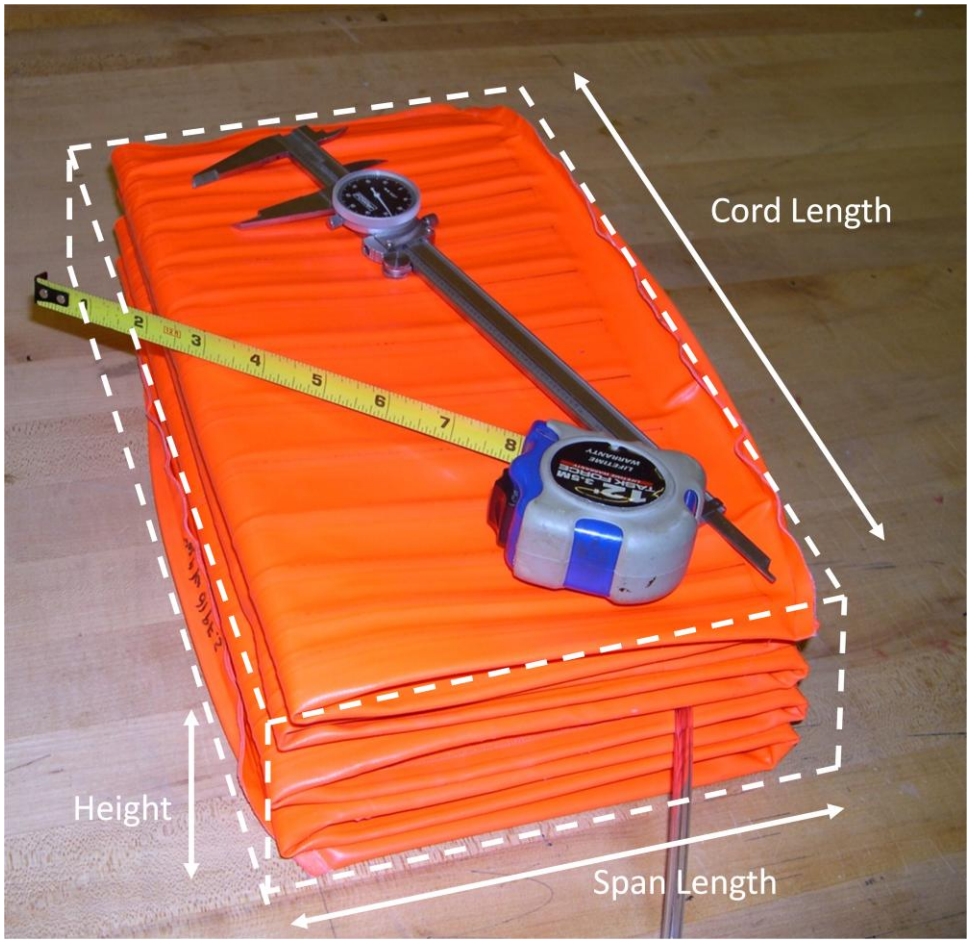

Figure 3.2 Packed boxed volume measurements

The packed volume divided by the deployed volume gives the packed percentage. Figure 3.4 used a log-log axis because of the large variety of wing sizes and large variety of packed percentages.

$$P = \frac{abc}{ABC} \times 100, \qquad \text{Equation 3.1}$$

Where P is packed percentage, as is the packed height, b is the packed span length, c is the packed cord length, A is deployed height, B is deployed span length, and C is deployed cord length.

Figure 3.4 presents a first look at the packing percentage results from these measurements. The horizontal axis is deployed boxed volume and is the normal flight configuration. The vertical axis is packed percentage. The deployed volumes range from 255-66,000 cubic inches, while the packed percentages range from 0.7% for flexible wings to 663% for rigid wings. An important observation is that hybrid wings pack from 7-59% depending on the rigid mechanism. Note that, the rigid wing values are approximated using a model constructed of two wood boards with a hinge at mid-span. All other wings were actual designs measured experimentally. All wings measured fit into the class of small UAV with a typical payload of 5-30 pounds except for the longest rigid wing calculation.

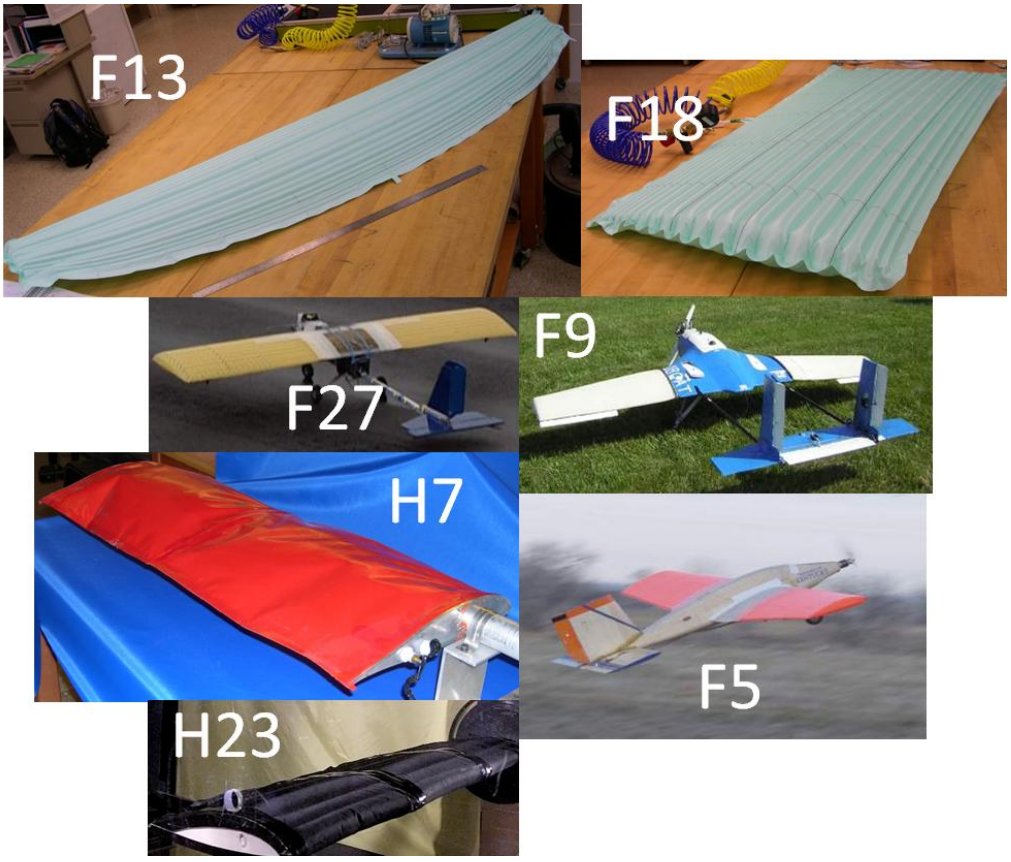

Figure 3.3 Images of a selection of wings measured for the Empirical Packing Study

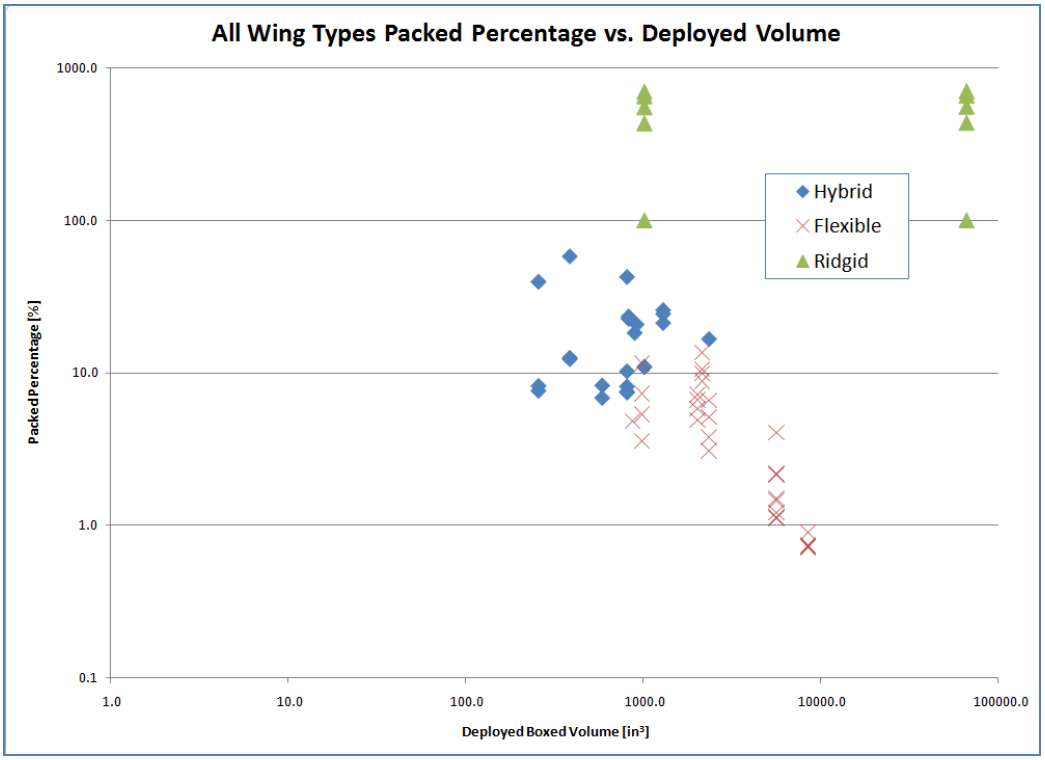

Figure 3.4 All wing types with multiple packing configurations

The first conclusion here is that the purely flexible wing class consistently packs to 10% boxed volume or less, which could be an advantage for mobile and deployable UAV wing systems. The majority of the hybrid class wings packed between 8-25% boxed volume. This could be an acceptable trade for a larger wing root buckling strength or for larger bending and torsion stiffness.

The second conclusion is that purely flexible wings having different packing configurations still pack into a comparatively small range of packed volume percentages. This is shown more clearly in Figure 3.5 below.

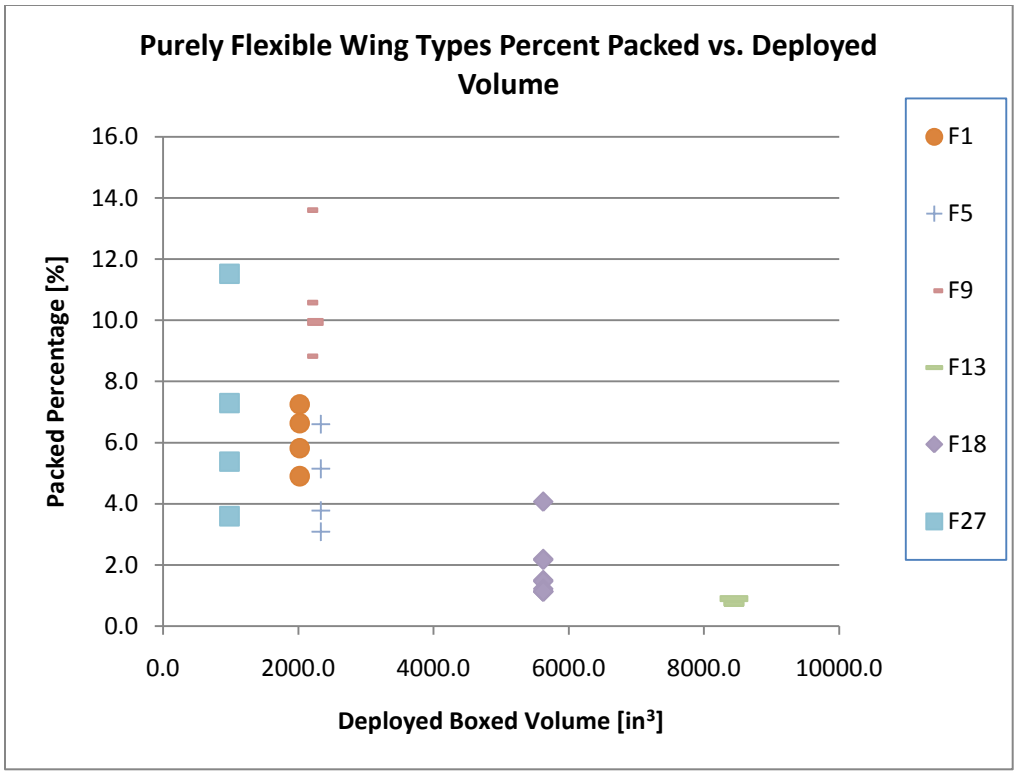

Figure 3.5 Flexible wing types packed percentage

The purely flexible class wing has an additional advantage that more than one efficient packing configuration is available for each design. An example where this could be beneficial is two UAV backpack missions with different shaped additional equipment to be packed within each backpack. A second example would be the recovery of the UAV could be packed and returned by another solider with different backpack requirements.

In contrast, the hybrid-class wings pack into a much wider range of boxed volumes as shown in Figure 3.6. These results suggest that consideration of wing packing for hybrid-class wings should occur during initial design stages in order to achieve optimal packed volumes.

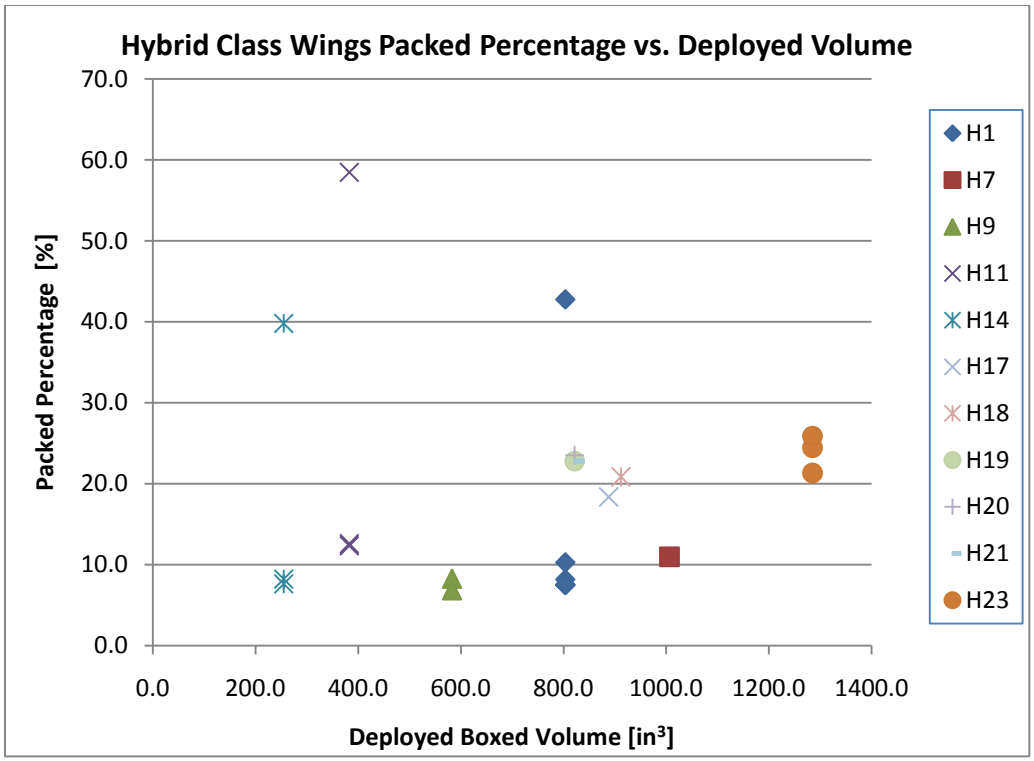

Figure 3.6 Hybrid wings packed percentage

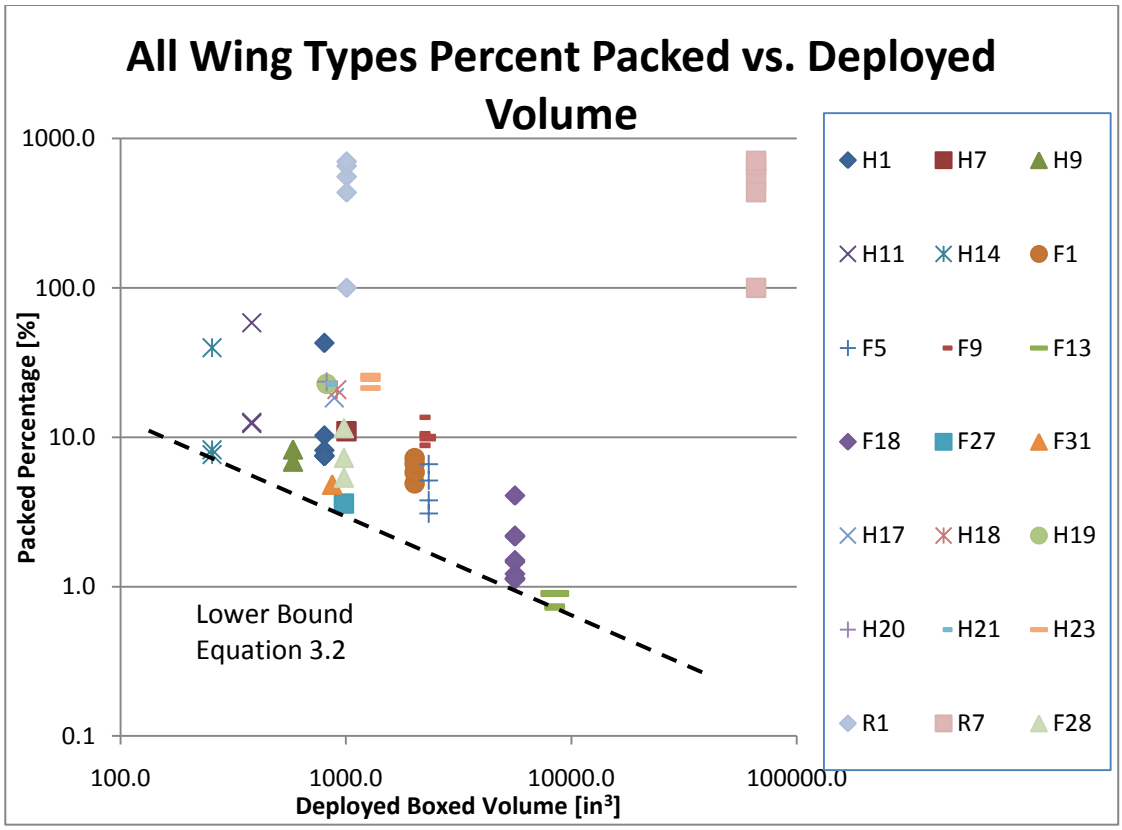

Figure 3.7 All wing types with multiple packing configurations and labels

In Figure 3.7, the wings of Figure 3.4 are labeled individually, so different packing configurations are identifiable such as for hybrid wing H1. There also appears to be a lower packing limit that is expressed by for the current wing technologies.

$$y = (-9.1963e^{-4})x + 255.007, \qquad \text{Equation 3.2}$$

Were the x-variable is the boxed deployed volume in cubic inches and the y variable is the packed percentage. Equation 3.2 reveals that larger wings have more benefits from packing.

All portable and deployable UAVs will benefit from wing packing, thus the packed percentage is not the only design criteria or even then most important criteria. The rigid wing's minimum packed percentage configuration was 100% which was greater than the hybrid wings'

packed configurations. Hybrid wing design has rigid structural components while maintaining good packing properties.

Figure 3.7, is a significant contribution to UAVs with deployable wings because it compares 23 wing designs and their packing properties together for the first time to demonstrate the design space. There were 67 packing configurations total.

A telescoping wing design from OSU, H23, was estimated to have a packed percentage of 16.7% before the wing was built and shipped to the University of Kentucky. This estimate was based on previously measured wings with similar size and hybrid telescope packed configuration. The actual wing packed percentage was measured 21.3%, 24.5%, and 25.9% for different packing configurations. This showed the value of Figure 3.7. The packing estimate was close despite using an estimated deployed volume that was 80% over sized. If the estimate would have used a smaller (correct) deployed volume this would have brought the predicted packed percentage volume up due to the trend explained earlier by Equation 3.2. The deployed volume was not measured prior to making an estimate because the wing was being designed and built at Oklahoma State University.

3.2 Packing Observations and Heuristic Rules

A hands-on approach was chosen to learn the basics of packing inflatable wings. Many observations were made and lessons were learned as different wings were packed and measured. Some wings were totally inflatable designs; some were hybrid inflatable/rigid designs. Different packing configurations result in different efficiencies.

The initial configuration was to simply roll the wing into a tube similar to a wall poster or wrapping paper. The next configuration was a single fold along the cord at the middle span of

the wing. The third packing configuration was a z-pattern fold. The more folds included with the z-pattern, the more efficient packing resulted.

Packing efficiency is one packing characteristic used to compare packed wings. Packing efficiency is the percent of a box that is full of material. A quarter full box would be 25% filled. Thus, more wing material can be packed before the box is full. A higher packing efficiency is better. Another judgment packing characteristic is packed wing length that fits into a box. A longer wing is better.

Heuristic rules are high level rules to guide problem solving. Heuristics can't be described with mathematical equations. They are learned and applied through experience. The first heuristic packing rule learned was that wing taper has little to no affect on the packing process or the overall packed efficiency. This is because the boxed volume is defined as a box not a wing-following volume.

The second heuristic rule learned was to minimize the packed volume of an inflatable wing, air was vacuumed out of a wing prior to packing. A wing must be cleverly vacuumed while being packed, though. For example, consider F5 wing with 25 inHg vacuum applied prior to packing. If starting at the tip and rolling or folding the wing towards the wing attachment/root, the wing may resist if the insides of the top and bottom are "glued" together. The vacuuming prevents the free shearing motion that would normally occur as the inner surface has a shorter radius than the outer surface. This layer-sticking result has a negative influence on packing efficiency.

To circumvent this glue effect, a small amount of air must be present while packing the wing. An observation was made that as more folds were included the vacuum pressure would need to be applied in stages due to the fold pattern. The need to vacuum out the air at an early

stage in the packing lends itself to being more efficient than the rolled packing option. Sticking prevents rolling or folding so both rolled and z-folded approaches are affected. The final vacuum was applied and shown in Figure 3.9. This packing configuration is flexible in the vertical plan (up and down) and leads to fuselage wrapping covered in the next section.

3.3 Fold Radius Length

Packing different configurations of z-packing was tedious because excess wing material that does not end flush with the entire pack. Applying vacuum at each fold stage and then finding out on the last fold that there is excess material was time consuming. Any material that does not end at the edges of the pack is excess waist. An additional material layer increases the packed box volume no matter how long or short the layer is. Therefore for an optimal pack, that last layer should end flush with the edge of the pack configuration. Trial and error is unacceptable for a long wing. A method has to be devised to guide the alternating vacuuming-folding process.

A method to predict where wing folds should be placed to have no excess material (or excess wing length) is presented. The first attempt was to take the length of a flat deflated, non-vacuumed, wing and divided by the number of layers.

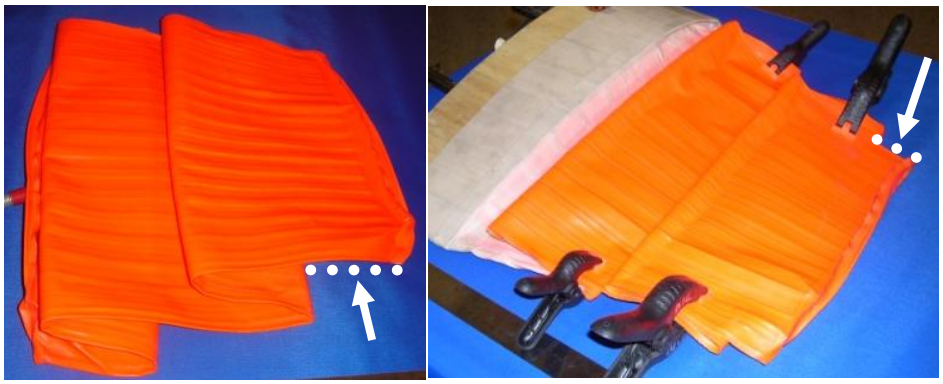

Figure 3.8 Excess wing material indicated with arrow and dashed line

Figure 3.9 Four pleat z-fold with no excess wing length

For example, a three layer z-pattern with the orange wing is 38” long divided by three layers equals 12 2/3” long layers. When this simple example is tried experimentally, each layer measures twelve inches. The percent difference between calculated and experiment is 5%. However, this simple theory does not account for the material length used in the fold itself.

This folded material length depends on wing construction, fold type, and the material properties of the wing. A correction factor is defined as "fold radius length", FRL, with units of length. A simple method to experimentally calculate the fold radius is to take the measured single layer length subtracted from the theoretical length and divide by the number of layers. The FRL will be useful both during the packing process as well as during the packing configuration design stage. The material properties leading to the fold radius for five wings are listed below in Table 3.2.

Table 3.2 UK wing properties used to determine FRL

Units=Inches	Orange	Yellow	Orange Root	Yellow Root	Vectran
cord deployed	18.11	12.125	19.5	12.125	17
length deployed	37	35.125	42.25	35.5	36
height deployed	3.54	2.3	3.58	2.42	3.5
cord deflated	18.25	13.5	19.5	13.125	17.75
length deflated	38	36.625	41.5	35.5	36
llayer deflated	0.055	0.075	0.055	0.075	0.19
height pac	0.3	0.22	0.5	0.135	1
radius factor	0.5	0.375	1	0.0625	0.125
root cord	0.00	0.00	19.5	12.125	0
root length	0.00	0.00	6.5	6.75	0
root height	0.00	0.00	3.58	2.542	0

Another observation is that the smallest packed volume does not guarantee the optimum packed configuration. The shape of the volume or enclosure that the wing must fit into has a significant effect. For example a backpack UAV could be modeled as a rectangular box. While a UAV mission for Mars might require a conical enclosure, and a missile-launched UAV might require a cylindrical one, the shapes for packing become complex when a rigid fuselage is alongside the packed wing. A systematic method to handle these enclosures will be determined.

A wing has at least four possible fold directions: span-wise, sweep, root rotation, 45^{o} fold along the fuselage. If fold lines are perpendicular to the wing span, then depending on the number of folds and wing length, the resulting packed wing may be stiff or flexible as illustrated in Figure 3.10 through Figure 3.12. The solid packaging will require an enclosure to surround it, but flexible-folding wings can conform to an enclosure shape as illustrated in Figure 3.13 and Figure 3.14.

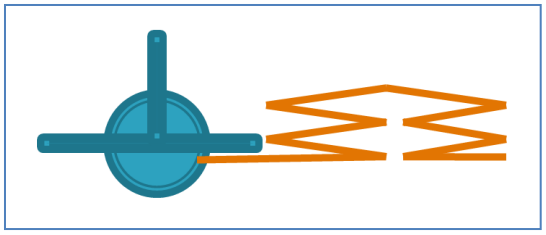

Figure 3.10 Flexible multiple z-packed configuration

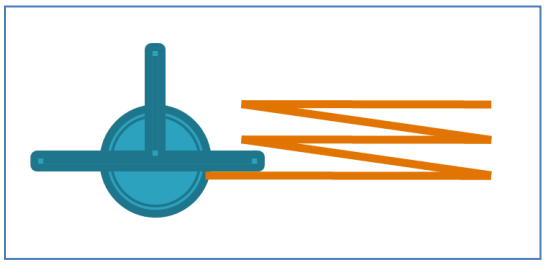

Figure 3.11 Flexible z-packed configuration

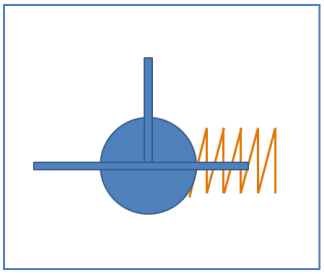

Figure 3.12 Non-flexible packing configuration

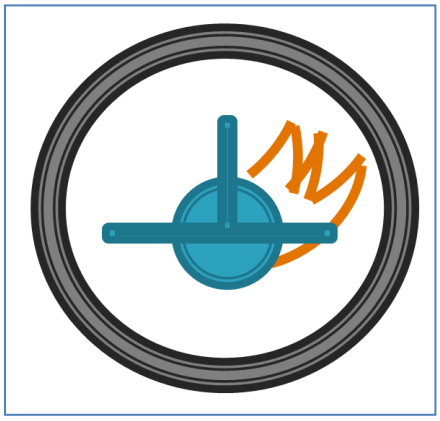

Figure 3.13 Flexible packing properties used inside tube enclosure

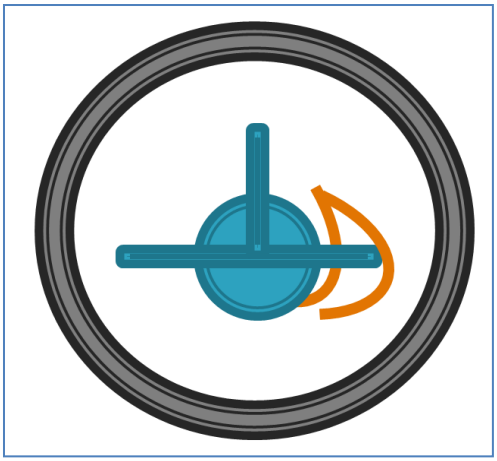

Figure 3.14 Fuselage following wrap

Additionally, a 45^{o} fold line with respect to the wing span can allow for long packed wings if the fuselage is long. Packing along the fuselage requires less layers of material for a given wing size.

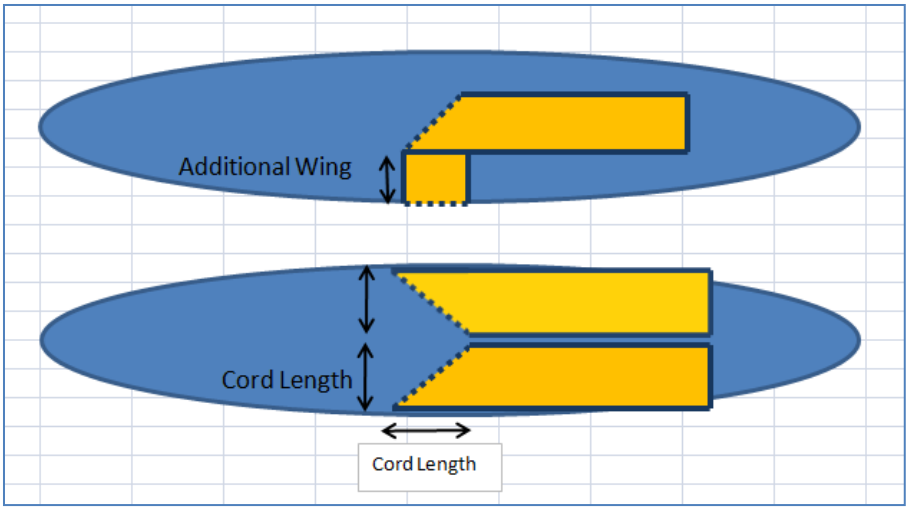

Figure 3.15 Fuselage limited 45 degree fold back

The z-pack can be modified from an accordion shape that grows tall with more folds. It can also be stretched out so that folds don't lie directly on top of the other folds. There can be a

slight offset or a completely different stack. These different versions of z-packing may or may not include a material bridge to the next stack depending on the orientation.

The mounting method also affects the packing. The method used in BIG BLUE III was a metal flange with bolts around the air foil. The metal flange had a neutral influence on packing direction. Mainly because the vectran wing with internal air bladder was quite stiff. BIG BLUE V used adhesive tape to attach the wings to the wing root. The tape limits the number of degrees of freedom that a packer can utilize. It also causes the rolled wing to climb up over the wing root. A future design might include extra material along the wing root seem. This material could have attachment eyelets like a flag. When pressure is applied the wing inflates to fill and wedge into the root, a press fit. The attachment method needs to be investigated for hybrid wings. Some hybrid wings have repeating hard-soft-hard portions. The attachment method does influence what shapes the wings will fit into.

Not only does the fuselage change the total shape of the wing packing enclosure but the tail, propeller, and landing gear do as well. For example, if no landing gear exists then the wings could be packed below the fuselage.

Now consider a triangular prism as a confinement space. The wing has to mount at some point. The heuristic rule discovered here is that long flat layers pack the best. The starting point should be in a corner such that the longest flat layers lay on the inside the longest wall of the triangle. The shorter layers are used later when moving into the crevice of the triangle.

When considering a rolled wing, the large outer radius layers are very efficient in that a new layer adds minimal size to the roll while using a large amount of material in length to wrap the circumference of the pack. Conversely, the inner most portion of this roll is inefficient as shown in the left pictures of Figure 3.16.

Figure 3.12 Rolled wings on wing roots, BBV ballon launch in Colorado

Wings on hand were packed and measured in various configurations. It was observed that all orange wings packed ended up with similar volumes by observation. The BIGBLUE V wing attachment method used tape to secure the wing to a wing root. The orange wing being taped to the wing root wasted a large volume. This also moved the whole packing configuration further away from the fuselage. When packing the wing tried to climb above the wing root when

roll packed which increased the height of the packed dimension with no benefit to packing volume as shown in Figure 3.16.

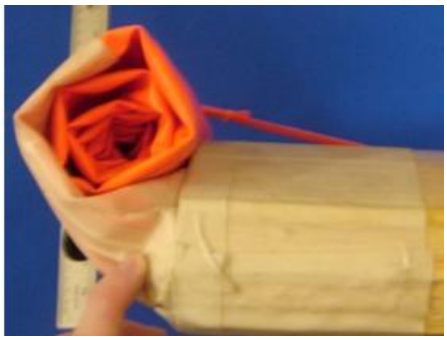

Figure 3.16 Rolled wing climbing over root

3.4 Glue effect and vacuuming

A vacuum pump was used in an attempt to further reduce the packed percentage for the BBV wings. A glue effect was discovered if all the internal air was removed the wing's top surface and bottom surface made interior contact. The resulting friction prevented the two surfaces from sliding across each other as if they were glued together. This vacuumed wing now had a larger bend radius and was stiffer and so packed less efficiently.

Figure 3.17 Glue effect from partial z fold

Figure 3.18 Glue effect from full z fold and roll packs on hanging wing

The glue effect could be used beneficially to help a packed wing stay in a particular configuration as shown in Figure 3.17 and Figure 3.18. The glue effect can be beneficial in maintaining a wing pack configuration. In order to control the glue effect, a portion of the volume of air is removed while packing the first fold. Then more air is removed and another fold can be made until the pack configuration is reached. If the internal air is not removed in steps during packing, the wing will seal off and trap the remaining air and lead to a wing that does not pack well. Not only does it not pack well, but trapped air at higher pressure will prematurely deploy or too-rapidly deploy wings in a lower-pressure environment. These considerations also lead to the necessity that the air inflation valve must be accessible while packed and throughout the packing and deploying stages. After the wing is vacuum packed, the wing can still be compressed to a smaller volume with external hand pressure. A UAV could have its inflatable wings vacuum packed then be shrink wrapped or be placed inside of an outer vacuum bag to further reduce the packed percentage. The wrap or bag can be cut or split during deployment. A second wing made from yellow material was packed with similar methods. The yellow wing's

smaller deployed volume made a more frequent evacuation interval necessary to prevent the glue effect. Thus, a larger volume wing will pack more easily by hand than a smaller volume wing.

The packed volume is less than the deployed volume for inflatable wings. This is because as the inflatable wing is deflated and flattened the root and tip ends extend out as show in Figure 3.19. These end effects cause a deflated wing to be longer than the inflated wing. Packing these wings caused the root and tip ends to pack in the thickness direction and thus adds only the deflated thickness to the packed length. Similarly the BBV wing taper does not result in a smaller packed percentage volume because the taper does not fill the boxed volume well.

Figure 3.19 Deflated and flattened inflatable wing

3.5 Improved Packing

Any tail, propeller, rigid wing root, and landing gear will limit packing options as shown in Figure 3.20. Also, detachable wings would allow more packing options. The wings could be user assembled or be attached with cables that would tighten up to remove slack. The fuselage could also be matched to the bottom of the airfoil for nestled packed. The fuselage could allow for internal wing pack with hinged doors or even an open fuselage like a convertible car.

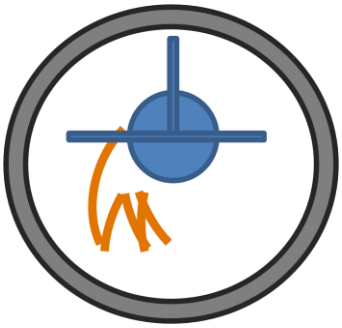

Figure 3.20 Single use UAV with no landing gear so wing could pack under fuselage

Packing improvement isn't volume limited, it is shape limited only. A wing packs to the same volume in any shape. The enclosure shape determines packing configuration. The enclosure is rarely a perfect curve. Therefore shape and packing direction are the keys to good packs.

The ILC Dover and UK Technology Demonstrator utilized inflatable wings and vertical tail so that the inflatable sections could be wrapped around the fuselage thus maintaining good packing characteristics [3].

The BIG BLUE V wing roots have been measured in the lab. They affect the final packed volume in several ways. The obvious effect is that the root sets all minimal dimensions before the packed wing is considered. The second root effect concerns how the inflatable wing is attached to the root. If tape it used to secure the top and bottom of the wing then this limits how the wing can fold. If the wing inflates inside of the wing root, then this creates sufficient pressure to retain the wing and transfer the loads to the wing root. The tape can be stuck to only one side of the wing only to retain a packed wing. If the inflatable wing has reinforced rivets like a flag would have then this would allow even better folding configurations thus packed volumes.

3.6 Hybrid Wings

Hybrid wings consist of flexible material as well as rigid parts. The rigid parts can be spars or telescoping rods. The rigid portions of the wing serve to increase structural strength. Some hybrid designs may be a rigid wing with inflatable tip such as the NexGen project. Hybrid wings and sections of hybrid wing designs were on hand and studied at the University of Kentucky.

When packing telescoping wings, an initial pleat or fold was initiated and maintained while compressing the spars together as shown in Figure 3.21. The initial pleat helped to control where the material would displace to while the spars were brought together. The H1 wing's spars could be packed tightly so that the spars would touch with the wing material above and below the wing. Alternatively, the material could be packed between the spars within the airfoil profile, but resulted in a longer packed length.

Figure 3.21 Wing reference H1, Telescoping wing with rigid spars

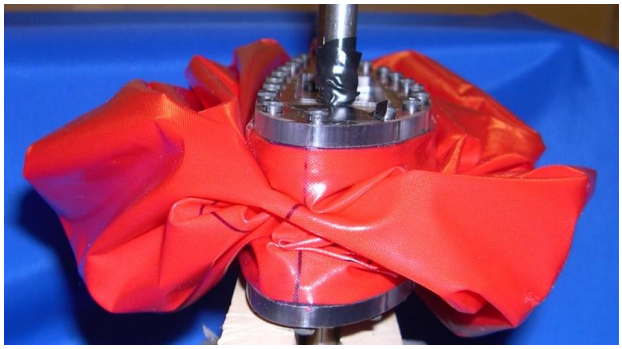

Figure 3.22 Packed telescoping wing with material out of top and bottom (H1)

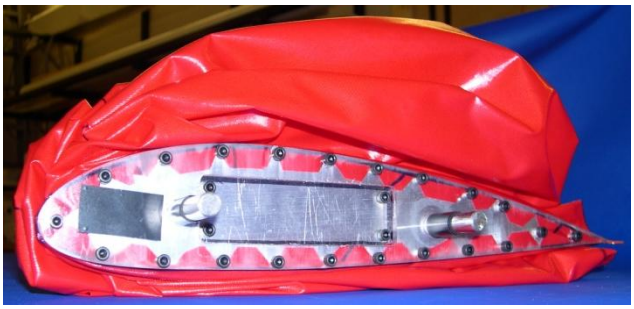

Figure 3.23 Packed telescoping wing with material out of top (H1)

The H7 telescoping wing, also red colored, had a packing limitation due to design. The rigid spars could not be packed to touch one another due to the telescoping rod. This lead to one packing configuration with the wing packed between the spars shown in Figure 3.24.

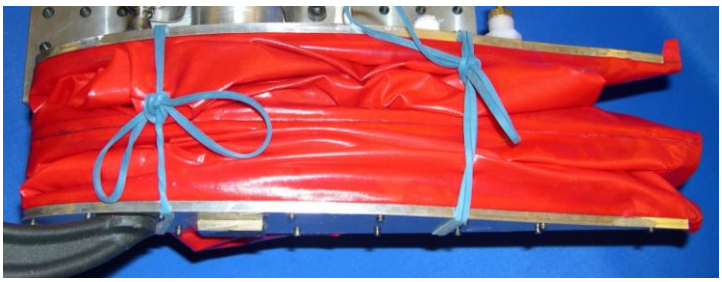

Figure 3.24 Wing reference H7, packed telescoping wing with material between ribs

Depending on the shape limitation the excess material can be constrained to stay within the airfoil shape or allowed to flow out. Furthermore, the excess material can be rolled or folded

or moved to a single side above or below the wing. A hybrid wing without guide rods or telescoping rod can be twisted for each section between rigid spars shown in Figure 3.25. This configuration does not produce the smallest packed percentage, but a long multi segmented wing may benefit depending on enclosure restrictions.

Figure 3.25 Wing reference H11,Hybrid wing segment with twist pack

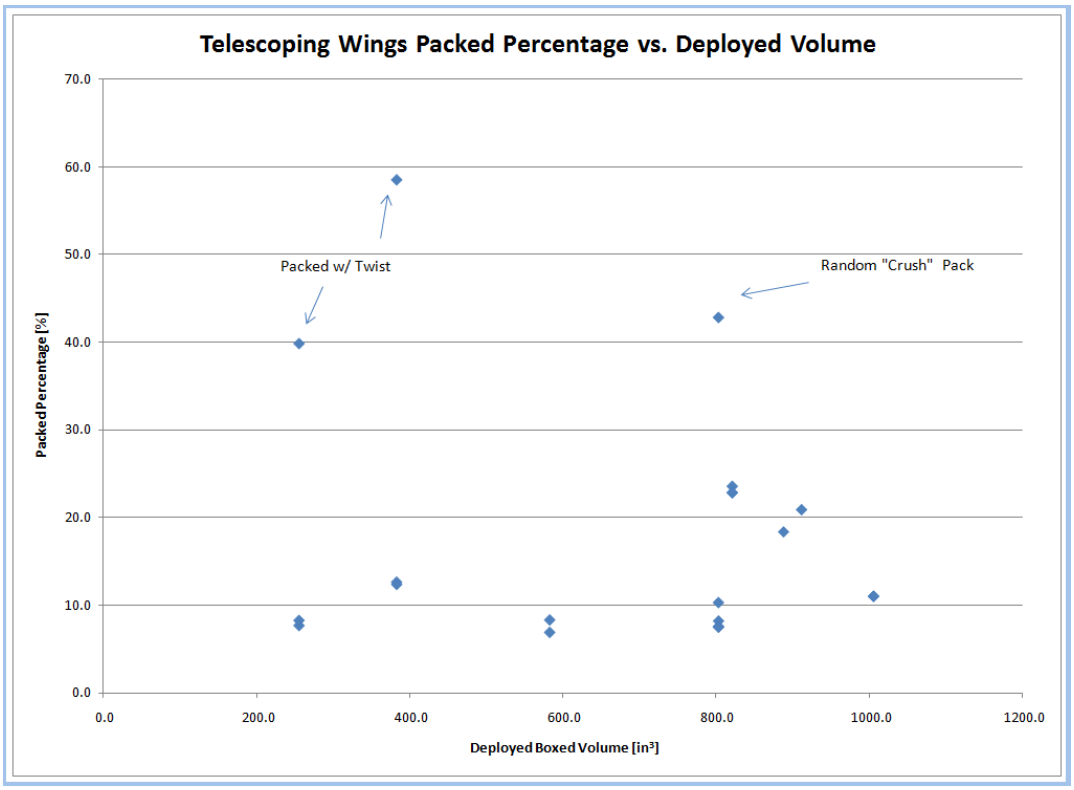

Figure 3.26 Telescoping wings packed percentage

This plot contains telescoping wings or wings with rigid spars that are packing restricted similar to telescoping wings. These wings pack into the accepted 10% rule for flexible wings as can be seen by the lower trend. The wings can alternatively be packed into a non minimal volume as shown by the three points above the 10 packed percentage volume. These packing configurations may fit into a shape restricted enclosure better. Also as the wing aspect ratio increases these points will have a lower volume packed percentage.

There are three high level packing values to be compared. Wing packed volume with shape, wing plus fuselage packed volume with shape, and lastly wing plus fuselage volume and shape inside of restricted enclosure. The packing value that considers the restricted enclosure is the most interesting value. If a UAV is to be packing into an enclosure, how long can the wings be? It depends on the shape of the enclosure and the wing type, rigid, flexible, or hybrid.

The folding or rolling of a flexible wing will result in a similar packed volume. As the scale of the wing increases these differences become negligible. The packing advantage to using a flexible wing or a wing with flexible parts is its inherent ability to conform to the void between the enclosure and the fuselage.

3.7 Rigid Wing with Hinge

A purely-rigid semi-span wing with a single top-folding hinge is shown in Figure 3.27. This simple geometric model was studied to understand modeling of simple packing configurations. The model assumes the left wing end is fixed to a fuselage. The hinge location is defined from the side of the fuselage. The rotating length of the wing is determined as the hinge location subtracted from the total deployed span. The packing (or rotation) angle is defined from the horizontal axis to the rotating wing tip as illustrated in Figure 3.27. Figure 3.28 shows a wing with the measured boxed volume represented by dashed line. Similar to Reference 13, the boxed volume ratio was plotted verses the tip angle, Alpha, in Figure 3.29. A rigid wing by definition cannot pack less than the original volume. The figure shows a distinct maximum for each hinge location. The maximum occurs near 45 degree fold. Each hinge location has its own angle where the maximum occurs do to the influence of wing thickness. At 90 degrees and greater a second region with better packed ratio is observed. For a single-hinge wing, we can imagine that the minimum boxed packing ratio of 100% can only occur twice. Once is when it is fully deployed. The second time is when it is fully folded (180^{o}) with the hinge at the midpoint, so that the total packed volume is the same with half the span length, but twice the thickness.

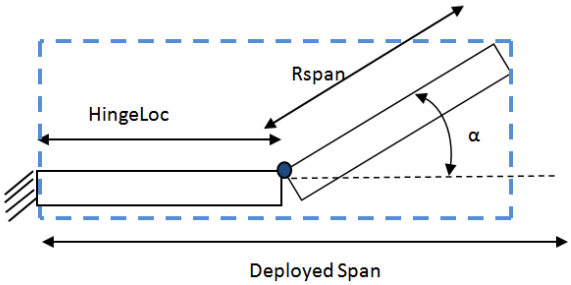

Figure 3.27 Rigid wing with top folding hinge

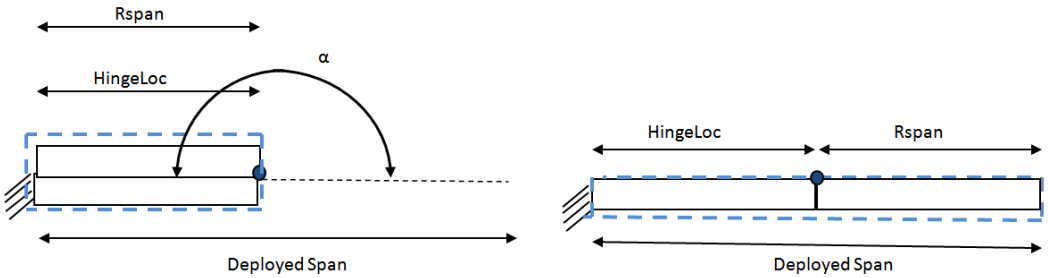

Figure 3.28 Two minimum packed percentage volumes with mid-span hinge

Figure 3.30 shows hinge locations less than 50% span length from wing root. This causes the folding wing tip to fold back into the fuselage region as shown in Figure 3.29. Thus the model implemented here calculates the boxed volume only from the wing root and results in a less than 100% packed ratio for the model. For hinge positions not at the mid-span, excess material (overhang) on either side will increase the packing volume similar to the excess material issue discussed in 3.3 Fold Radius.

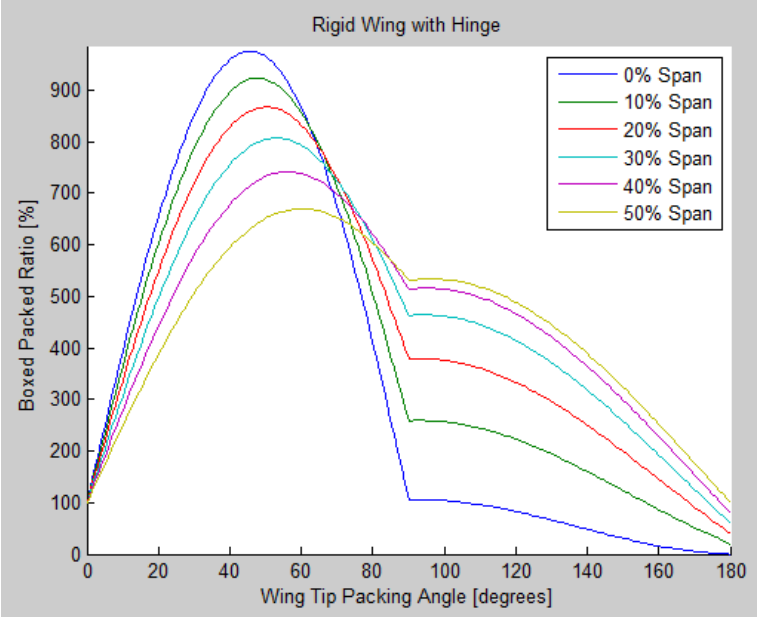

Figure 3.29 Various hinge locations with small tip effects

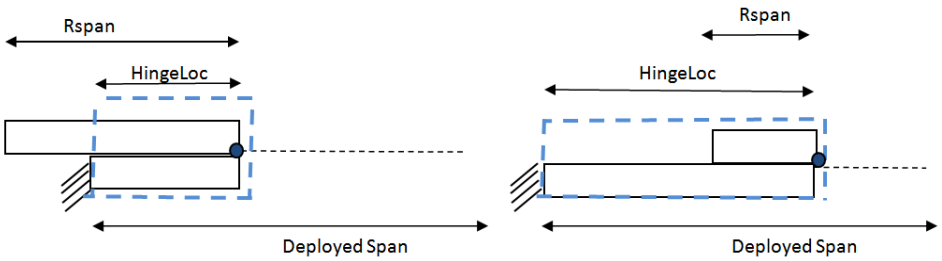

Figure 3.30 Hinge located less than 50% span (left), hinge located more than 50% span (right)

In Figure 3.31, the wing from Figure 3.29 was simulated rigid wing with a hinge location greater than 50% of the semi-span. The maximum packed ratio occurred at 60 degrees and should be avoided for most designs. At 90 degrees and greater, the second region shows more efficient packing. The two regions in Figure 3.31 are similar were as the two regions from Figure 3.29 are drastically different. Therefore, designs wing with root hinge location should be folded greater than 90 degrees every time. Figure 3.31 shows a unique theoretical wing with a hinge at 100% span with an infinitely thin wing tip. As the wing tip is rotated it added to the packed

percentage ratio, but it not useful for actual use because there is no practical use for a hinge at the wing tip.

To understand these results in the context of the small UAVs under primary consideration, a theoretical wing was considered a hinged-rigid wing the of the BIG BLUE V project [7]. A mathematical model was created to determine the boxed packed ratio for each tip angle. Two wings were modeled one with a span 36, cord 14, and height 2 inches similar to BIG BLUE V wings and a high aspect ratio wing with a span of 100, cord 15, and height of 5 inches. The horizontal axis of Figure 3.31 shows the range of tip folding angles from 0 to 180 degrees. The vertical axis shows the boxed packed ratio which is the boxed packed volume divided by the boxed deployed volume. The model only handles folding above the wing for two reasons. To fold the wing below would be a symmetric case study. Also, folding down is rarely a practical mode of packing due to the ground and landing gear located below the fuselage.

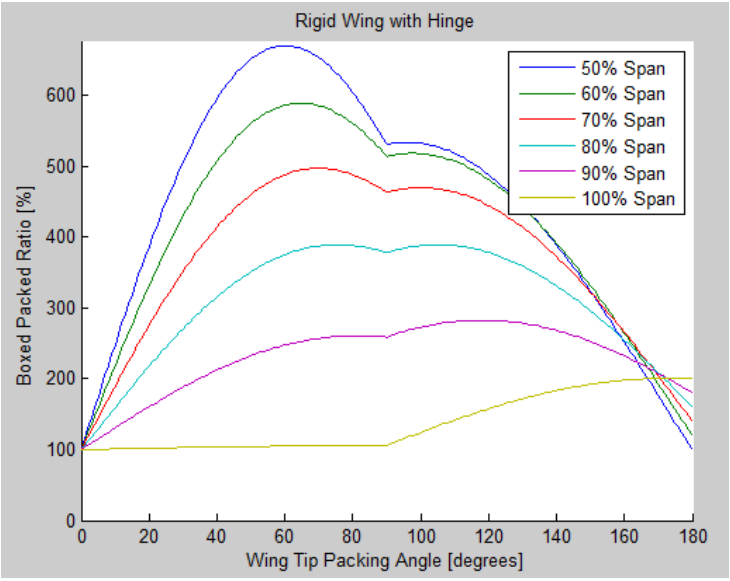

Figure 3.31 Various hinge locations, rigid wing with similar dimensions as BIG BLUE V wing

The first observation of results is this model with mid-span hinge verifies the two minimum boxed volumes are fully deployed and a fully folded wing configuration. The fully folded wing configuration has a more desirable shape in that it has a smaller footprint area, and thus leads to a better pack. The second observation is that all other configurations have a packed volume ratio greater than 100% of the deployed volume, but with smaller footprint which leads to a better shape. With wing tips folded upward, there may not be a total aircraft boxed volume increase with a traditional vertical tail section. All aircraft and many UAVs don't pack 3-dimensionally, i.e. they must be resting on designated landing gear. The third observation is that the largest packed ratios occur when the wing tip is packed less than 90 degrees.

The programmed rigid wing model also takes into account the small end effect due to the rotating wing tip's cord height. This model could also be combined with a later model presented in this thesis for flexible wings to make estimate a hybrid wing's packing configuration. The rotating wing tip could be set as the enclosure for the flexible wing. The code could also be modified to have multiple hinges for more complex wing designs. It was decided to forgo multiple hinge studies due to the added parasitic mass of additional hinges.

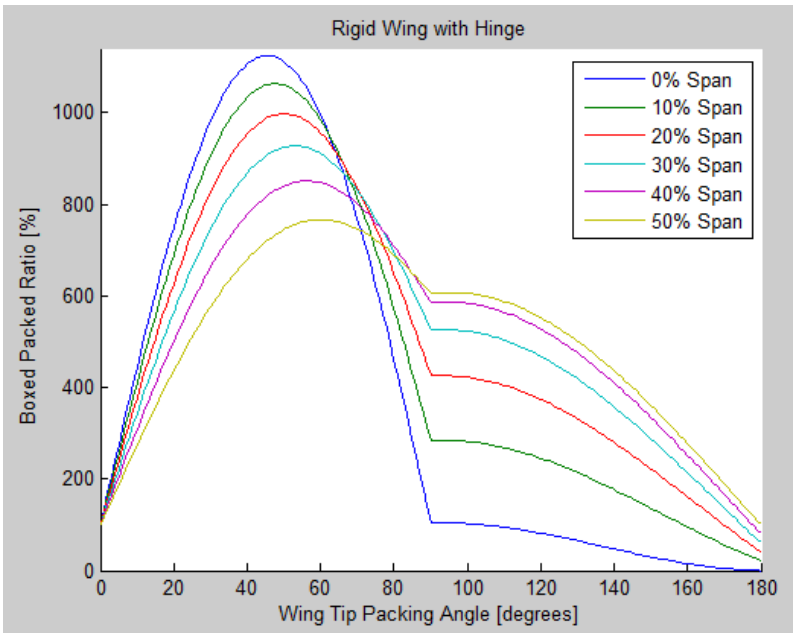

Figure 3.32 Various hinge locations less than 50% span, high aspect ratio wing

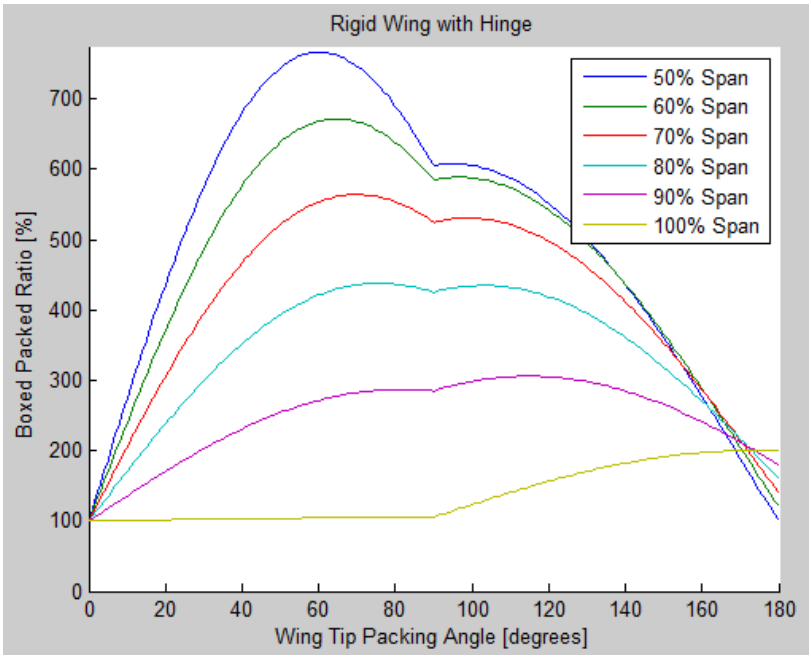

Figure 3.33 Various hinge location greater than 50% span, high aspect ratio wing

Figure 3.32 and Figure 3.33 shows a high aspect ratio wing with a hinge located at 0 to 100 % span. The same two regions are seen in each result. By changing the location of the hinge

there are large changes is the maximum boxed volume packing ratio. Locating the hinge close to the fuselage allows causes the largest boxed packed volumes. It also allows a theoretical packed volume to be less than 100 % at 180 degrees. This is due to a long wing tip folding back past the left most point where the wing attaches to the fuselage. This is a possible scenario mathematically, however most UAVs today have symmetric wings and small fuselages thus the wing tips would contact and prevent this case from happening. Therefore, all results below 100% were eliminated as unfeasible. This may be a design benefit when considering a UAV hinged rigid wing design such as NRL's XFC [14].

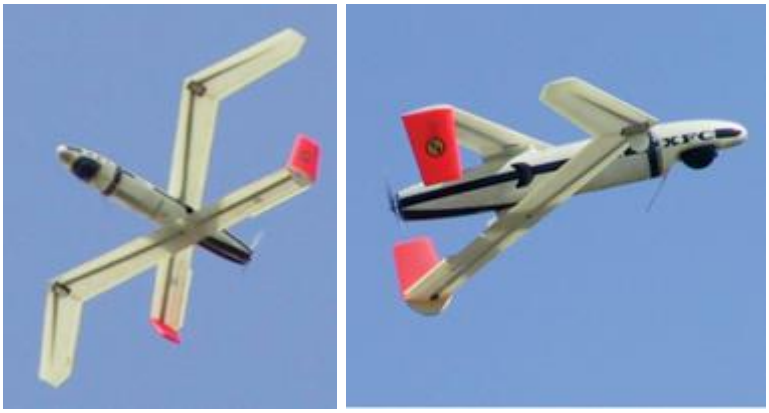

Figure 3.34 NRL's OFC non symmetric folding wing UAS

The high aspect ratio wing model has a higher maximum boxed volume packed ratio. All hinge locations past 50% are less efficient overall since the symmetric wing tips would fold flat and have a gap of wasted space directly above the fuselage. This is indicated on the plot by not reaching the 100% boxed volume packed ratio at 180 degrees. The files used for these plots were RunRigidWingPackingVolTEN.m and adjHingeRigidWingPackVolFunc.m included the list of files section, Packing Simulation Files.

For a wing tip to physically fold a large angle, it must not have cables or control surfaces due to the hinge limitations. This leads well to a simple inflatable tip design. The mathematical

model could be slightly altered so that the wing tip boxed volume is larger than the rigid fixed wing section. This larger boxed volume could be studied for optimal fold angle. Then the boxed volume could be used as an enclosure for an inflatable wing simulation as shown in the next chapter. For the cases with a hinge past 50% span, the 180 degree fold is always the best packing configuration.

3.8 Packing Estimates with BBV Wing: An Example

To design a deployable inflatable wing along with its enclosure the BIG BLUE V plane will be used as an example. This plane exists so its wing can be directly measured. From initial measurements, trends were studied to understand packing volumes.

For example, consider a case were the BIG BLUE glider wing must fit into a rectangular shaped enclosure measuring 1.25”x20”x5.5”. The BIG BLUE V wing was folded and measured to determine the packed thickness for a given number of folds and layers. The folds were all parallel, with fold lines perpendicular to span-wise direction. Each additional layer was packed on top of the last so that the packed thickness was measured in the vertical direction. The folds are thicker than the multiple layers between the folds, so unless the packing design addresses this geometric aspect, the multiple stacked folds determine the packed size. Depending on how much material compression or risk is acceptable, a relationship can be generated to predict the maximum wing length and the corresponding packed volume.

This packed region is located above the fuselage. A wing of similar construction, but different semi-span length, could fit inside of the enclosure. Depending on the folding design, various length wings of similar construction can be packed, as this example illustrates. Two assumptions here are that the wing is attached at the root and that the available packing space is above the fuselage. In order to optimally pack above a fuselage the first fold at the wing root

is up and then the second fold is a 45-degree angle so the wing semi-span becomes aligned with the fuselage as shown in Figure 3.37

3.9 Straight forward z-folding

Figure 3.36, shows the wing packed with a straightforward z-configuration above the fuselage. Here, the 45^{o} fold is not used, so the 5.5" dimension of the enclosure limits the folded section length to 5.4". Table 3.3shows the various numbers of layers of deflated wing that can be packed into enclosure. Here, more layers packed result in more total wing length. The minimum fold thickness for a deflated wing depends on the wing material and wing construction as well as the total compression on the fold. The minimum fold thickness multiplied by the number of layers determine the height (or thickness) of the packed configuration. This assumes that the folds stack on top of each other. This also assumed that the wing's airfoil and structure were constant along its span. The cord length is set by the airfoil shape and thus this packing dimension is constant.

Meeting the goal of having the longest glider wing depends on how much fold compression is acceptable for the folded wing. Practically, the more compression used to pack the wing increases risk of deployment sticking and storage damage.

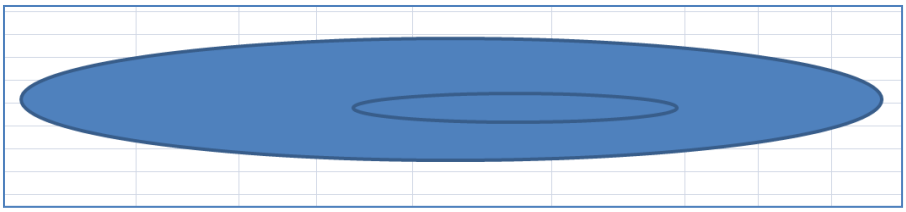

Figure 3.35 Side view of wing attachment to fuselage

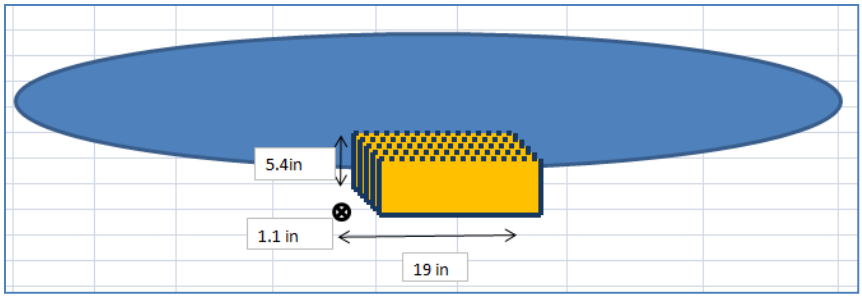

Figure 3.36 Top view of fuselage with z packed BIG BLUE V wing

Table 3.3 Typical z-fold packing arrangement

Height [in]	Cord [in]	Layers	Pack L [in]	Deployed L [in]	Packvol [in^3]
0.5	19	6	5.4	32.4	51.3
0.7	19	8	5.4	43.2	71.82
0.9	19	10	5.4	54.0	92.34
1.1	19	12	5.4	64.8	112.86

Alternatively, the packed region can be enlarged during the design stage by either increasing the enclosure size or by decreasing the fuselage width and height. The packed region height only needs a slight increase to pack additional folded wing layers so this packed dimension should be considered first for design improvement. Red in the table indicates that a min desired fold thickness has been violated by adding more packing layers which leads to higher compression. Therefore, the maximum length wing that can be z-packed without changing the enclosure or introducing excessive compression is 54". The largest inaccuracy for this estimation method is that most fuselages have a curved surface which is not accounted for.

3.10 Packing with Folds in Two Directions

The second packing approach maximizes the wing length that can be packed and uses a second fold direction. For this example, the packed region and packed configuration are designed together. In this case, the wing is folded at a 45 degree angle to pack alongside the longitudinal dimension of the fuselage. It should be noted that the fuselage is not flat and the final packed configuration will be improved because the wing will conform to the fuselage. A

rigid wing could not conform to the shape of the fuselage. After the 45 degree fold, the z-fold pattern is used with longer fold sections, so a longer wing is packed while having minimal increase in the overall packed shape of the enclosure. Multiple long layers add to the total packed wing length while slightly increasing the packed thickness. Table 3.4 shows that this packing approach results in wing lengths ten times greater than Figure 3.36 in packed volumes of comparable thickness.

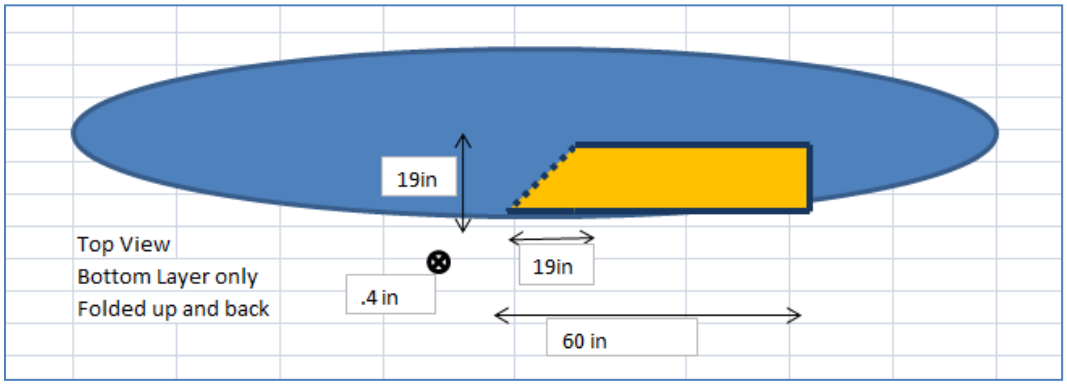

Figure 3.37 First packed wing layer 45 degree fold to change packing direction

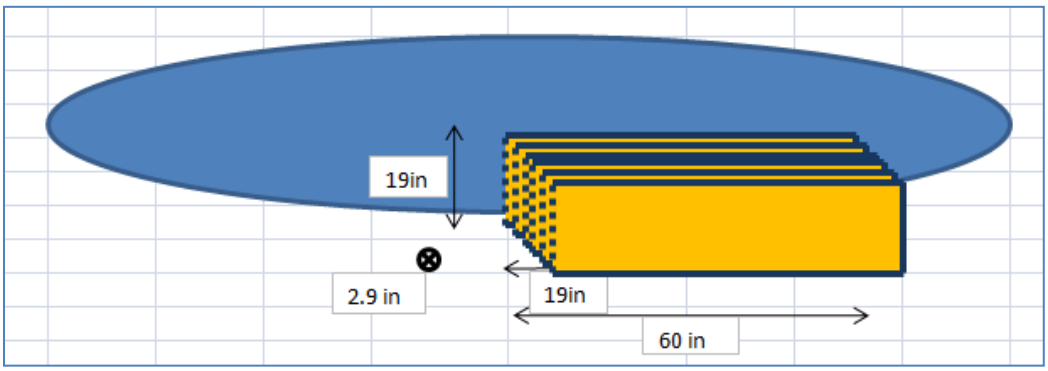

Figure 3.38 Z-pack layers in fuselage direction

Table 3.4 45 degree fold along fuselage combined with z fold

Height [in]	Cord [in]	Layers	Pack L [in]	Deployed L [in]	Packvol [in^3]
0.6	19	6	60	360	684
0.8	19	8	60	480	912
1	19	10	60	600	1140
1.2	19	12	60	720	1368

The calculated deployed lengths in Table 3.4 do not account for fold radius length and thus are conservative lengths. The minimum 45 degree fold is limited by the cord length and the diameter of the fuselage. The fuselage diameter must be greater than twice the length of a single wing cord as shown Figure 3.39. The top pack configuration of Figure 3.39 does not allow for the opposite wing to pack unless it packed on top or below the first wing. The cord length set the minimum packing length across the fuselage in the span direction.

Depending on the shape of the enclosure, the total packed length could be a better performance parameter than packed percentage volume. The folded back wing was measured at the thickest point, the fold, to be 0.4 inches. The free pack space extended back 60 inches.

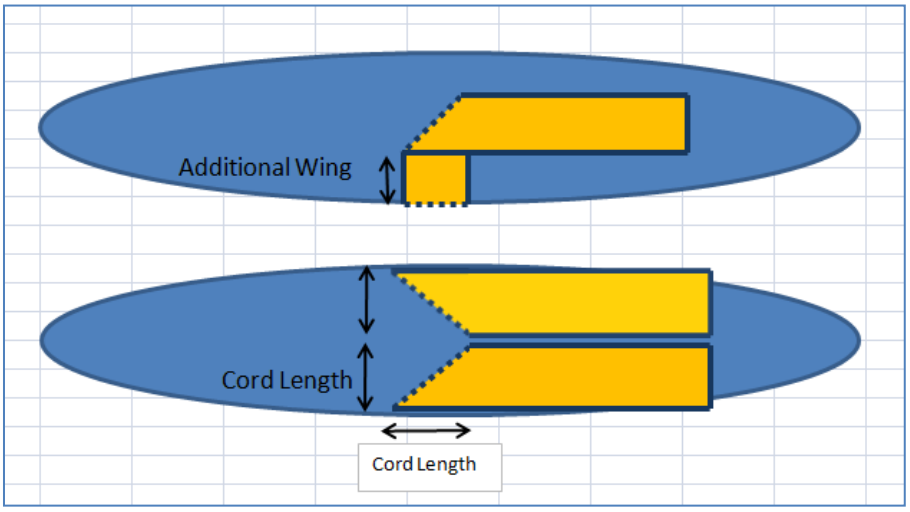

Figure 3.39 Fuselage limited 45 degree fold back

3.11 Fold Radius Length and Pleat Length

During these measurements and estimations, it became necessary to predict the pleat length of the folds so that no excess wing length would occur. Excess wing length results in a less than optimal packed percentage. Physically, the entire wing would need to be repacked, leading to a time consuming trial and error process.

Computationally, these quantities are necessary for more accurate estimations of packing. Fold radius length (FRL), an inflatable wing property, has been determined and is illustrated in Figure 3.40. FRL is the length of material that is used in the radius of the fold. The fold radius length can be used to determine the pleat length for an optimum pack with a given number of layers. The wing shown in Figure 3.40 was repacked using FRL calculations to eliminate excess wing overhand and is again illustrated in Figure 3.41. The figure also shows a ruler measuring pleat length.

Figure 3.40 Fold radius length along dotted line

Figure 3.41 No wing overhang, measuring pleat length with ruler

3.12 FRL Determination

The fold radius length is determined by z-folding a deflated wing so that there is no excess wing length. The pleat length is measured and multiplied by the number of layers in the pack. This length is subtracted from the deflated wing length to get the total length of material used in all the folds. Then the total material used in folding is divided by the number of folds to determine the FRL. FRL was determined for F5, F27, and F9 and recorded in a data file entitled WingMaterialPropertiesText.txt listed in Table 3.2 UK wing properties used to determine FRLfor use with calcPleatExcessLength.m.

The script reads in the measured lengths of cord deployed, length deployed, height deployed, cord deflated, length deflated, layer deflated, height packed, radius factor, root cord, root length, and attached root height. Next, the program allowed for the user to adjust variables representing pleatlength, pleatgroup, and foldfactor. The outputs are excess wing length and the packed percentage volume. The goal is to eliminate the excess wing material that results in a

final packed layer that does not span the full pleat length. The FRL becomes a significant length for packed configurations with many folds. Note that different wing materials often have weaves resulting in orthotropic properties aligned with the warp and full directions, but the effective bend radius was found empirically to be the same in each direction for all materials measured. FRL must be for a single z-pack group. It will not account for multiple groups of z-packs due to the material between groups.

With the understanding gained from the empirical packing study and initial folding computation, a new approach to simulating flexible (inflatable) wing packing was developed. Chapter 4 presents a chronological summary of initial developments followed by Chapter 5 with details of the final simulation and results.

Chapter 4

4.1 Random packing section

To better understand optimal packing, a simulation was developed to randomly pack a deflated wing into an enclosure. The primary goal was to rerun the simulation to generate many random packed configurations, then to see which packing patterns emerged that produced the longest packed wing lengths. The literature review determined there is no method to estimate the length of an inflatable wing that can be packed into an enclosure. The simulation produces a conservative wing size estimation in that results from random packing in general do not lead to the best packing configurations (as seen by inspection). Therefore, random packing is a way to provide a lower bound for valid results during development and a starting point for packing simulation development.

A MATLAB program was written with the goal of predicting the total wing length that could be packed into a given two-dimensional enclosure.

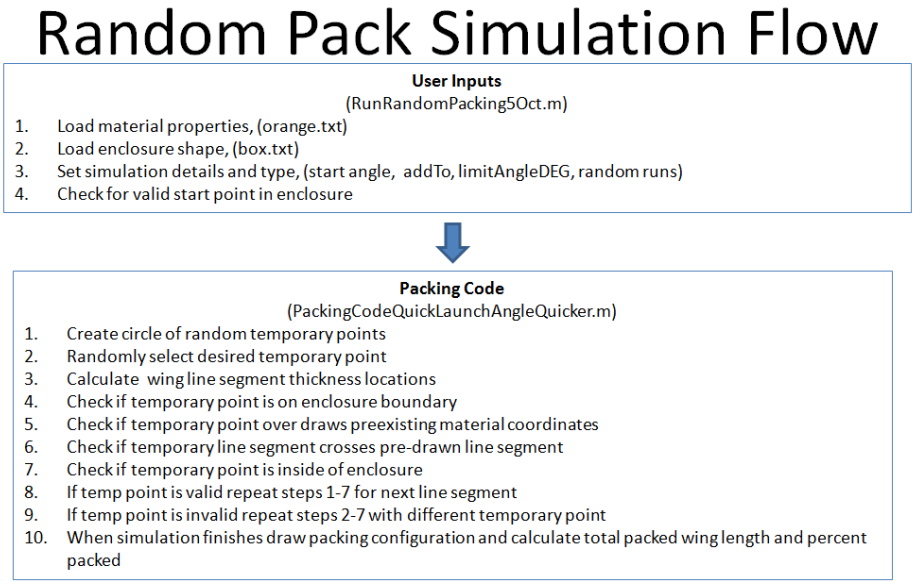

Figure 4.1 Simulation flow diagram

The enclosure is first defined by a text file of the Cartesian coordinates for each corner. The points are connected sequentially to form a closed polygon. This method allows any shape to be entered and analyzed. A circle is approximated as a series of straight lines. Additionally, difficult convex and concave shapes can be handled such as a star shape. Any real-world two-dimensional enclosure should be able to be modeled using this approach.

The program also defines the starting point, material thickness, and minimum fold radius. A function, inpoly.m written by Engwirda [15] is used to check if the starting point is within the closed polygon. This is a point location problem, a classical geometric computational topic. The random packing simulation then creates a set of candidate points (also referred to as temporary points) around the initial starting point. From these, the next valid point is randomly selected.

The basic mode for the simulation to run uses two user defined variables, "pathOpt" and "addTo", to determine how many candidate points are created for each path iteration of the simulation. For example, if pathOpt is set at four, then there would be four candidate points created ninety degrees apart with a distance from the starting point of "addTo". The least amount of candidate points is three. There is no upper limit of number of candidate points. The code then uses a random number generator to order and select the candidate points.

All these points are checked with three criteria to be valid points. The first check is all candidate points against all previously drawn points so that no over drawing will occur. The second check is to make sure the random points won't cause a crossing of previously drawn lines. The third check is that the random points are inside of the polygon enclosure. After all points have been identified as valid options, the first random point that passes all tests is selected as the path for the packed wing, then the creation and checking process is repeated

until no points pass all criteria. At the end of filling up the wing region the total length of the wing packing configuration is calculated.

The simulation was first run and the packed length of each simulation was saved. The simulation was run in a loop with the five longest packed lengths saved. As the number of runs increased the chances of having a longer random packed configuration increased. Five simulations were run in parallel, each with a total of 100,000 runs for both attachment locations. More runs increase the wing packed length but the efficiency of the random packing method is low.

Simulation 1: Random Packing without Improvements

The first random packing simulation used a centered attachment point. In a square enclosure four wings with different stiffnesses were simulated by setting the stiffAngDEG variable to 60,90,130, and 160 degrees. The smallest angle allowed for a tighter radius and thus is a more flexible material. The largest angle limit simulated a stiff deflated wing. The stiffAngDEG is a physical combination of material property, inflatable wing construction and effects of being deflated. Table 4.1 presents the input variables for the simulation, with results in Figure 4.2 Random pack simulation best and Figure 4.3 Center attach results. Wing packing simulations are judged by long wing lengths packing into the standard 4"x4" boxed enclosure. A secondary method is to use packed percentage. Packed percentage is deflated wing area divided by box area.

Table 4.1 Simulation data for centered root random packing

Center Initial Root				
start point	Stiffest	Stiffer	Flexible	Most Flexible
pathOpt	5	5	5	5
addTo	0.2	0.2	0.2	0.2
stiffAngDEG	60	90	130	160
runs	10000	10000	10000	10000
material file	orange.txt	orange.txt	orange.txt	orange.txt

Figure 4.2 shows the longest two simulations for 10,000 trials for each of the five parallel loops. The enclosure is shown, with the random-pack results from the two best cases for a relatively flexible material. These are typical of random trials and show the large amount of unused space. Unlike real-life, the simulation does not allow for the packed wing to be manipulated or squeezed. Thus, the root attachment simulation starting position has an important influence on the resulting packed length. The center attachment point is not the optimum starting point for a box enclosure simulation.

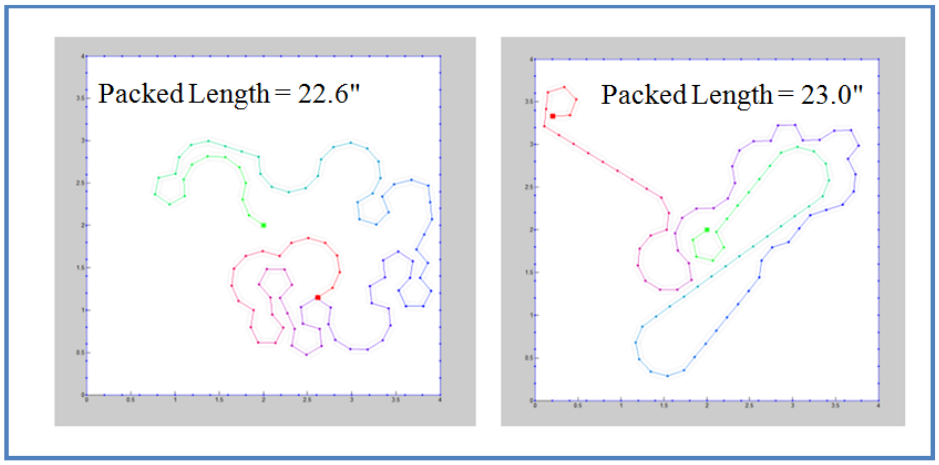

Figure 4.2 Random pack simulation best two

The number of runs and the stiffAngDEG variables were studied to determine how effective a random packing configuration could be. First, note that the pathOpt and addTo variables influence the simulation time with more (or fewer) calculations per line-segment

iteration. These variables were held constant throughout this study for consistency. They should be tailored for a specific inflatable wing to study actual packing. A shorter addTo length allows for better contour-following which will slightly increase the total packed wing length. Increasing the number of path options for the pathOpt variable also increases the contour-following resulting in additional packed wing length. These two variables could be adjusted after initial wing sizing simulations for more accurate, and therefore less conservative, estimates.

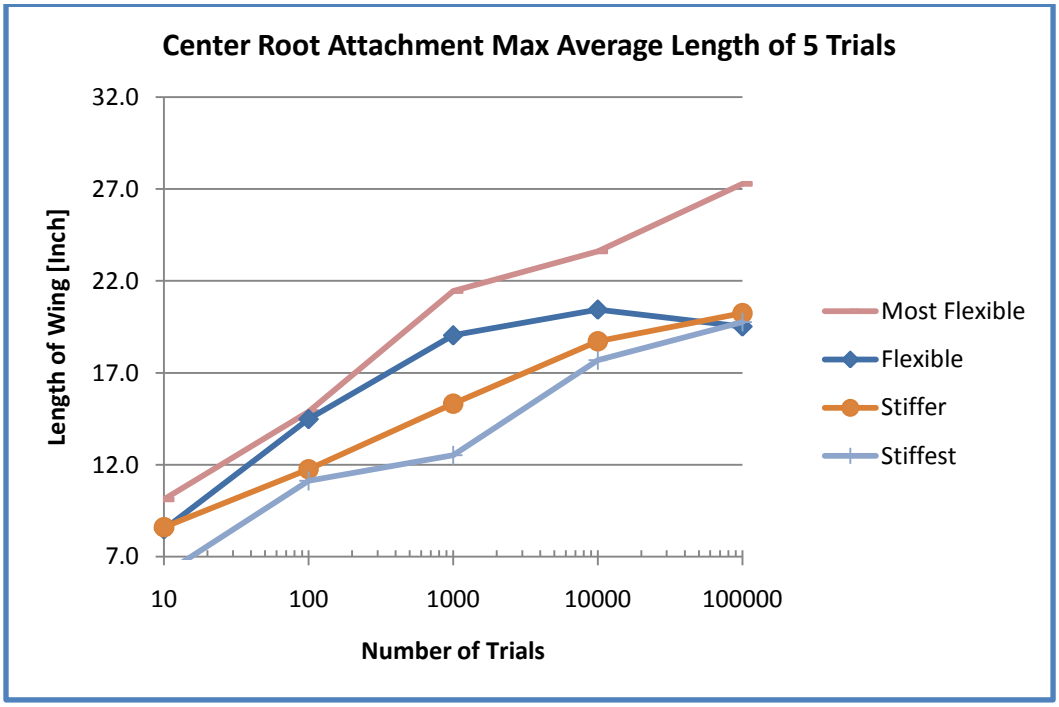

Figure 4.3 Center attach results

As expected the most flexible deflated wing resulted in the best packing length for all runs. When designing a packable UAV for low-density, high-altitude or extra-terrestrial use, flexible wing designs should be considered to help maximize the wing length.

Simulation 2: Random Packing with an Edge-Centered Wing Root

The simulation was rerun for the same cases, but with the starting point at the middle of the left wall. The material file used to define this was orangeLeftWall.txt. The wall attachment

resulted generally in shorter packed wing lengths although the longest achieved were slightly longer than those with a center starting pack. This is due to the method's inability to move points that were previously defined. If the packing starts at the wall and begins validating a path that is perpendicular to the wall, the enclosure is essentially halved, or at least the probability is severely reduced for the random-packing path making it back to the other half of the enclosure, top or bottom. Table 4.2 shows that the same test cases where run except a wall starting position was used. The symmetry of the boxed enclosure makes starting at top, bottom, left, or right walls the same.

Table 4.2 Simulation variables

Wall Attach				
start point	Stiffest	Stiffer	Flexible	Most Flexible
pathOpt	5	5	5	5
addTo	0.2	0.2	0.2	0.2
stiffAngDEG	60	90	130	160
runs	1.00E+05	1.00E+05	1.00E+05	1.00E+05
material file	orangeLeftWall.txt	orangeLeftWall.txt	orangeLeftWall.txt	orangeLeftWall.txt

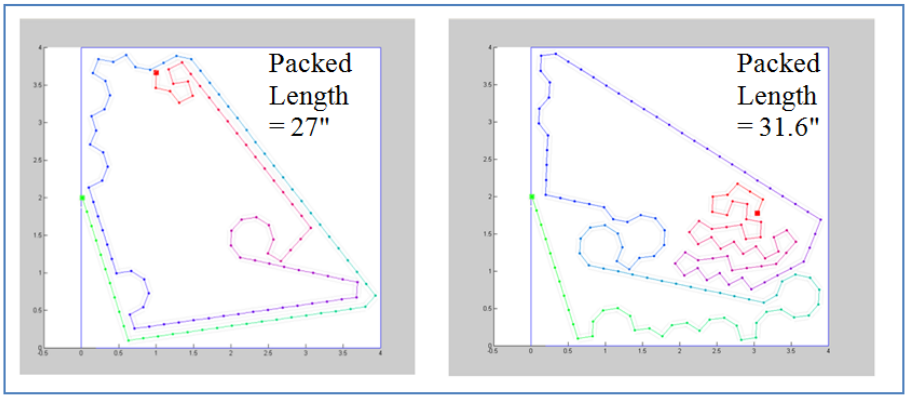

Figure 4.4 Two best runs for simulation settings 1e5, 160, .2,5

Figure 4.5 shows the best packing results occur when the first few path segments follow near the enclosure wall instead of taking a perpendicular path.

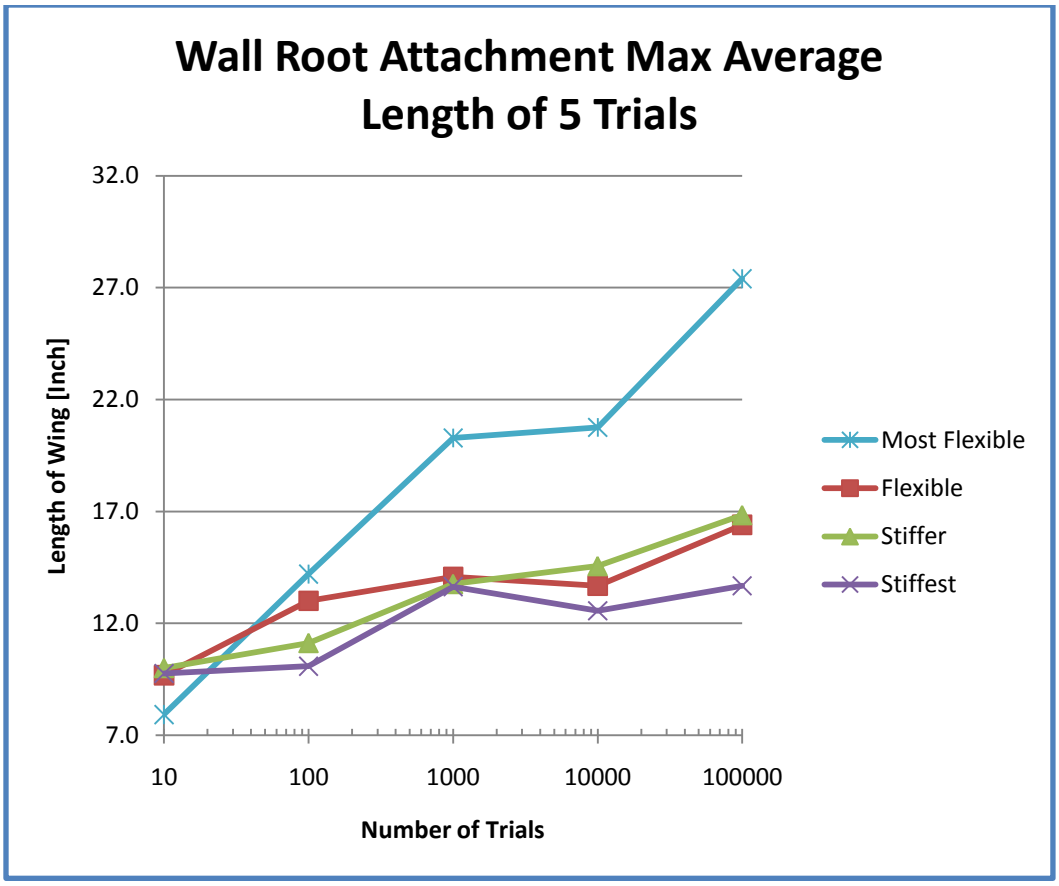

Figure 4.5 Wall attach simulation results

Figure 4.5 shows that increasing the number of runs does increase the total packed length, but at a slower rate of length increase than the center attachment case. This slower rate shows that the center start point is a better packing configuration in general. However, the most flexible material is able to achieve a 27 inch length for both attachment positions. The less flexible, stiffer, and stiffest materials achieve a maximum length of 16 inches for wall attachment and 20 inches for center attachment. Note that the center attachment point is less physically realizable because the wing root has to be attached to a fuselage. However, if the last point of the simulation ends at a wall, the center attachment point could be thought of as the wing tip and the wall point could be thought of as attached to the fuselage.

Upon analyzing the results for random packing simulations, an improved simulation was desired. A method to keep the simulation away from the walls by attracting the simulation to the center was developed. It consisted of defining a potential energy plane throughout the enclosure were the simulation still produced random candidate points, but the points have potential energy values to influence the simulation. This method is presented in Chapter 5.

Chapter 5

5.1 Potential Energy to Control Packing Path

The random packing method did not yield a fully packed enclosure therefore a "potential energy" method was developed to guide how the simulation would prioritize randomly packing the wing material. Figure 5.2 shows the same four inch by four inch square enclosure with a low "potential energy" region at the center of the enclosure. The centered low potential energy (PE) attracts the packing process and prevents random packing path from being trapped at the walls and ending the simulation before filling the enclosure.

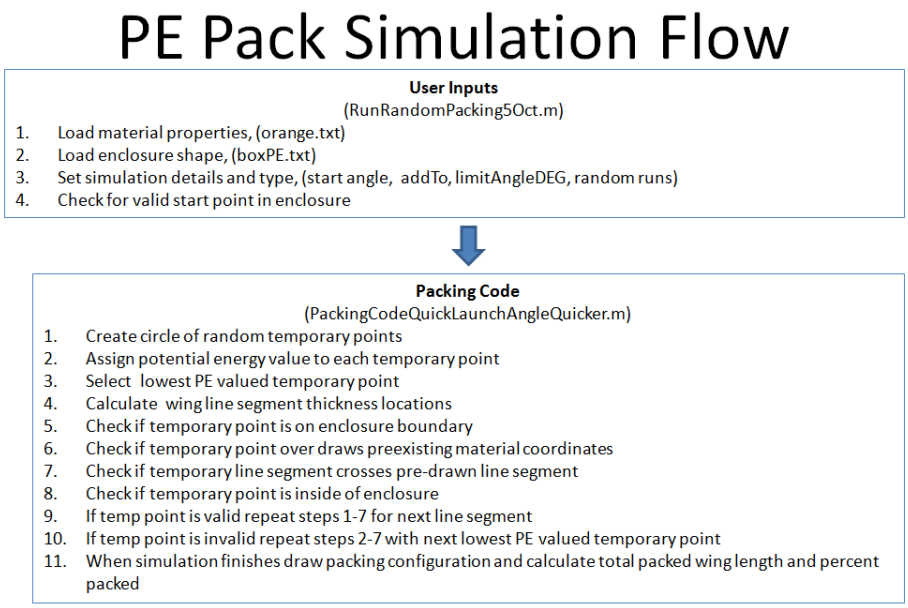

Figure 5.1 Potential energy guided simulation diagram

The enclosure input text file has coordinates for a PE point and a value. The PE function is defined with the same equation as gravitational pull. It uses a point mass, gravitational constant, and the radius from the point mass to determine the PE value. The point mass value is defined in the enclosure input text file and is indicated on the packing configuration plot with a circle and dot or a circle and cross symbol. The size of the symbol grows with a larger point mass

value. With a low PE value assigned to each set of random temporary points, the packing simulation chose the lowest-PE-valued path.

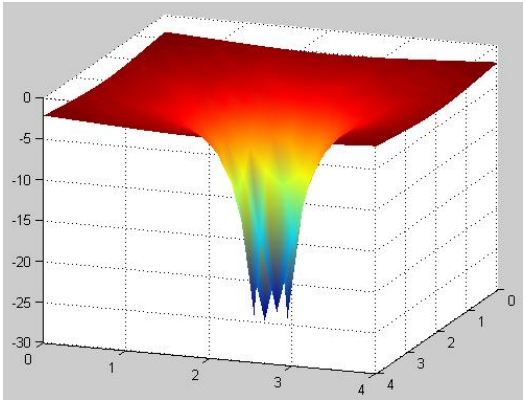

Figure 5.2 Low potential energy plot of four inch by four inch box enclosure

Both low (attracting) and high (repelling) "potential energy" points or regions can be defined. Figure 5.3 illustrates high PE corners as an alternative to a low PE center.

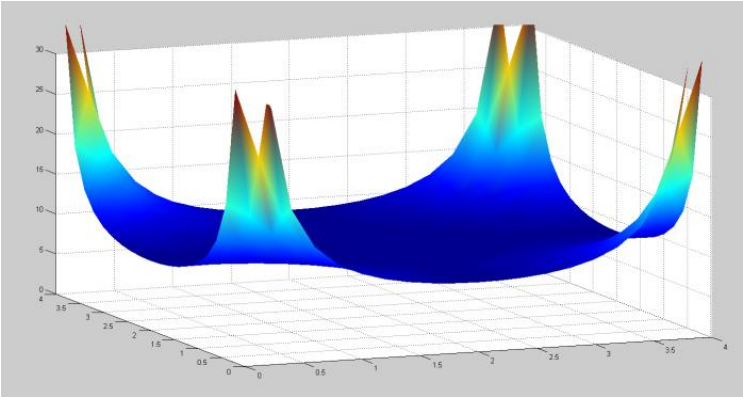

Figure 5.3 High PE regions at corners of box enclosure

Simulation 1: Initial Potential Energy Trials

Four simulation results are seen in Figure 5.4. The difference among them is that the random path option is in conflict with the low "potential energy" region. The top two packing configurations made it out of the exponential PE region. The bottom two pack configurations

had a random path selection that kept inside of the exponential PE region. The packing simulation stopped many times due to attempted path crossing near the low PE region. Two examples of this are seen in the top two results of Figure 5.4. The diameter of the PE marker indicates the relative PE value used and its location. The circle with a cross represents a low or negative PE point. The circle with a dot represents a high or positive PE point.

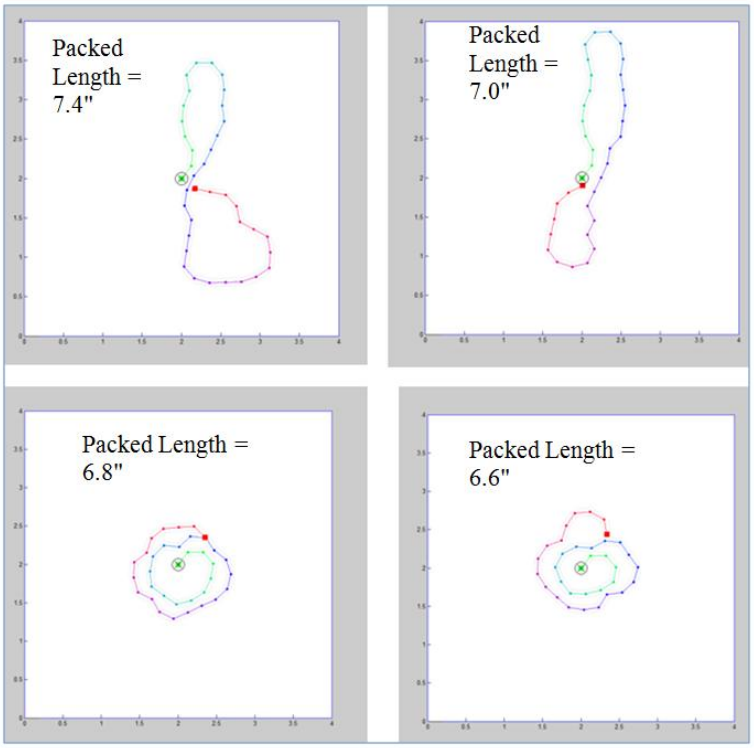

Figure 5.4 Typical results of center-attach, low-PE center simulation

In an attempt to increase the packed wing lengths, the starting point was moved to the lower left corner while still having the low PE point at the center. A quick trial of 50 simulations was conducted. Figure 5.4 shows the results with packed lengths from 6.2 to 7.2 inches. The PE method influences packing near the center of the enclosure, but as the simulation passes the low PE point and comes back to center, the simulation runs into already packed material and stops, resulting with poor packed wing lengths. The results can be improved with more

simulations as shown in the random packing section. However, due to the short wing lengths a different approach was chosen for the next simulations. From prior experience obtained from 3.1 Empirical Packing Study, these PE controlled simulations are lacking. To improve probability of long wing packed length the simulation was run through a series of loops. A circle and dot symbol indicates high PE out of page like an arrow head.

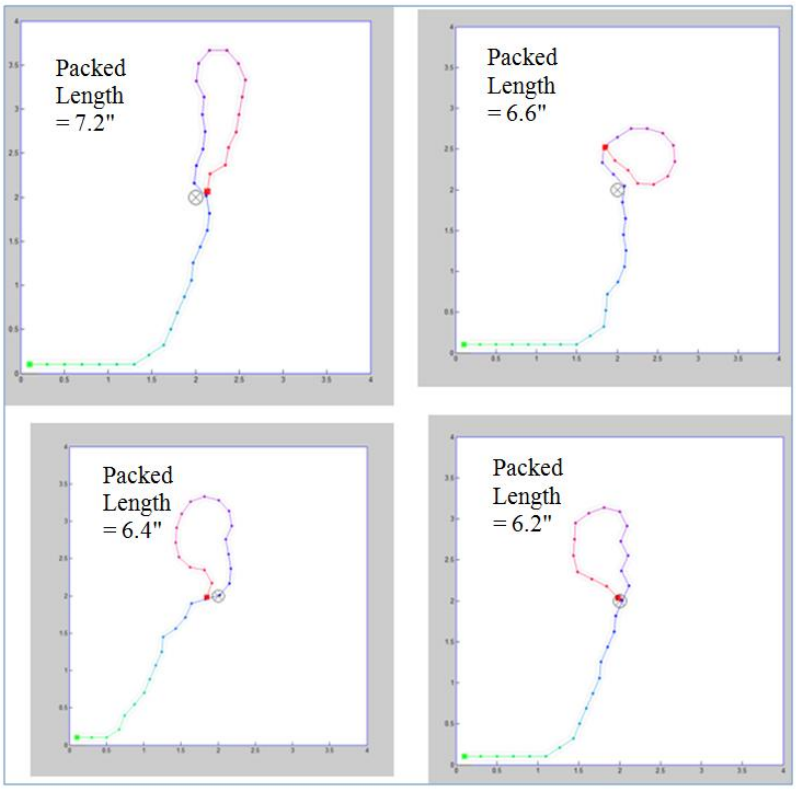

Figure 5.5 Longest four of 50 runs with low PE center and corner start

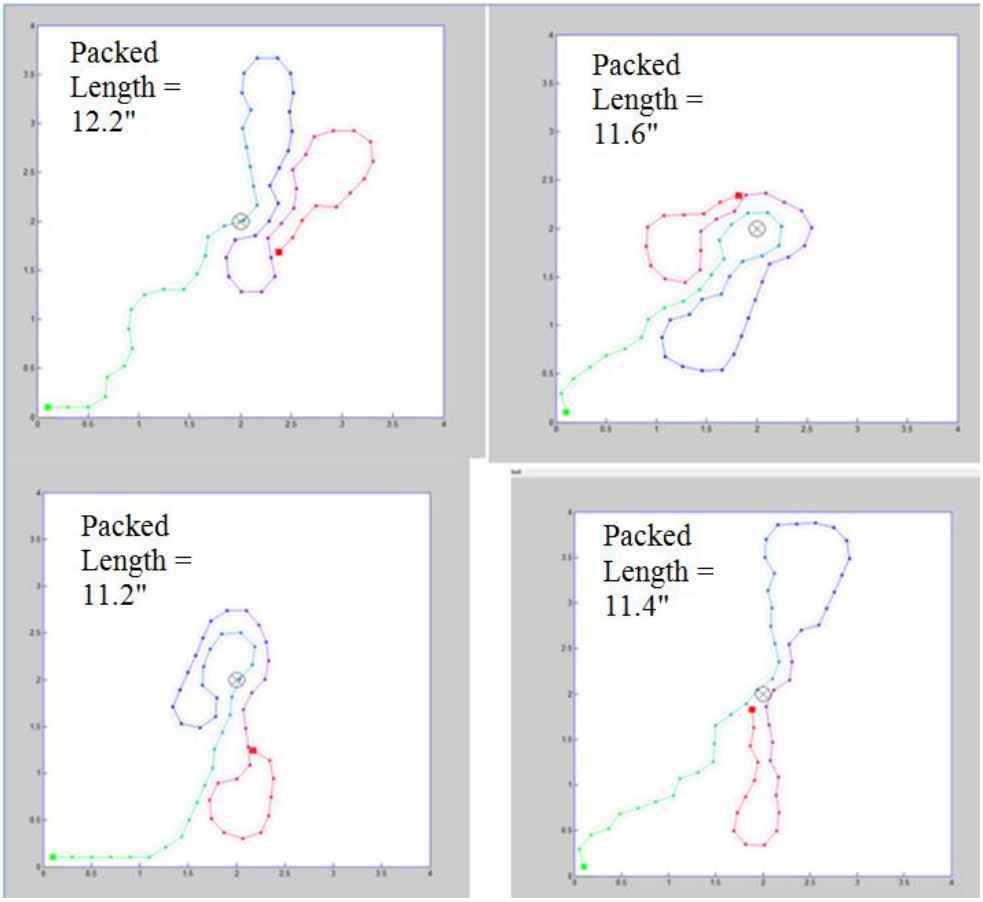

Figure 5.6 Best four of 5000 runs for random packing with center PE and a corner attachment

Simulation 2: High Potential Energy Corners

High PE corners were used to prevent path crossing issues that resulted from center attraction PE guidance of the random packing material. The longest wing lengths were recorded and plotted in Figure 5.7. Note the high PE corners indicated with the circle-enclosed dots.

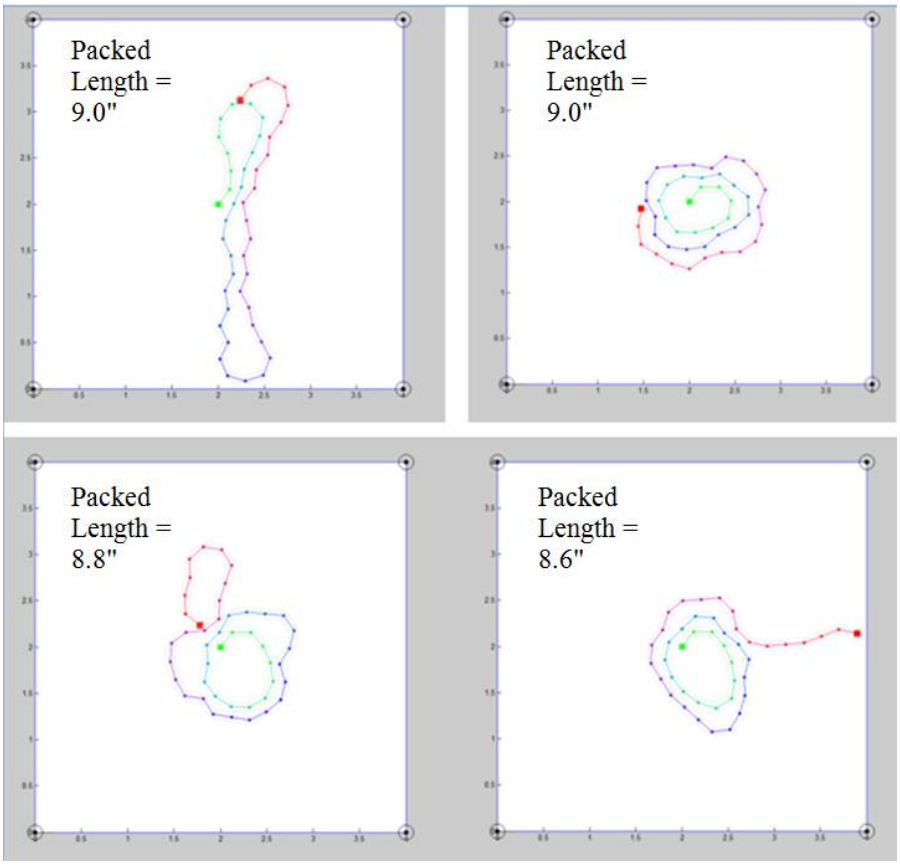

Figure 5.7 Longest wing lengths of 5000 simulations high PE corners

The simulation was set to run autonomously 5000 times and save the longest resulting packing schemes. All simulations start with a central fixed point in a square enclosure. All sub plots of Figure 5.7 except the top left sub plot showed the start of a roll wrap configuration. The top two tied for the longest of the simulation. The top left shows characteristics of a z-pack configuration. This produced the longest packed wing of 5000 runs. Compared to the center-low-PE approach, the longest results were 19.5% longer. The simulation with four high PE corners encouraged the packing path to stay away from the walls yet was not attracted to a single point to help prevent early simulation termination.

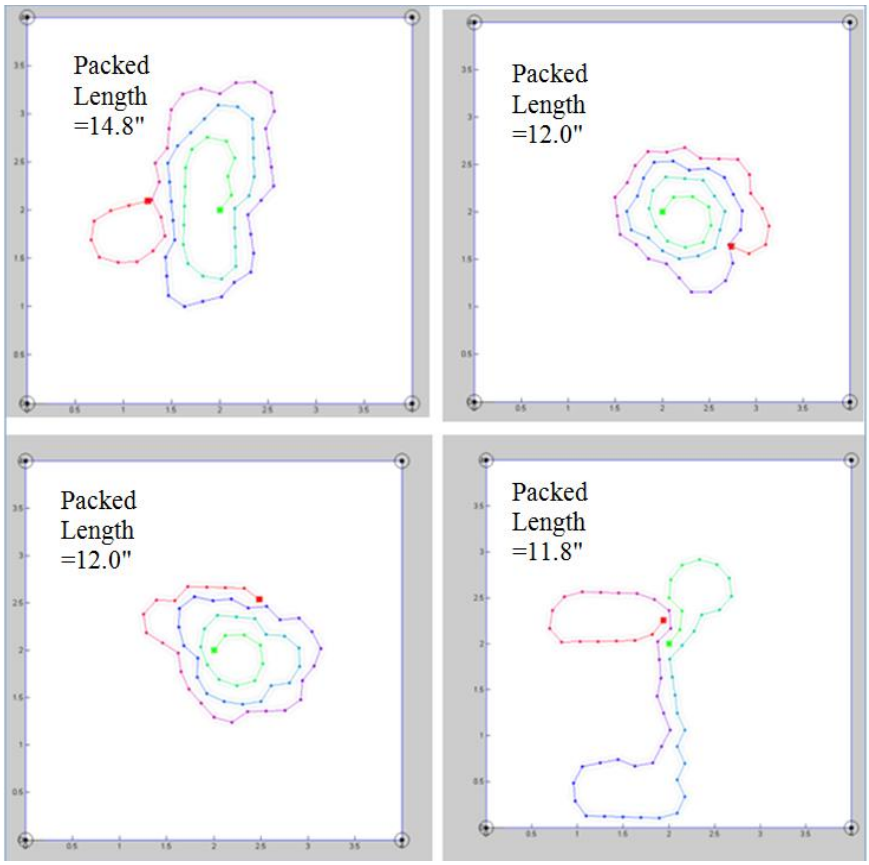

Figure 5.8 Longest four of 865,000 runs

However, the lengths achieved in the previous example were still disappointing compared to empirically-based results. Figure 5.8 shows the best four results after 865,000 runs of the simulation. This number of runs was chosen to complete in one evening on a desktop computer. Packed lengths varied here from 11.8 to 14.8 inches. All but the lower right sub plot showed a wrap packed configuration. The wrap packed configuration is a simple configuration that resulted in many of the simulations.

Simulation 3: High Potential Energy Corners with Corner Start

A similar simulation to Simulation 2 is a high potential energy at the corners with attachment at corner. The object was to prevent early terminations at the walls and to prevent

common line crossings at the center low PE point. Simulation 3 used 4 high PE points at the corners.

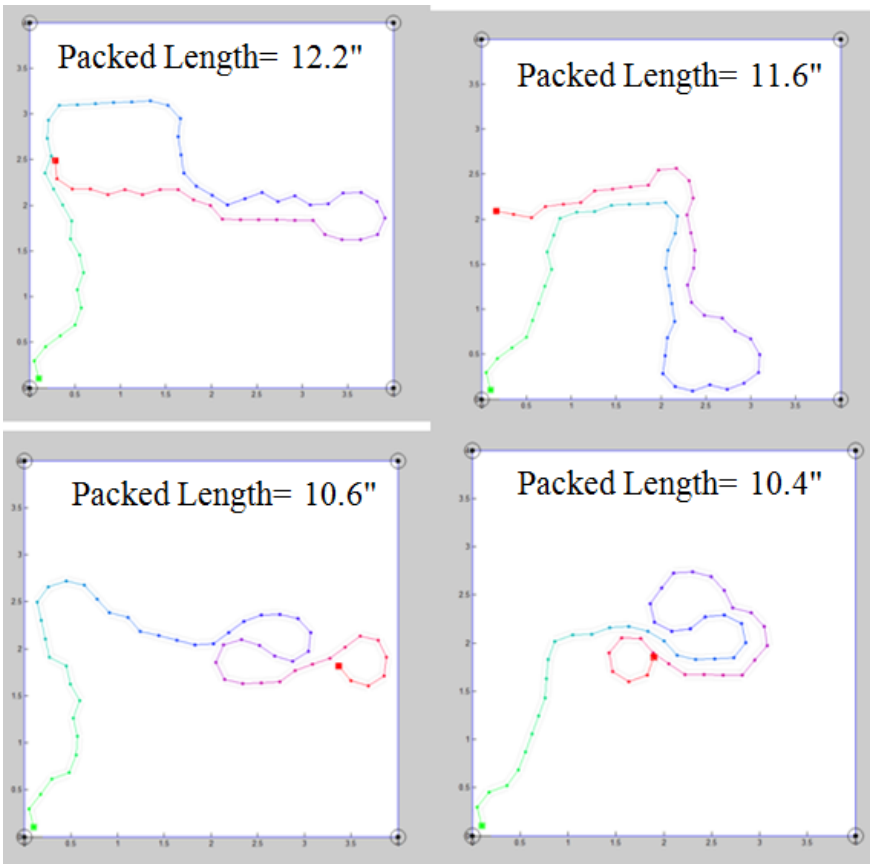

Figure 5.9 Best four of 5000 with high PE at corners

Having PE control resulted in acceptable packing configurations. However, all simulations stopped before reaching any useful configurations. In general, the PE control method produced slightly longer packed wings than the random method. The corner start with high PE corners results tied the corner start low PE center. Ultimately, the large unused area of the enclosure motivated further improvement of the simulation approach.

5.2 Genetic Algorithm Section

The random and potential energy methods of controlling inflatable wing packing in an enclosure resulted in short wings that did not show the packing benefit expected of inflatable wings. Therefore a genetic algorithm was implemented for the same cases and led to longer packed wings and fewer simulation runs to reach the better results.

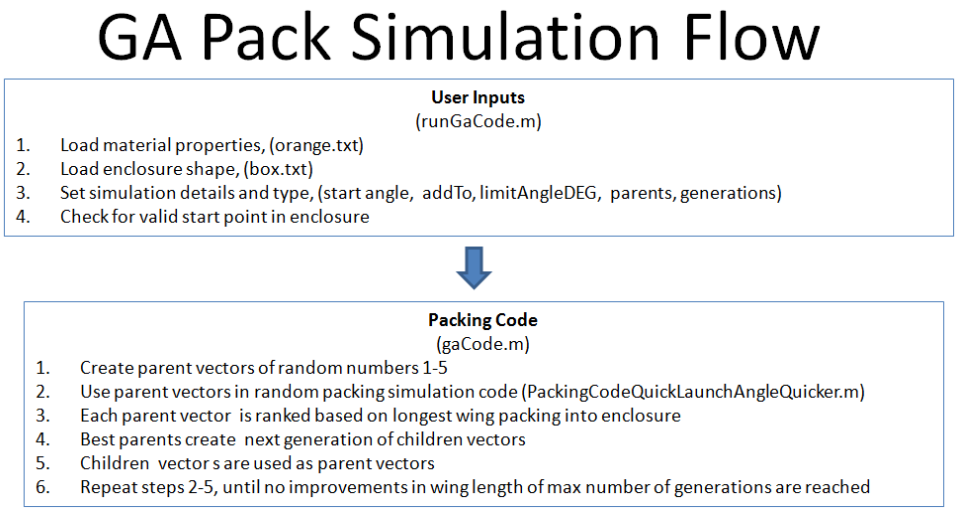

Figure 5.10 Genetic algorithm simulation flow diagram

The genetic algorithm creates random parent vectors of numbers. These parent vectors are used to control which path will be taken for each line segment iteration. Each simulation runs until the path has no additional valid locations. The parent vectors with the longest packed wing are used to create similar child vectors for the next generation of simulation runs. The genetic algorithm method is automated and requires a minimal amount of work from the user.

The variable nvars sets the parent vector length to be 500 path options from one to five. The longest wing this vector produced was the addTo length of 0.2 inches multiplied by 500 for a maximum packed length of 100.0 inches. The variable Population_Size set the number of

parents for each generation. The variable Generations_Data set the number of generations for each simulation.

Five trials were run for four different wing stiffnesses and two attachment points as summarized in Table 5.1. The number of parents and number of generations were selected here to have a similar number of total simulations as in the random and potential energy sections for comparison.

Table 5.1 Summary of GA trials

Trial	1	2	3	4	5
Parent Vector Length	500	500	500	500	500
Parents	20	100	200	500	1000
Generations	50	50	75	75	100
Total Runs	1020	5100	15200	38000	101000

5.2.1 Center Attachment

For comparison, the first GA case used the same center attachment, box enclosure, pathOpt, addTo, and material file as in the Random and PE simulation sections. Four wing stiffnesses were simulated as shown in Table 5.2.

Table 5.2 Center attachment variable inputs for GA

Center Attach				
start point	Stiffest	Stiffer	Flexible	Most Flexible
pathOpt	5	5	5	5
addTo	0.2	0.2	0.2	0.2
stiffAngDEG	60	90	130	160
material file	orange.txt	orange.txt	orange.txt	orange.txt

The genetic algorithm resulted in longer wing packing configurations for a given number of runs as shown in Figure 5.11. The longest packed wing lengths for the 5th trail of 101,000 runs resulted in packed lengths of 37.8 inches, 38.4 inches, and 33.4 inches for 160 deg, 130

deg, and 90 deg stiffAngleDEG variable respectively. These packed configurations are shown in Figure 5.12.

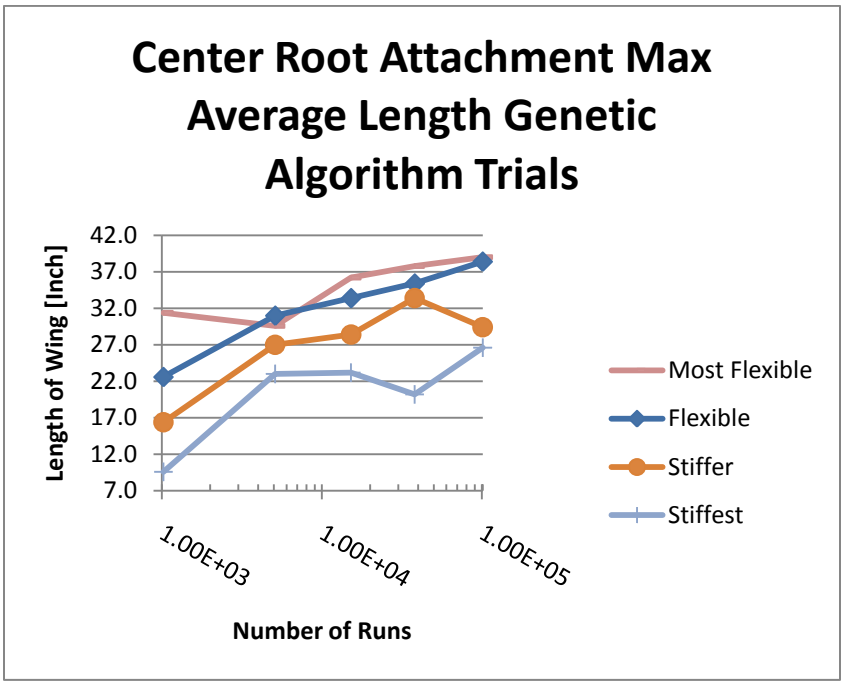

Figure 5.11 Center root attachment GA trails

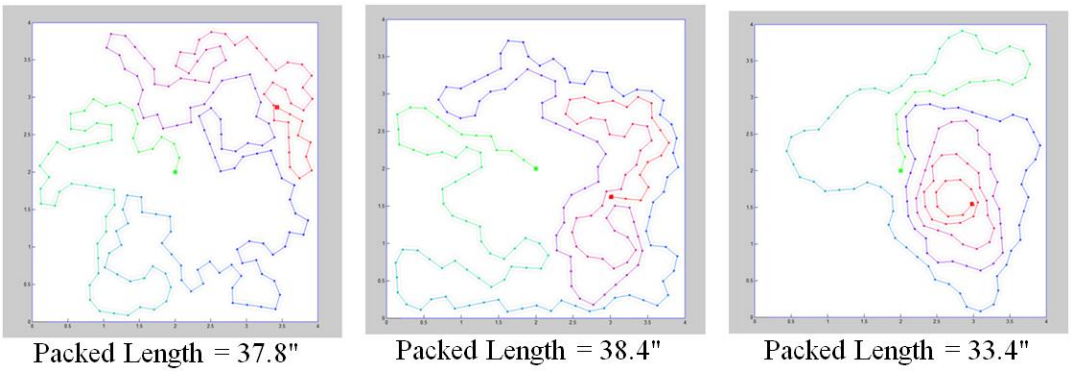

Figure 5.12 Longest packing configurations from GA

5.2.2 Wall attachment

The same wing stiffnesses, box enclosure, number of parents, and number of generations were simulated again with a wall attachment. The fifth trail with the most runs had

40.0 inches, 32.2 inches, and 33.8 inches, for 160 deg, 130 deg, and 90 deg respectively. The center attachment had similar packed wing lengths for the longest runs. Thus with better packing control methods the wing attachment has less influence on the total packed length.

The wing stiffness was the primary factor determining the total packed length in the enclosure. Table 5.2 shows the stiffness labels and their respective angle limits. The total packed lengths for each wing are shown vs. the number of runs required in Figure 5.13. The best packed lengths were 40.0 inch, 32.2 inch, and 33.8 inch for the 160deg, 130deg, and 90deg respectively. These packing configurations are shown in Figure 5.14. Figure 5.14 shows the general trend that a flexible wing packed better than a stiffer wing. The genetic algorithm still uses randomly generated parent vectors, but the sequential generations are selected based on longest wing length packed. The best parent vectors are used for the next generation to create longer packed lengths. The random parent vectors results in stiffer wings occasionally packing better than flexible wings for any given run.

Table 5.2 GA variable settings

Wall Attach				
start point	Stiffest	Stiffer	Flexible	Most Flexible
pathOpt	5	5	5	5
addTo	0.2	0.2	0.2	0.2
stiffAngDEG	60	90	130	160
material file	orangeLeftWall.txt	orangeLeftWall.txt	orangeLeftWall.txt	orangeLeftWall.txt

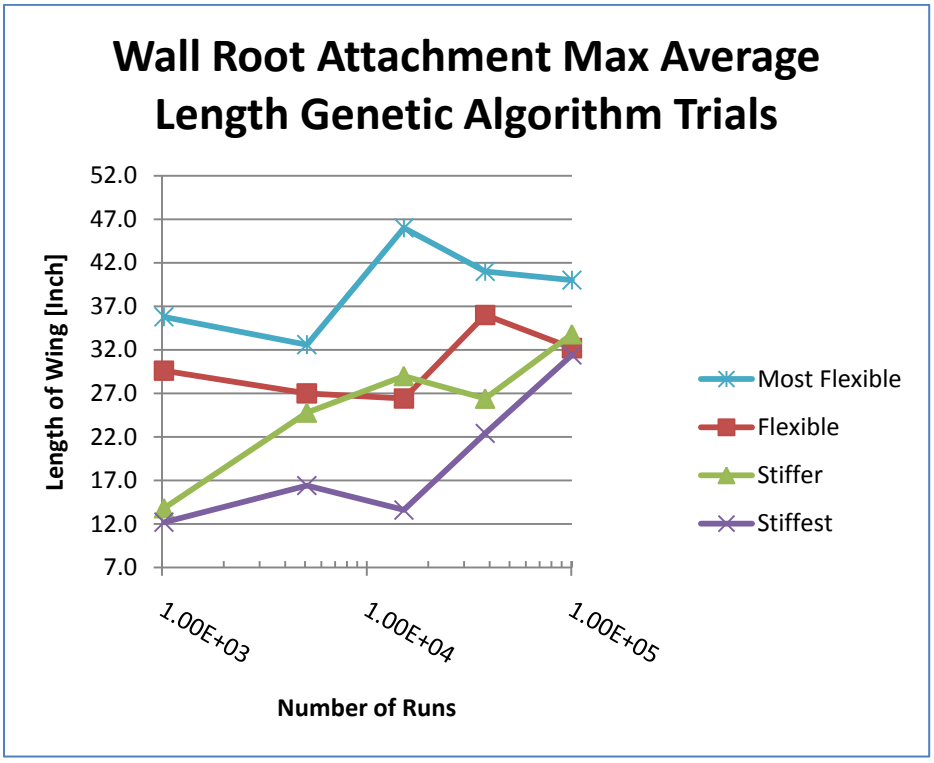

Figure 5.13 GA packing results

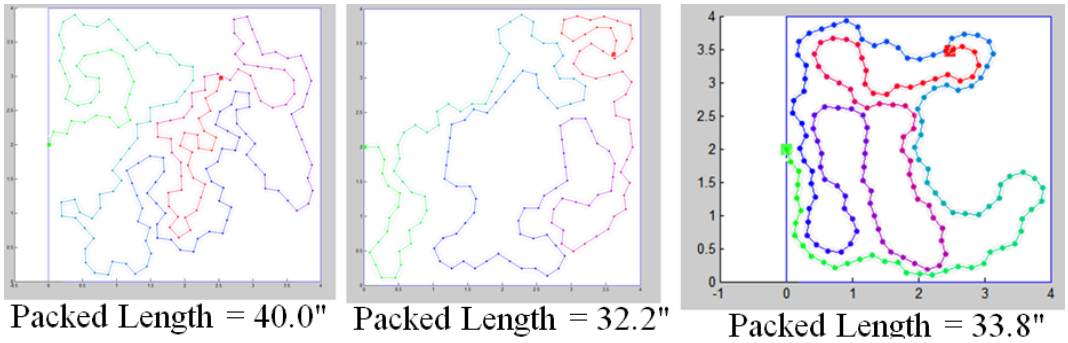

Figure 5.14 GA wall root attachment results

The genetic algorithm is a method for quickly comparing many different wing stiffness, enclosure size, enclosure shape, and wing attachment locations to determine high-level trends. These trends could then be used in the later "User Trace" section for best packed lengths. However, the GA packing method did not reveal optimal packed lengths or practical packed configurations. The packed configurations are typically too complex for a hand-packed wing.

The GA method also suffers from the simulation's inability to relocate the packed configuration. Once a material point is determined it can't be shifted. A physical wing can be loosely packed, then squeezed to fit an enclosure. Lastly, the parent vector is often not a physical geometry vector due to invalid path selections. So the best parent vectors combine to form a future generation that is not based exactly on the packed configuration. It is based on the vector learnPathCyc instead of the vector pathCyc. The files used are listed in Genetic Algorithm Files.

Chapter 6

6.1 "User Trace" Option

The goals of the packing simulation code are to enable designers to define an enclosed polygon then to assist with determining the optimal packing strategy and to arrive at an initial conservative estimation of wing length. Inflatable wing properties are inputs to the simulation. Multiple two dimensional packing arrangements can be tested, so that during the aircraft sizing and enclosure design phase, the design team can have numerical estimates of wing length.

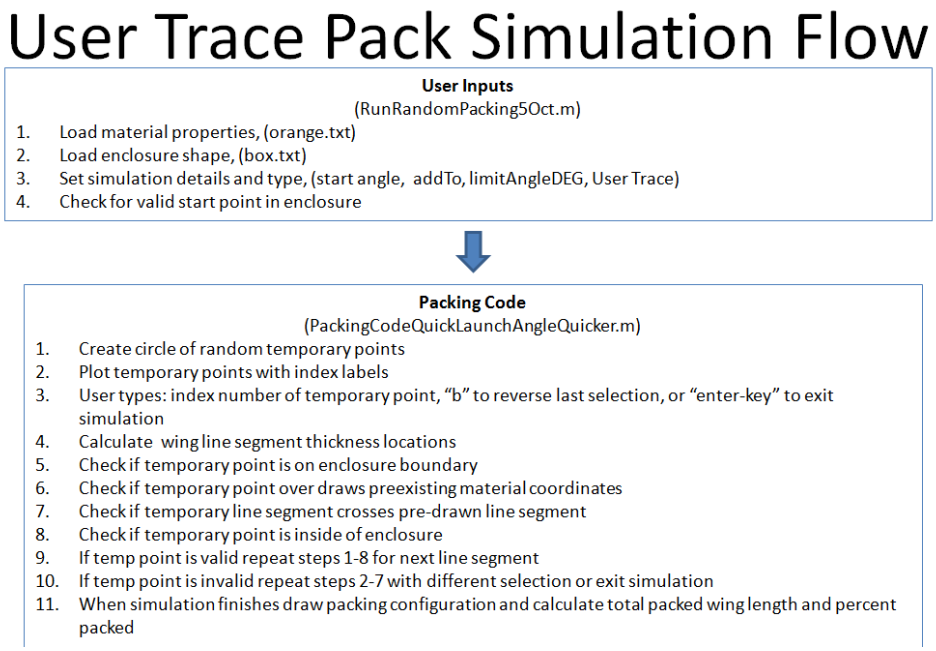

Figure 6.1 User trace guided simulation flow diagram

The user selects from three to nine path options. The code generates the selected number of temporary points that alternate indexes left and right from the center path. The path option index alternates with even and odd creation; if a majority of the path selections are even, then the packing configuration will be wrapped counter clockwise around a central starting point.

To help the user make a valid path selection, the deflated wing thickness is shown with grey parallel lines. The thickness can be turned on or off for any plotted pack configuration by means of the variable traceOpt. Choosing an even number for the path option, leads to option one not being straight ahead (straightforward). The user is encouraged to use an odd number of packing options in order to have one straight option at each step of the simulation.

A situation may arise during the "user trace" simulation in that an invalid path was selected or a mistake was made. The simulation is reversible by typing the letter "b" instead of a number when prompted to make a path selection. This reversing feature allows the simulation's most recent packing selection to be altered without starting over at the beginning.

The first simulation uses an addTo length of 0.2 inches, stiffAngleDEG of 130 degrees, deflated wing thickness of 0.1 inch, startAngDEG of zero degrees, and a pathOpt of seven. These simulation variables represent a typical inflatable wing previously studied at the University of Kentucky. The files used in this simulation are named runPackingCodeONCE.m, orange.txt, and box.txt.

The attachment angle matters. If a stiff material is being used and attached to a wall, a neutral launch angle should be used. A neutral (or zero degree) attachment angle would be defined as perpendicular to the left wall. A traditional aircraft with deployed wings will have a near zero launch angle. For stiffer materials wing designs, when a dihedral is required the launch angle will be positive (above the horizontal) and will help increase the packing efficiency.

The first series of simulations with the "user trace" option will use similar wing stiffness as in the Random Packing section (Chapter 4) and Potential Energy Packing section (Chapter 5), but with the user directing the packing path.

Simulation 1: Flexible Wing

The step-by-step simulation process is demonstrated and key packing improvements are discussed in this chapter through the means of a sequence of simulations. The first simulation starts at the center of a square enclosure. The first seven temporary points are seen in Figure 6.2.

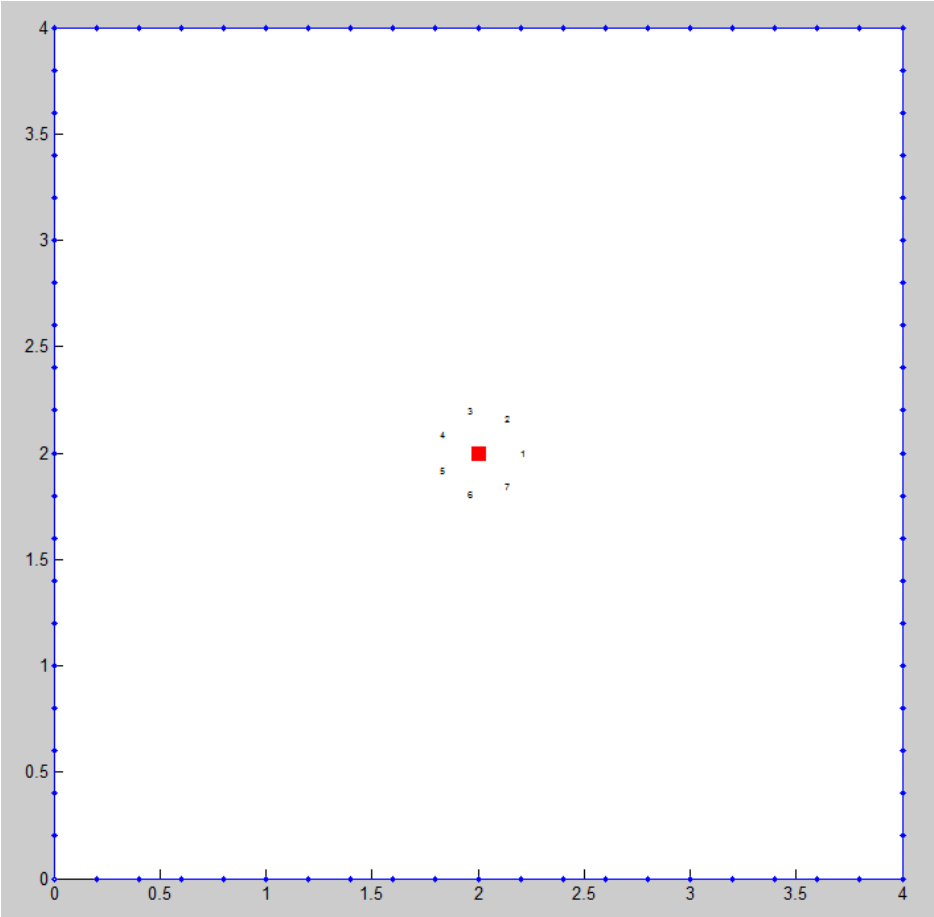

Figure 6.2 Shows the enclosure, start point, and the seven path options

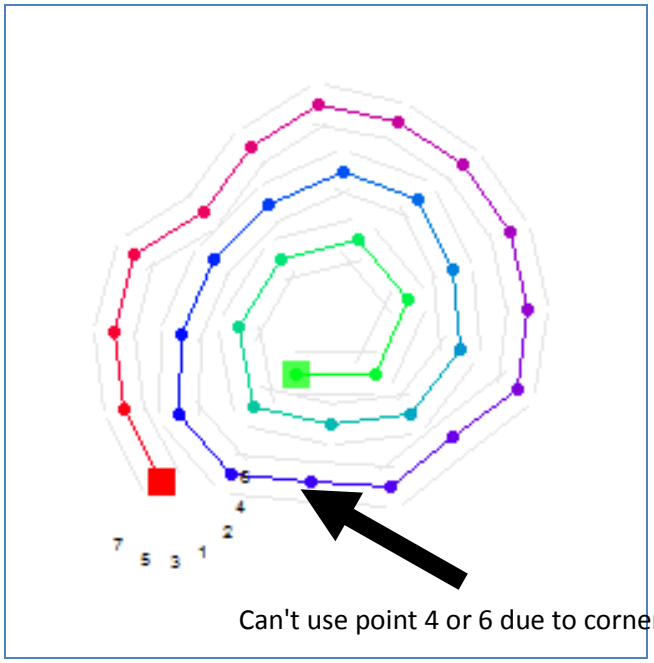

Figure 6.3 Shows a corner effect common to first few wraps

The first three complete "rolled" paths were more difficult then later rolls because the most recent point drawn might be inline or just behind a material point on the adjacent inner layer. This interaction caused a corner effect indicated with arrow in Figure 6.3. As the simulated wing wraps additional layers, the packed radius becomes larger. Therefore the user naturally selects path option number two more often without the need to reverse the simulation and try again. The goal is keeping a very tight pack configuration. Figure 6.3 shows path option six is invalid by inspection and path option two and four are possibilities. Path option four will stop the simulation or require a step back, therefore select path option two to continue the simulation. The larger radius leads to a smoother layering which makes valid path selection easier.

It was found that due to the left and right alternating index, if an invalid path is selected it's obvious to the user that the point was invalid because the path will be on the opposite side of the straight center line of path option one. This indication is used to keep the wing path close

to other packed wing layers. Another method to tightly wrap the wing is described next. If all the odd choices are invalid by user inspection, then chose path option one. The choice of path option one, despite being invalid, causes the next valid index to be selected and is the closest valid point every time. This is a useful and time saving strategy for the user. Figure 6.4 shows a close up of this strategy.

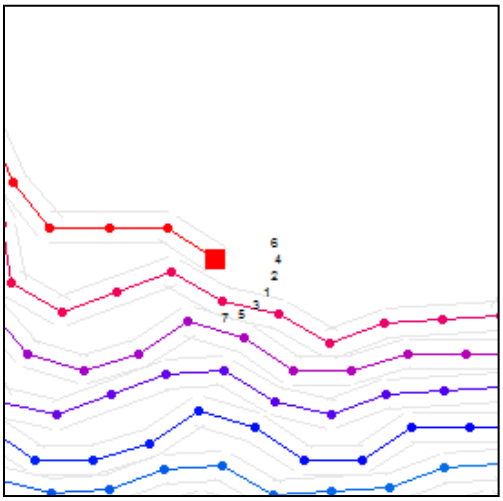

Figure 6.4 Choose path option one to get the tightest pack by default valid index

The simulation does not allow a material to flow and move after being partially packed. A plastic or rubber type of wing material would prevent the sliding and movement do to a high coefficient of friction. An ideal wing material could be coated with a friction reducer with almost no negative effects as is done in automobile airbags. This would help both packing and deployment. Future work could consider a dynamic adaptable packing simulation to improve packed wing length simulations.

When using the code, I found that a user will grow tired of using the backup option and therefore will tend to choose the less tightly packed path selection which leads to a more conservative, shorter wing length estimate.

When comparing the simulation rolled pack with a real physical wing roll pack the general shape is the same. It is also noted that the edge of a real wing has some distortion so that the inner wing cord does not perfectly match the wing edge packing profile. Thus, the real physical three dimensional wing is approximated when only viewing the side of the rolled wing pack Figure 6.5. The two-dimensional simulation similarly approximates the three-dimensional wing in two-dimensional space. The simulation and cross section view of a packed wing should be used to determine a general packing strategy and to approximate the total wing length to fit inside of an enclosure. The simulation could be thought of as a side view of a packed wing trailing edge or it could be an arbitrary cross section. The wing coordinates are less important than the general strategy, and will change every simulation. This is also true of every physical packing, no two will be identical.

Figure 6.5 Rolled orange wing

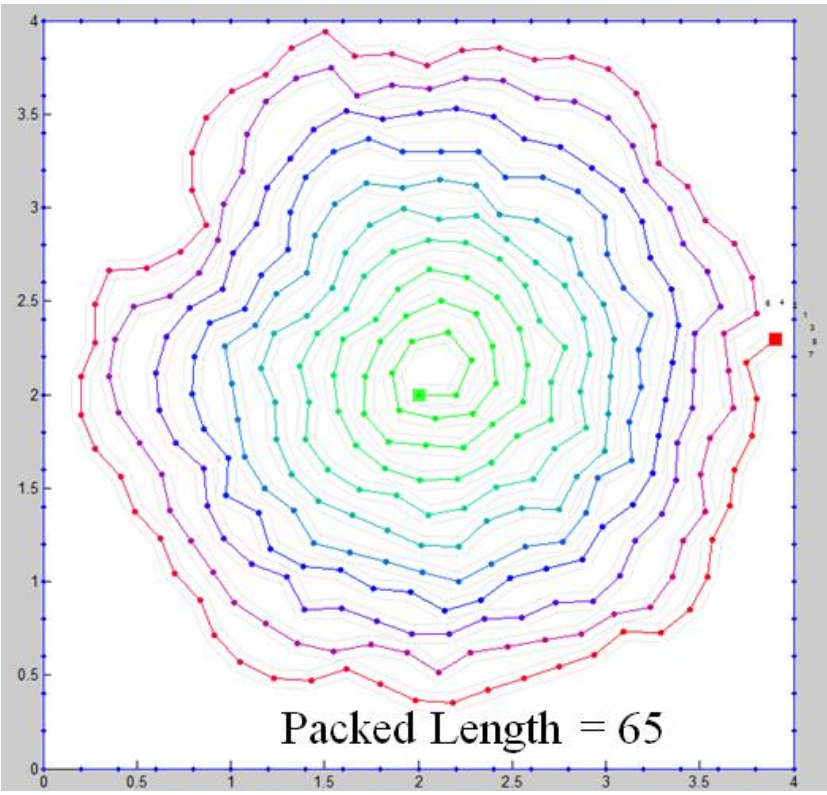

Figure 6.6 Complete wrap packing configuration

A partial learnCycRand vector is shown bellow.

0	1	6	6	6	4	4	6	2	4	4
2	4	4	2	2	2	4	4	1	4	1
4	2	2	2	2	4	1				

A partial PathCyc vector with first different path option shown below.

0	1	6	6	6	4	4	6	2	4	4
2	4	4	2	2	2	4	4	1	4	1
4	2	2	2	2	4	2				

At the 29th path option the two vectors differ, thus are not the same vector. These vectors are only saved if a particular packing configuration needs to be repotted. For the rest of

this thesis the vectors won't be shown. Instead both histograms will be shown, or only the histogram from pathCyc for simplicity and ease of reading. The desired input vector is pathCycRand. The actual valid path that is plotted is pathCyc. Many times an input vector consists of invalid path choices due to path crossing which is physically impossible or the path may leave the confinement area. In the case of an invalid path option the next temporary path index is selected when valid and causes the discrepancy between the two input vectors. Comparing Figure 6.7 and Figure 6.8 it can be seen that the user attempted to input pathOpt one many times, but these were invalid and the next index of two was valid thus getting the most common path section for that counter clock wise wrap packing configuration.

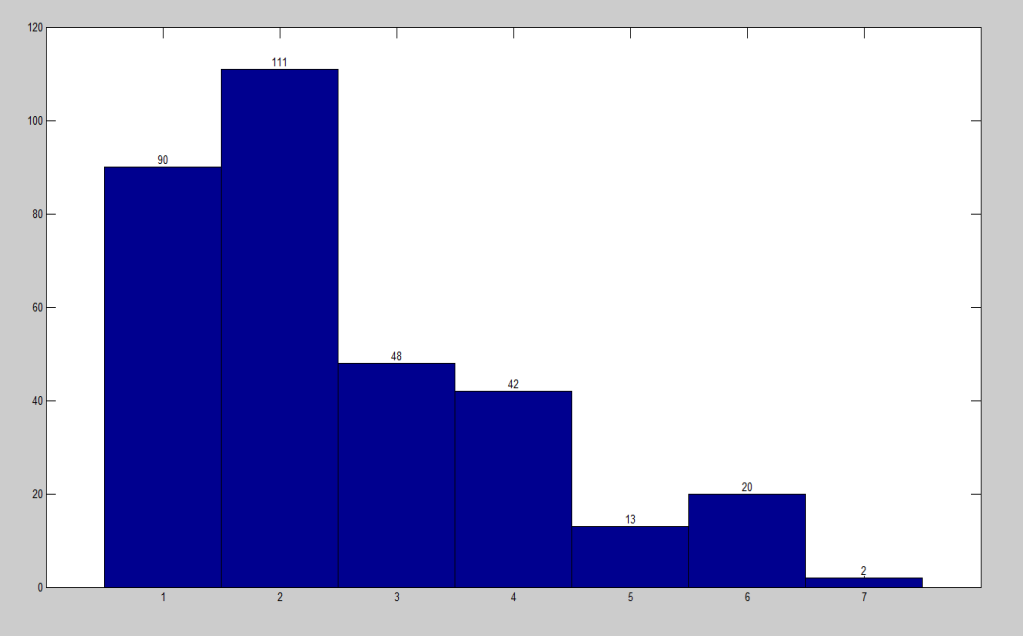

Figure 6.7 Histogram of learnCycRand vector

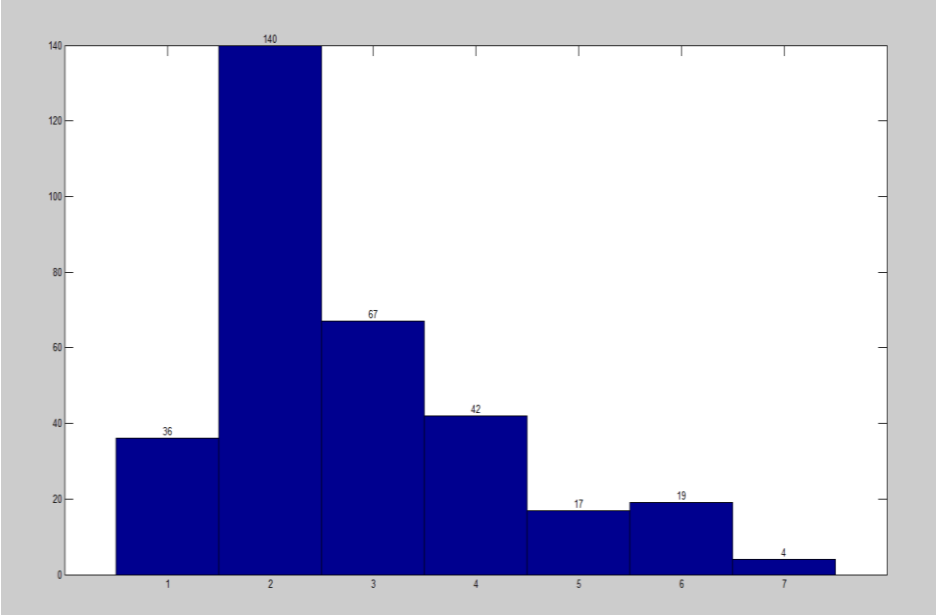

Figure 6.8 Histogram of pathCyc vector

Simulation 2: Stiff Wing

The second simulation will hold all variables the same as the first, except the limit angle is set at 100 degrees instead of 130 degrees. This smaller angle limit simulates a stiffer, less flexible wing. The user selected the typical wrap or roll pack similar to Simulation 1: Flexible Wing. In Figure 6.9, notice that the most important and influential section of packing is the first complete wrap of the rolled pack. Choosing the minimum bend radius may allow an intersection on the first complete wrap which formed an oval shape. The inner most wrap being oval caused the outer most (last) wrap to interfere with the enclosure sooner. This discovery leads to an important heuristic. If the deflated wing packs tight into a non-symmetric enclosure then the larger dimension (oval shape) of a first-wrap should be aligned with the larger region of the enclosure. This will allow additional material to be packed. A design strategy for a square enclosure could be to not use the tightest bend radius with a goal of having a more circular inner most wrap. Figure 6.9 shows that the initial inner most oval wrap will cause an early wall restriction (resulting in less efficient packing) because of the enclosure at the top of the plot is in

line with the major axis of the oval. A more circular inner region could be obtained by not using the most extreme curvature for the first five path options. The best packing of the spiral/wrap/roll pack with symmetric enclosure is to offset the center starting point.

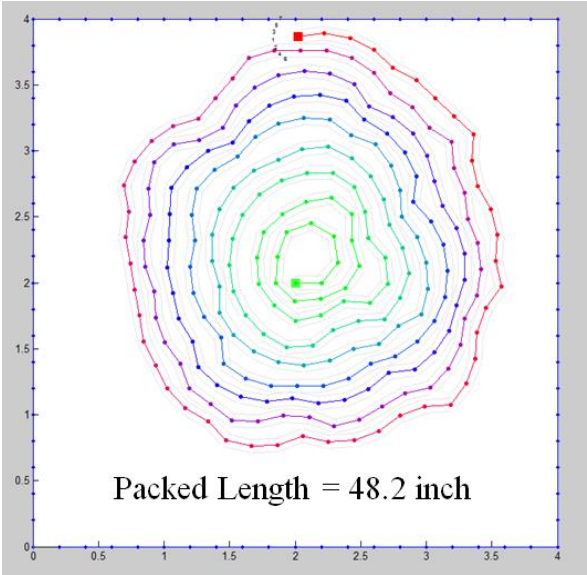

Figure 6.9 Completed stiff wing roll pack

Simulation 2 showed that reducing the stiffness angle while keeping the same number of path options effectively smoothed out each layer (by inspection) for the entire packing configuration. The smoothing is because the user-avoided selecting invalid points that were too close to the adjacent layer. Additionally, reducing the stiffness angle and keeping the same number of path options causes all candidate point to be centered closer to the desired path. Thus invalid path choice causes the next valid index with closer proximity to the path option of the desired invalid path.

Many times the backup option is used not because of the lack of valid points, but because a tight radius was used and led to a near-future point, two or three points away, being

invalid and stopping the packing simulation. Therefore the backup option once recognized to be needed will actually be needed several times, two to three times, to create the recent section.

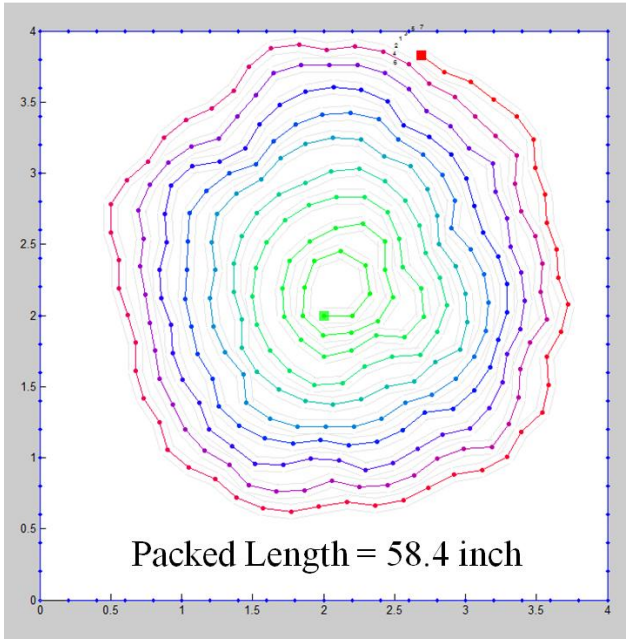

Figure 6.10 Completed Simulation 2 packed percentage of 36.5%

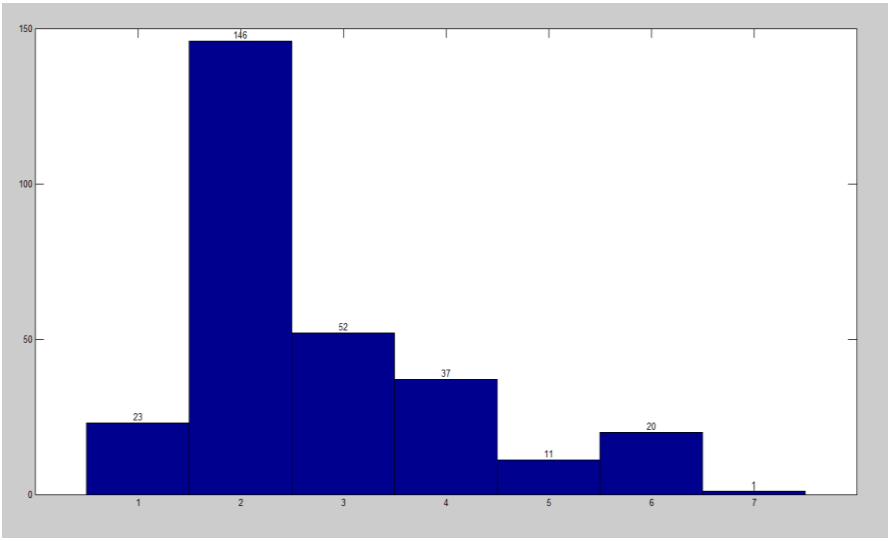

Figure 6.11 Histogram shows mostly path option number two selected for Simulation 2

The conclusion for a purely wrap/roll pack configuration is that the minimum bend radius is less important. The minimum bend radius is represented by path options six and seven. However, if packing the maximum wing length into an enclosure is the goal, minimum bend radius helps by storing a slightly larger amount of material at the inner radius and helps by allowing wrapping-direction reversal as in the next simulation, Simulation 3.

Simulation 3: Reversal Packing Direction

The packing could terminate as in Figure 6.10 or the user could be realize that more space is useable if the path can be reversed in the upper right hand corner and then wrapped clockwise. Figure 6.12 presents an illustration of this reversal in the upper right region.

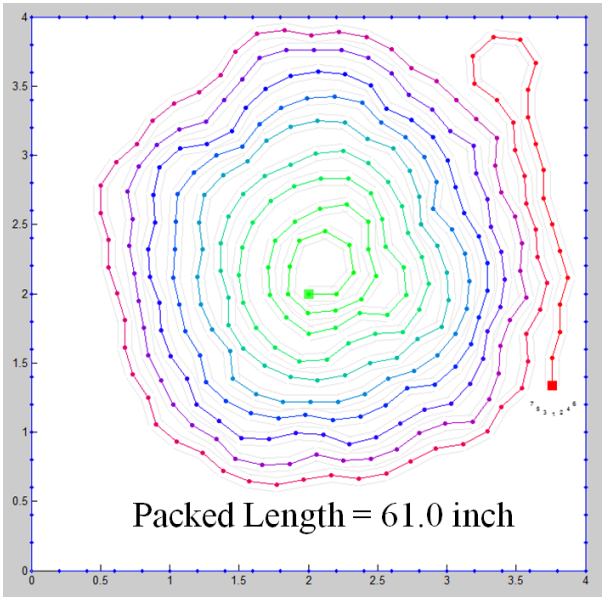

Figure 6.12 Roll pack and reversed direction

Also note, if a backup option is exercised and the reverse-direction wrap is desired then the new wrap should occur along the side with the most space. In the Figure 6.12 more space is available on the left or bottom due to the inner-most wrap being off center up and right. In

Figure 6.13, the packed length is increased from 61.0 inches to 80.6 inches using direction reversal to fill the unused space.

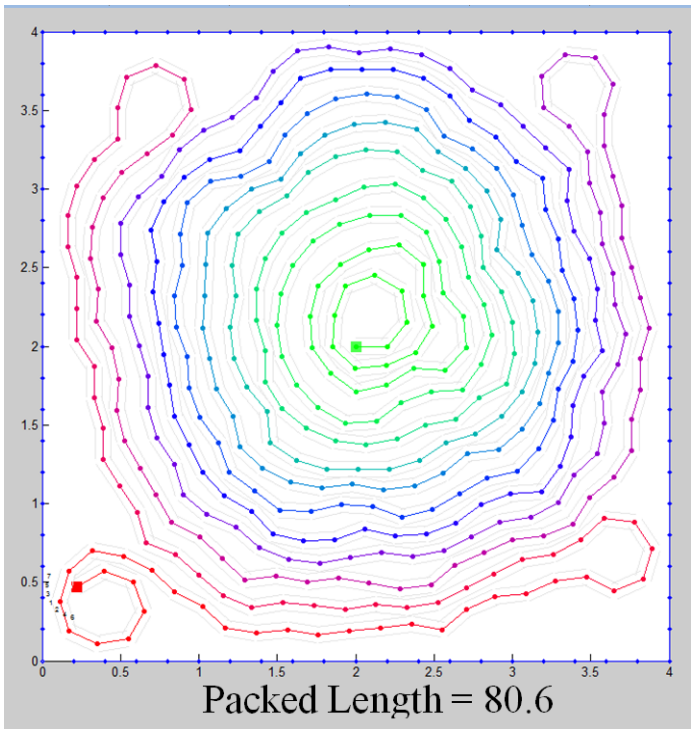

Figure 6.13 Roll pack with corners filled 50.375 % packed volume

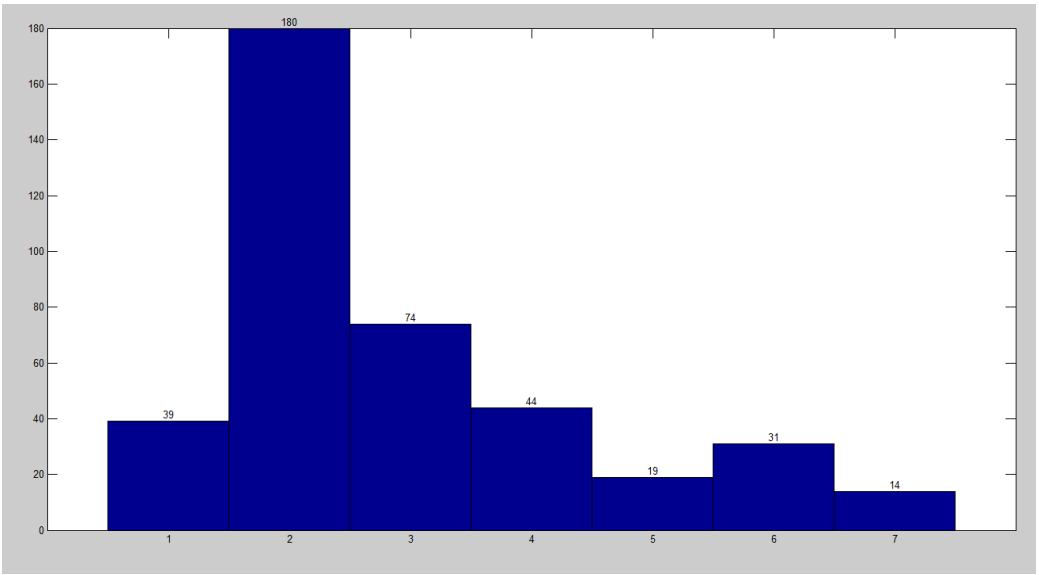

Figure 6.14 Full pack with corners filled; low left corner has loose wrap with other corners tight wrap

There are two cases to be aware of when packing. The first case encountered was a "free pack". Simulation 1 is an example, since the packing progressed with no direct wall influence as if packing in free space with no enclosure. The goal was to keep the wrap pack as tight as possible. The term "wrap pack" is used here with respect to the simulation, and the term "roll pack" is a physical description. The difference of reference frame leads to the two terms being interchangeable during this discussion. A physical wing is rolled during packing by the user. During a packing simulation the user wraps wing material around the center point. This is another difference between a static packing versus a dynamic packing where the material moves continually during packing.

The second case to be aware of when packing is the “constrained limited pack”, as the simulation packs more material into the free space the walls influence the available choices as well as near future choices. In Figure 6.12, the upper right hand corner the path was reversed instead of being terminated. Here the packing simulation switched to the second case, constrained pack. The user should have switched goals to using a loose pack that had used a maximum radius to match the enclosure. If there is significant space and the minimum fold radius is too large to make use of the immediate region, i.e. won't return to region during simulation, then a wave like path could further use the corner space. The lower left corner used the second goal of following the enclosure to allow as much material as possible into the confinement. Figure 6.13, used the free pack in upper left, upper right, and lower right corners, with the constrained limited pack goal in the lower left corner. This lead to a packed wing length of 80.6 inches with a packed percentage ratio of 50.375%

Figure 6.15 is a simulation with the last four corners with constrained limited pack method utilized along with a wave pattern instead of straight path. This lead to 3% more wing

length and 1.25% larger packed percentage. It is a small gain, but two more inches of wing could be fit into the enclosure.

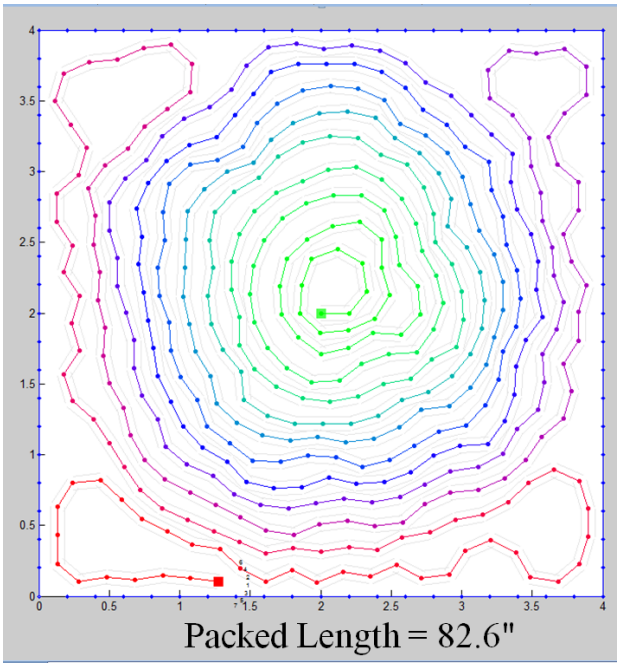

Figure 6.15 Rolled pack with four corners filled using second case goal, 51.625 % packed

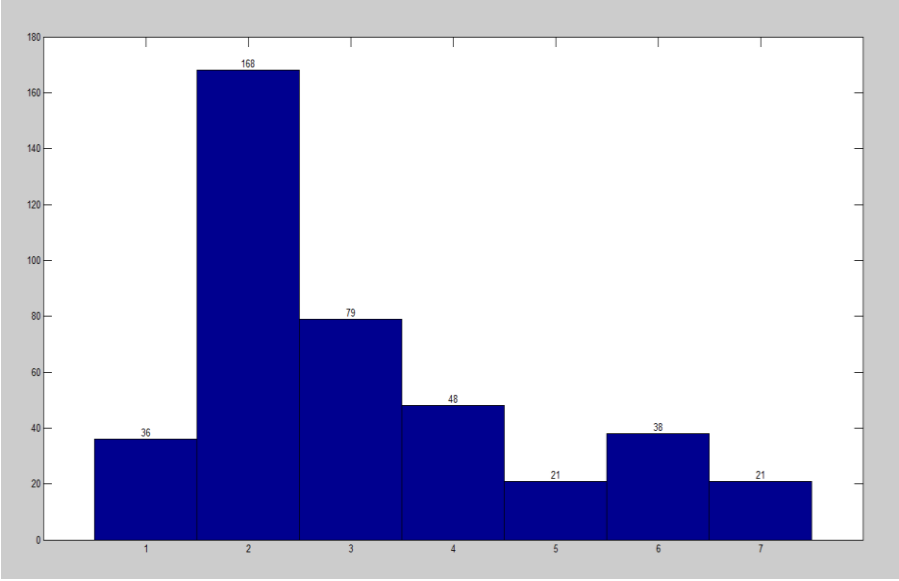

Figure 6.16 Utilized constrained pack method in corners along with wave pattern

If the user haphazardly chooses the tightest pack, eventually a corner problem will occur that causes an index to be chosen such that the path radically juts out away from the tight packing. In this case it is best to back up two or three choices and select a smooth and less tight packing path to avoid the radical outward path which will continue to build up worse and worse each additional material layer.

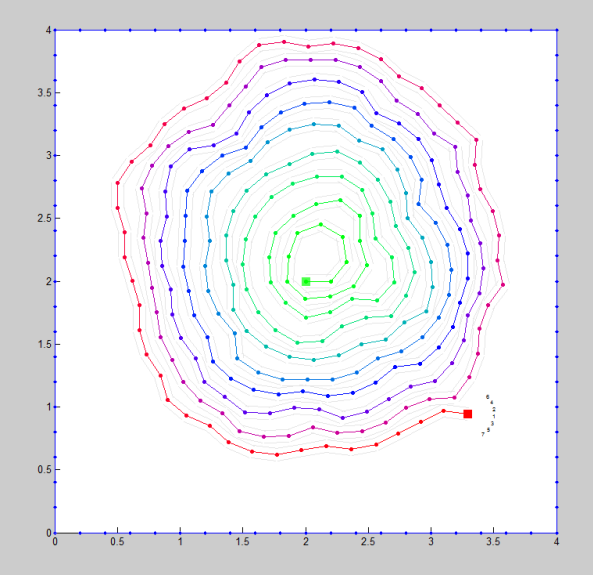

Figure 6.17 Radical index change due to corner effect, affects future wraps

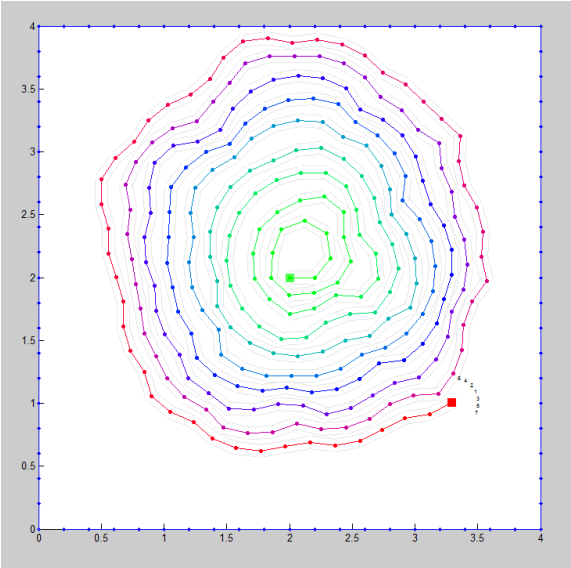

Figure 6.18 Less tight pack to allow a smoothing effect to help future wraps

Simulation 4: Offset Start/Attachment Point

The roll pack simulation should be centered about the center of a complete wrap of the smallest circular diameter. It is this inner wrap that should be centered not the material start point. The equation to determine the minimum diameter should be defined for a material folded 180 degrees. The following method was developed so that material properties are used to calculate the minimum diameter of the inner most circle.

Every deflated wing has a theoretical minimum inner circle, that doesn't include material thickness or the requirement to continue on, i.e. not connecting the ends of the circle. The theoretical minimum inner circle has connected ends forming a complete circle. It is based on the addTo length variable and the stiffangleDEG variable.

One wrap intersection is defined by a material simulation that results in the smallest inner circle with tightest wrap path selection. When the material can intersect itself with one wrap it should be called one wrap intersection OWI, otherwise it should be classified as normal spiral intersection, NSI. An OWI is oval or non-circular shape as shown in Figure 6.19. The Matlab

file minCircle.m can be used to match a simulated deflated wing to a physical model. Also the minimum circle diameter must be defined at the center thickness of the material. To measuring experimentally, just subtract one material thickness or two half thicknesses from a deflated wing that is folded back onto itself at an angle of 180 degrees and measure the largest diameter.

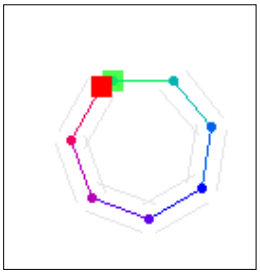

Figure 6.19 OWI simulation, variables same as Simulation 2: Stiff Wing,

In Figure 6.20, the material properties and the addTo length were constant while decreasing the stiffangleDEG from 180 to 20 degrees. The user must realize if the points intersect the current temporary point is invalid so the code chooses the next index and thus selects the outer path. This could miss lead the user to thinking that 60 degrees causes a normal spiral intersection instead of a One Wrap Intersection if they didn't notice the change in concavity. This may only be for a short addTo length ratio. The 20 degree case needed a larger enclosure due to the large MCD size.

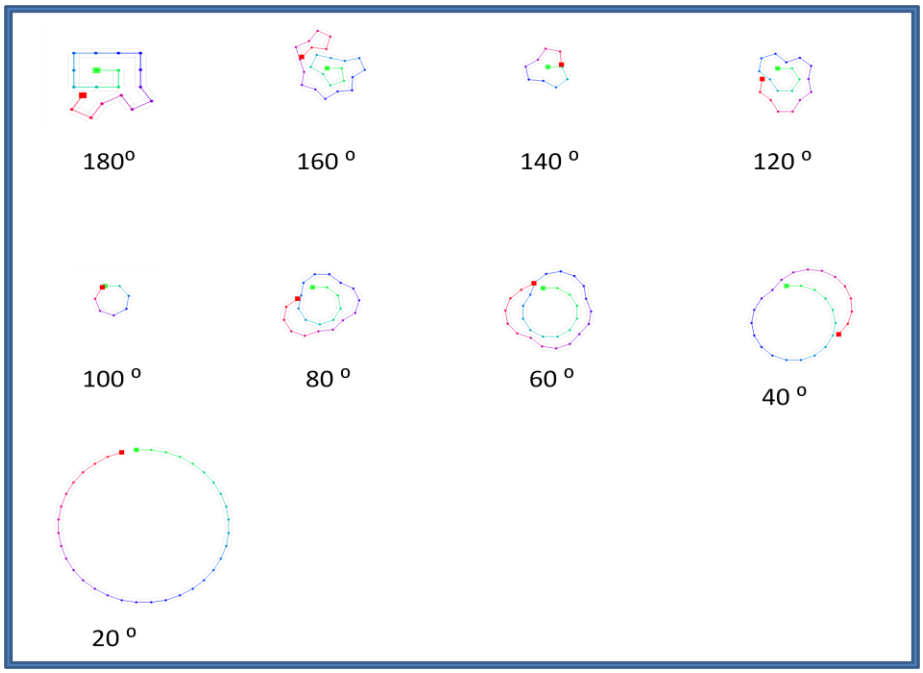

Figure 6.20 MCD plots for different max angle limits with addTo set at 0.2 inchs

A graph from One Wrap Intersection case study on addTo length and stiffAngDEG variables is show with trend lines in Figure 6.21 and Figure 6.22 below.

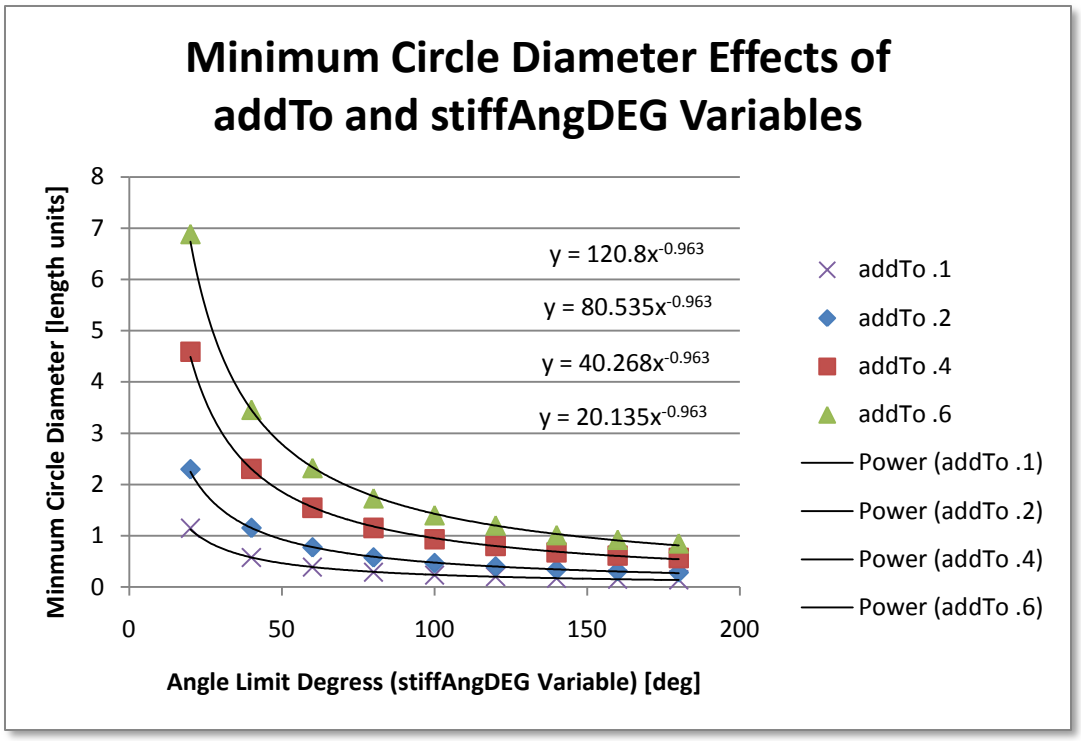

Figure 6.21 Minimum circle diameter of wing case study

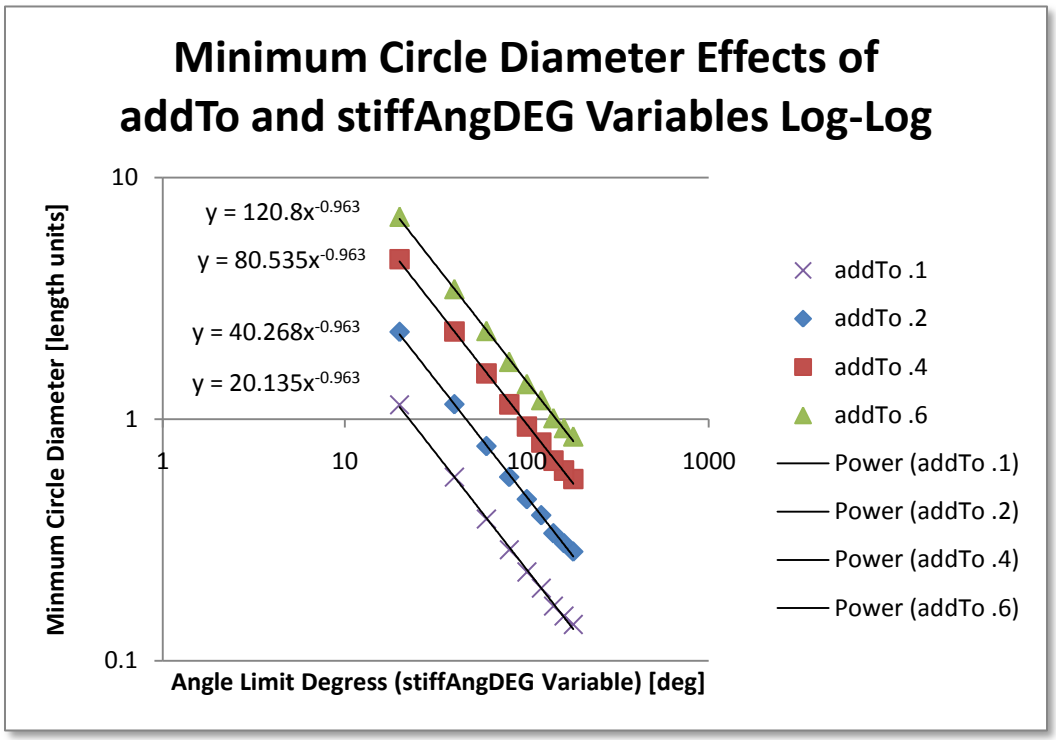

Figure 6.22 Minimum circle diameter of wing case study Log-Log plot

The equation for the theoretical Minimum Circle Diameter from power trend line is

$$MCD = L\left(\frac{604}{3}\right)\theta^{-.963}, \qquad \text{Equation 6.1}$$

with units of length that correspond to the same units. The variable L is the addTo simulation variable, and it is the length of the line segment that is added for each path option selected in the user trace simulation. θ is the simulation variable stiffAngDEG, and it is the extreme angular limit in units of degrees for the possible path for each line segment. The MCD percent difference is less than 5% for all cases with the highest error of 4.33% for 180 degree cases. The typical percent difference is 2%.

$$L = \frac{MCD}{\left(\frac{604}{3}\right)\theta^{-.963}} \qquad \text{Equation 6.2}$$

$$\theta = \mathrm{e}^{\left(\frac{\ln\left\{\frac{\mathrm{MCD}}{\left(\mathrm{L}\frac{604}{3}\right)}\right\}}{-.963}\right)} \qquad \text{Equation 6.3}$$

Equation 6.2 and Equation 6.3 are useful when a material's MCD has been experimentally measured and a packing simulation model is needed. The method for experimentally measuring MCD was described in Simulation 2: Stiff Wing. The MCD is closely related to the material fold length. This mathematical relationship is determined by first measuring the material fold length, MFD. The MFD is doubled to get a theoretical minimum circle circumference. MCD is mathematically determined from this circle circumference.

From Figure 6.10, a spiral pack should not be centered about the start point. A better solution would be to use the center of the MCD. A slightly better solution will offset the MCD's center by one material thickness from the first over lap that starts the second wrapping layer.

Note that the material thickness is the deflated wing's thickness. This thickness is at least twice as thick as a single piece of wing material and can have a larger average thickness due to internal baffles and wing construction.

During packing simulation from inner region to outer most region of a spiral pack, slight non-optimal path selections caused propagating fabric ripples to effect where the enclosed packing method should first be utilized. A OWI is shown in Figure 6.23. The desired input vector pathCycRand is 2,2,4,4,4,4, but the fourth path option 4 is invalid so the actual input vector pathCyc is 2,2,4,4,4,5.

Figure 6.23 Path option four is invalid so next index, 5, is chosen

When a four is input the code advances to the next index of five. This is where pathCyc vector differs from learnCycRand and indicates an OWI.

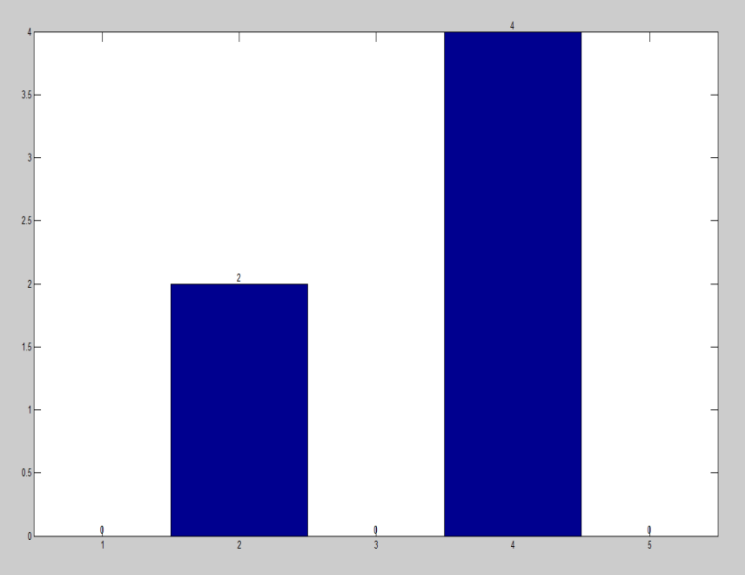

Figure 6.24 PathCycRand shows input vector

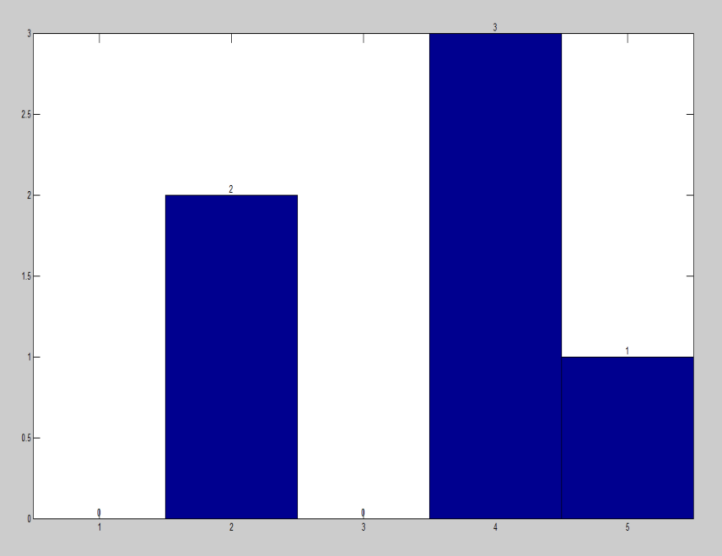

Figure 6.25 LearnCyc shows actual path vector

Simulation 5: MCD Improves Packed Length

The MCD Equation 6.1 with addTo of 0.2 inches and path option of seven gives MCD=.4775 inches. Therefore the starting point should be shifted half the MCD, 0.2387, from the center (2.0, 2.0) of the box enclosed region, so the start point will be at (1.7616, 2.0).

Simulation 5 shows that MCD Improves packed length and shows the improvement of using a better starting point. Further length improvements can be made by starting with path option number seven or using startAngDEG set at (360/7)*6 for a CCW wrap direction. The key is to align the center of the MCD and align the starting path angle with a line segment on the MCD.

Another possible combination would have been to use the first path option two with the same starting coordinates of (1.7616, 2.0) but to wrap in a clock wise direction.

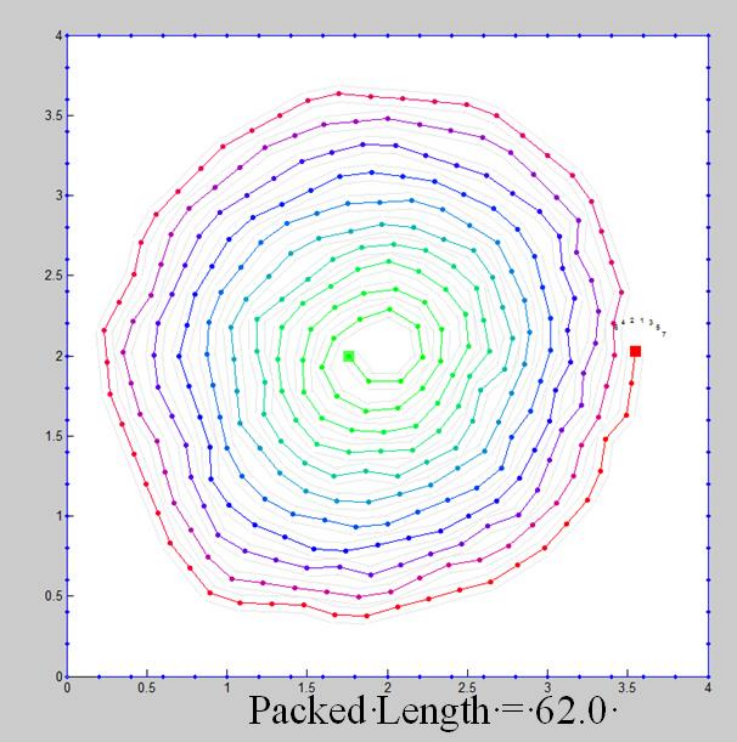

Figure 6.26 Centered at (1.7646, 2.0) using simple MCD method

The optimum center needs to be offset to include the radius of MCD, alignment of first segment on MCD, and wing thickness.

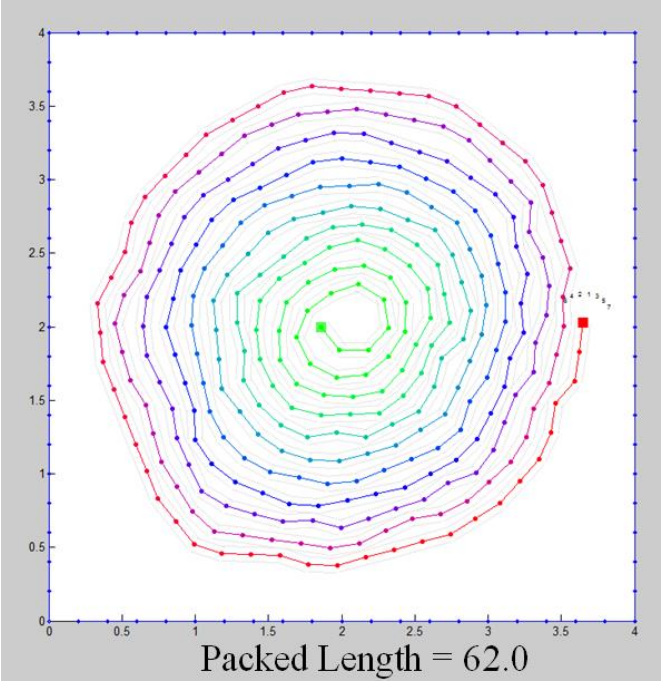

Figure 6.27 Centered (1.8613,2.0) shifted left half of MCD and shifted right one thickness

Simulation 5 shifted the start point left half of MCD and then shift right one thickness. The right one thickness shift accounts for the first point that occurs after the first complete wrap. The starting x coordinate is 2.0-.4775/2+0.1 for a coordinate of 1.8613. I used the MCD Equation 6.1 instead of the actual determined MCD because it is more common to not have the actual MCD during the initial design process. There is only a maximum 5% difference using the theoretical trend fit MCD Equation 6.1.

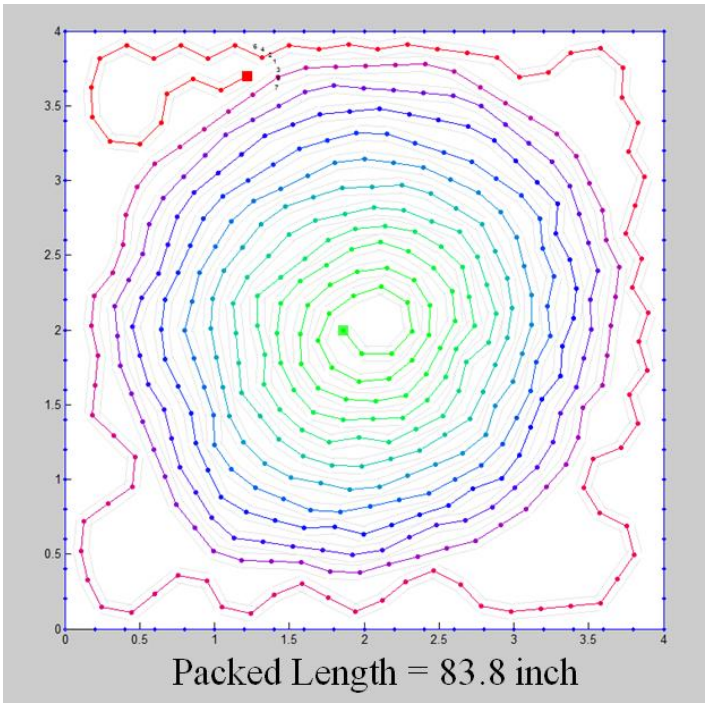

Figure 6.28 MCD and thickness shift with constrained limited packing case goal in corner, packed percentage 52.375%

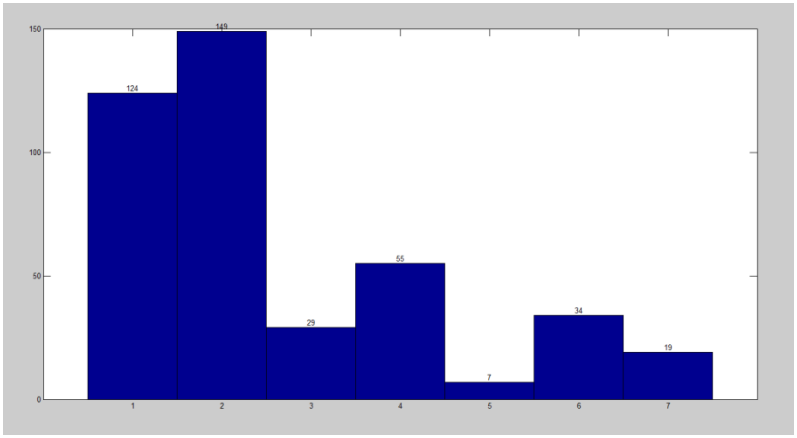

Figure 6.29 Simulation 5 histogram

Using the MCD, material thickness and constrained limited pack case in the corners resulted in the best packing length of 83.8 inches and a packed percentage ratio of 52.375% with an angle limit of 100 degrees.

Simulation 6: Z-Packing

The second common method of packing an inflatable wing is the z-packing configuration as shown in Figure 6.30 below. The z-packing and several variations are covered in Simulation 6.

Figure 6.30 Z-packing configuration

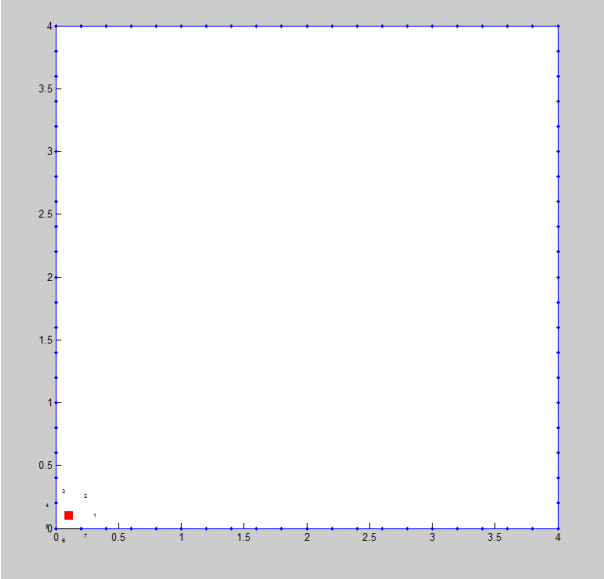

Figure 6.31 OrangeLowLeft.txt start point for z-pack

Figure 6.31 shows the starting point of (0.1,0.1) and is used throughout Simulation 6. The first z-packing configuration is simply using a 180 degree fold at each wall to change direction. The wing is built up along the bottom of the confinement region as show in Figure 6.32.

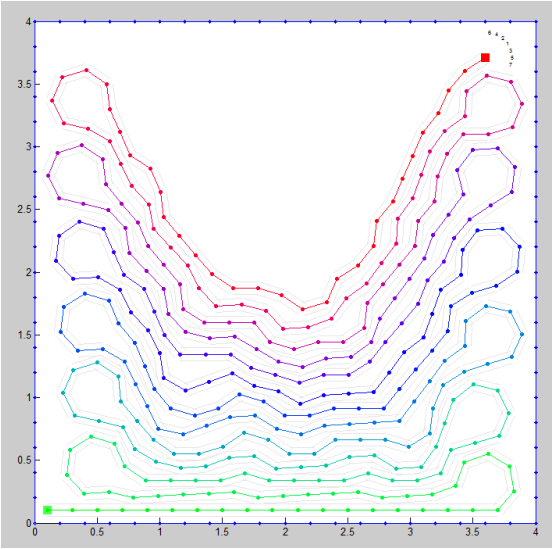

Figure 6.32 Z-packing configuration has to be modified to

Figure 6.33 shows the z-packing configuration pattern continuing into the remaining opening region.

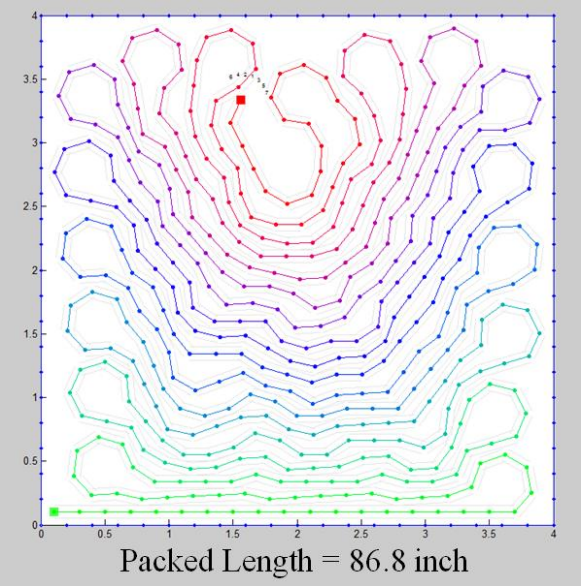

Figure 6.33 Shows inefficient packing with many minimum bend radiuses used

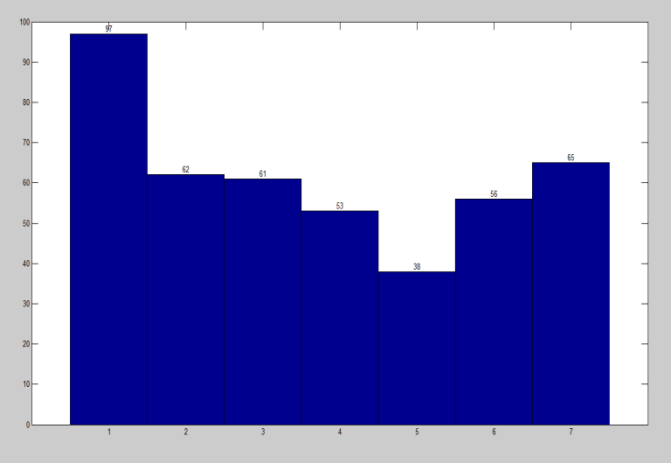

Figure 6.34 Z-pack histogram shows even amount of each path option

Figure 6.33 resulted in a packed length 86.8 inches and a packed percentage ratio of 54.25%. This is a slight improvement over the MCD optimized wrapped packing configuration. The histogram of Figure 6.34 shows a more even distribution of path option selections. Simulation 6 was retried with a wrap pack of constrained limited pack case to complete the remaining region of Figure 6.35, this lead to a wing length of 91.6 inches and a packed percentage ratio of 57.25%.

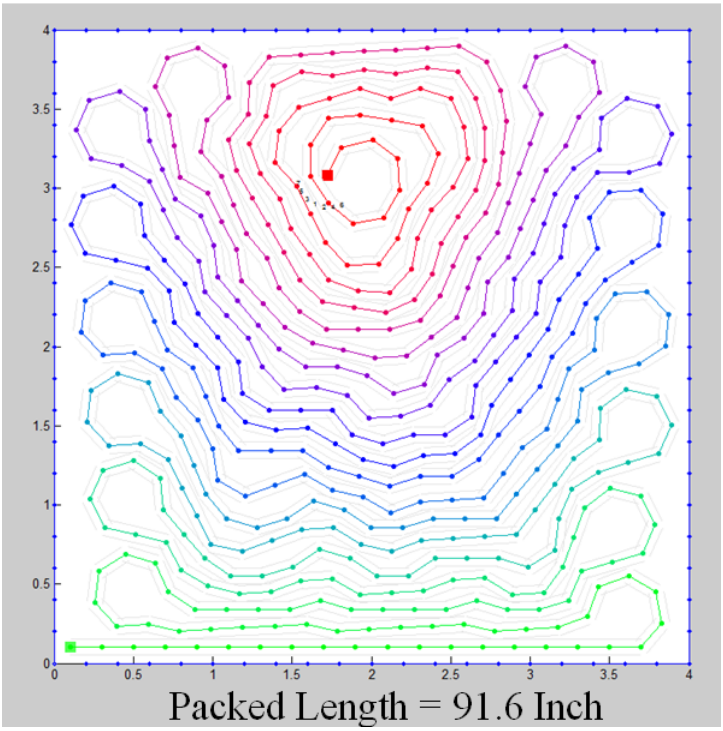

Figure 6.35 Z-pack with roll pack at end of simulation

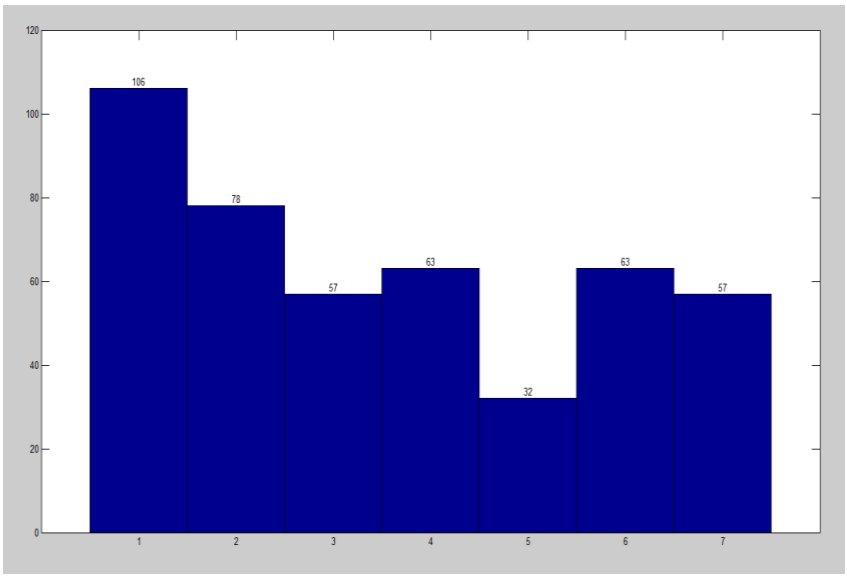

Figure 6.36 Z-pack with secondary confined enclosure wrap pack histogram

A staggered z-packing configuration was simulated but was less efficient that the first z-pack simulation. The staggered z-pack length was 82 inches and packed percentage ratio was

51.25%. This staggered packing simulation would become more efficient if the wall length to MCD ratio was increased.

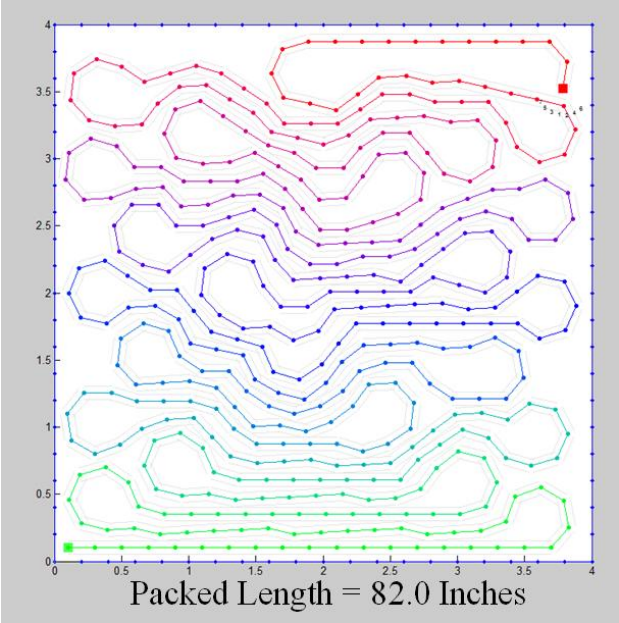

Figure 6.37 Staggering inefficient packing regions

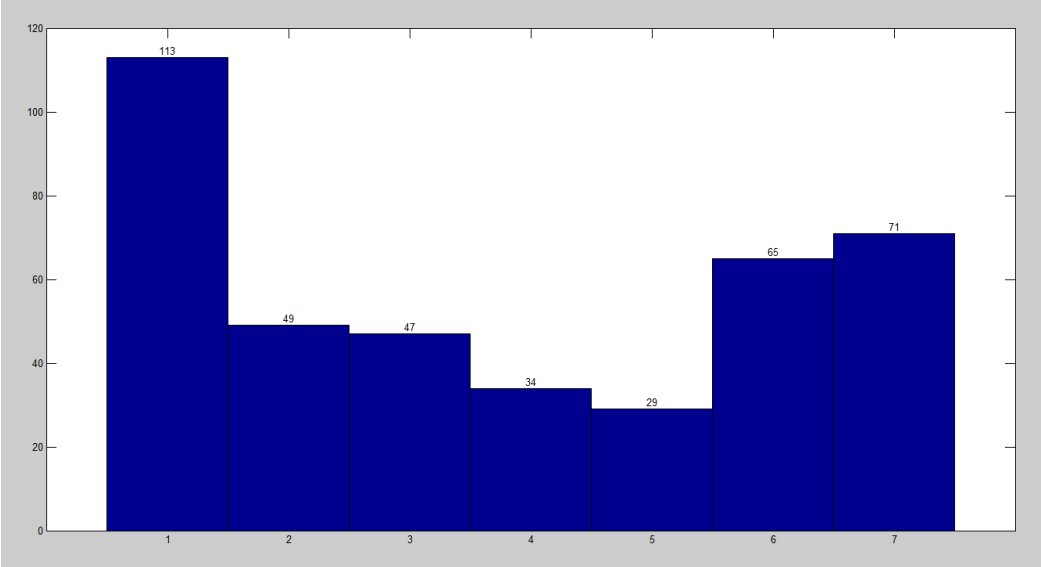

Figure 6.38 Staggered inefficient wrap

Simulation 7: Constrained Limited Wrap Pack

The second packing strategy, constrained limited pack method for wrap pack using the same material variables and enclosure from Simulation 2 was run for Simulation 7 and resulted in the longest wing packed, 109.6 inch, and highest packed percentage ratio, 68.5% shown in Figure 6.39. The goal is to follow the enclosure instead of trying to tightly wrap around a central point.

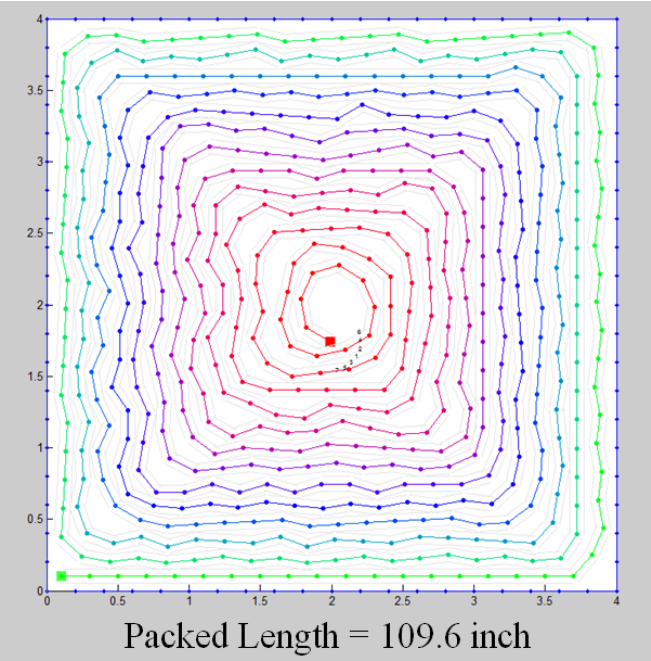

Figure 6.39 Best box packing strategy

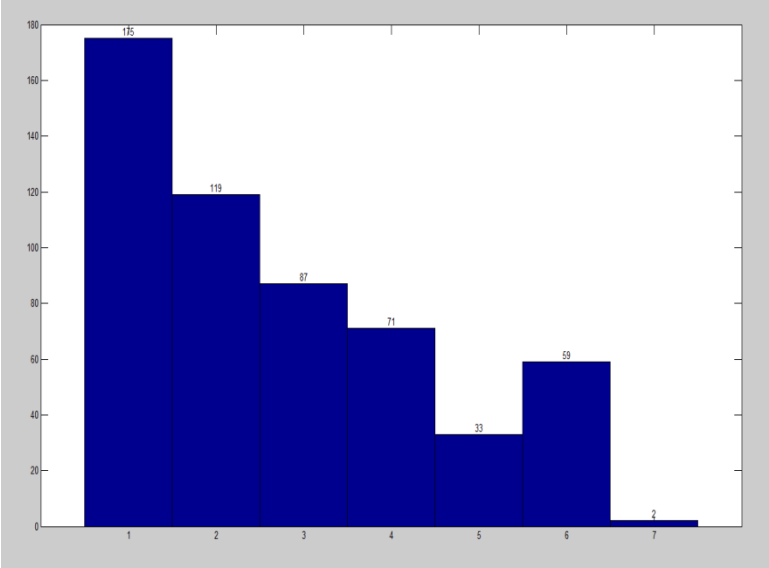

Figure 6.40 Best box packing strategy histogram

The strategy was to follow the wall as close as possible. This minimized wasted space. During Simulation 7: Constrained Limited Wrap Pack, packing from the outer to inner region there were wall confinement effects propagating through each wrap layer that lead to a packed configuration that does not reach the MCD. By achieving the longest pack inside of the standard box, this indicates an even better method than the MCD centered packing strategy.

It must be mentioned that due to symmetry, I could have started packing along the left vertical wall and ended up with a similar result, it would be flipped about a diagonal line from (0,0) to (4,4). Since the simulation is a tool to determine the final packing configuration it does not matter if the start or end point is the true attachment point. It only matters that the attachment point actually corresponds to the aircraft's design limitations.

Simulation 8: Circular Enclosure

A circular enclosure with an enclosed area of 15.98 square inches was modeled with a goal of having the same 16-square-inches area as the four-inch by-four inch box enclosure. The circular enclosure has a radius of 2.2568 inches and is centered at (2.2568,2.2568). The circular

enclosure is approximated by many straight lines. The wrap simulation used the MCD and thickness shift from the center of the enclosure. The starting point's x-coordinate was at 2.2568-0.2387+0.1=2.1181 inches and a y-coordinate of 2.2568 inches. The input vector was the same as for the box enclosure simulation with MCD shift and thickness shift. The input vector was then continued with the user trace. The wing packing simulation resulted in a tightly packed volume with wing length of 94.8 inches and a packed percentage of 59.3%.

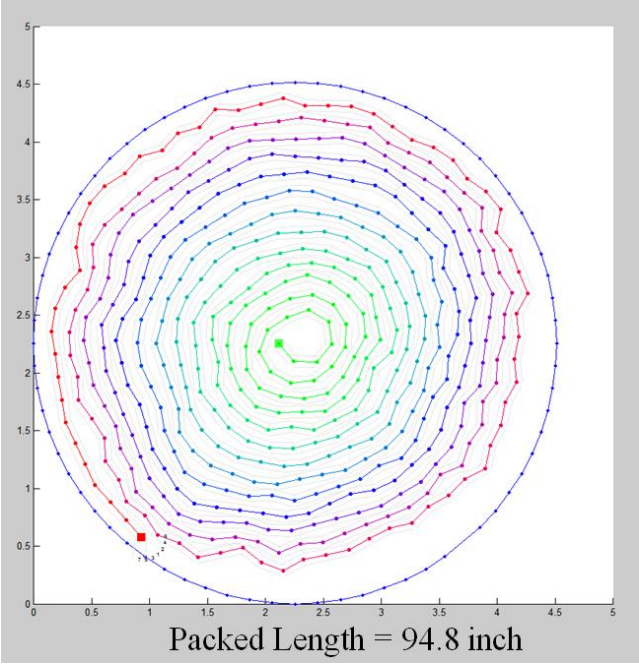

Figure 6.41 Circular enclosure

The corner effect causes a jut out from the closely packed wrap and produces a shorter packed wing. For example, a path choice of two is a very tight pack, but if chosen and the point is invalid the next index is three. The order from tightest wrap to loosest wrap is two, one, and three. The code automatically chooses path option three instead of the path option one which would have been the tightest pack. This leads to the wrap pack simulation result not being the longest wing inside of an enclosure, thus a conservative wing length estimate. When packing a physical wing the roll pack is a useful packing configuration do to the simplicity.

Packed percentage shows how well a packing configuration fits into an enclosure. Packed percentage should only be compared for different wing designs in the same enclosure. The circular enclosure simulation packed percentage should not be compared against the box enclosure packed percentage. The input text files used were orangeCir16.txt and circle16.txt.

Simulation 9: Fuselage in Tube Quarter Symmetry

The purpose of Simulation 9 is to show a common tube packed UAV situation. The defined enclosure is limited by the inner wall of the tube and the out wall of a cylinder shaped fuselage. Quarter symmetry was used to shorten the simulation time. However, after simulations were run it was discovered that symmetry should not be used because this limits packing options. The enclosure is symmetric however many packing configurations are not symmetric with respect to the enclosure. The quarter symmetry is still a useful tool for studying packing trends.

The start point was chosen to be at (4.01, 0.01). The simulation represents the rear view of a UAV fuselage (small arc) and the inside of a launch tube (large arc). The start point is at a traditional wing root location. The attachment angle variable can be adjusted to rotate the initial path option to a value more reasonable for an irregular shaped enclosure or for wings with a dihedral angle.

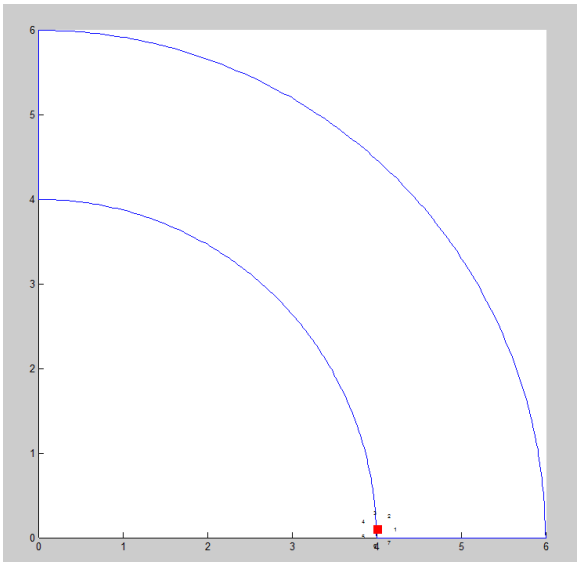

Figure 6.42 Start point for fuselage simulation quarter symmetry

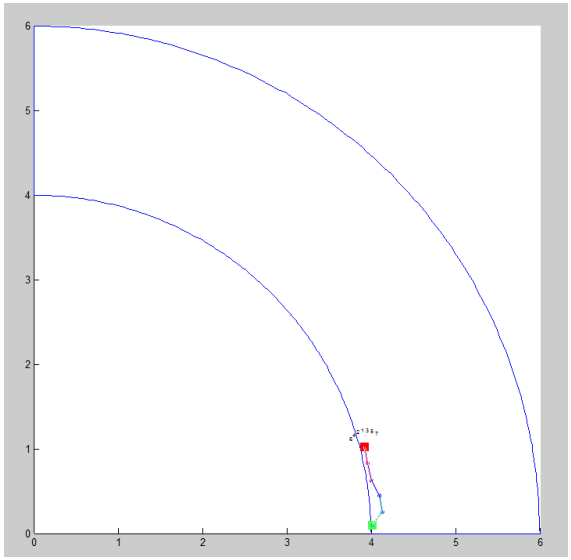

Figure 6.43 Used path two with zero degree start angel rotation

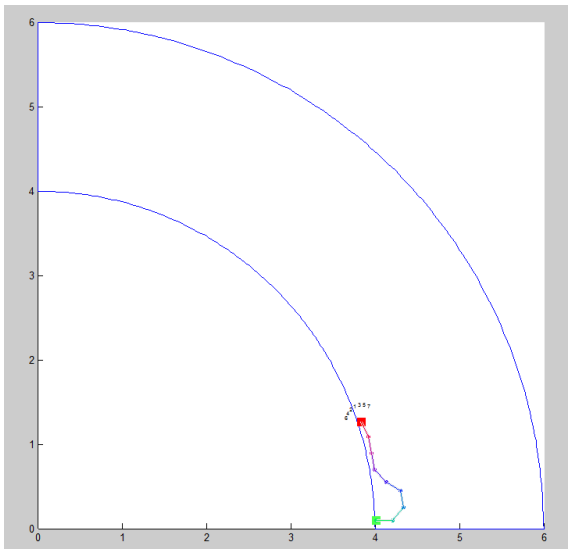

Figure 6.44 Used path option one with zero degree start angle rotation

The attachment method has an affect on the model. For example, The BIGBLUE V UAV with orange ILC Dover wings used wing roots that did influence the attachment angle. Therefore to model that type of wing, the attachment angle should be matched to the physical UAV.

The initial path option choices are spread around an entire 360 degrees with seven options, thus the start angle was corrected. The start angle used 100 degrees divided by seven path options which used a CCW shift of 14.3 degrees multiplied by three to have a start angle of 42.9 degrees. By rotating 42.9 degrees this allows for the theoretical minimum bend radius. In the simulation, the rotated start angle allows the simulation to follow the wall from the beginning, thus avoiding the first line segment protruding into the packing region. The simulation again uses path option of seven, addTo length of 0.2, and a stiffLimDEG of 100 degrees.

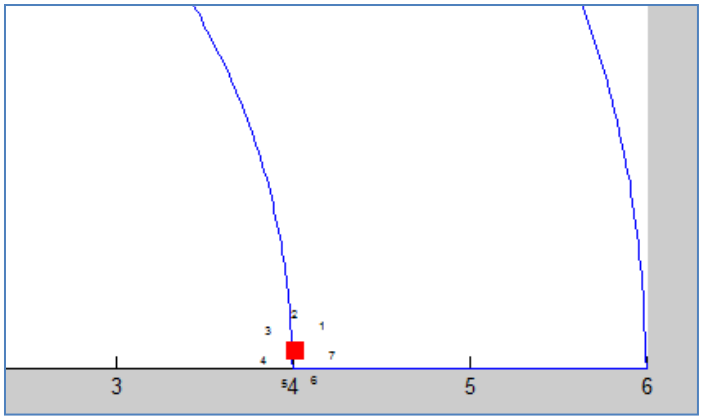

Figure 6.45 Start angle rotated CCW 42.9 degrees

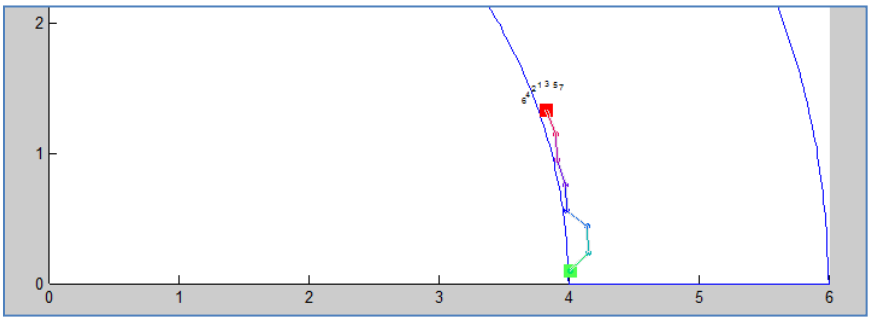

Figure 6.46 Start of packing simulation showing the minimum bend radius

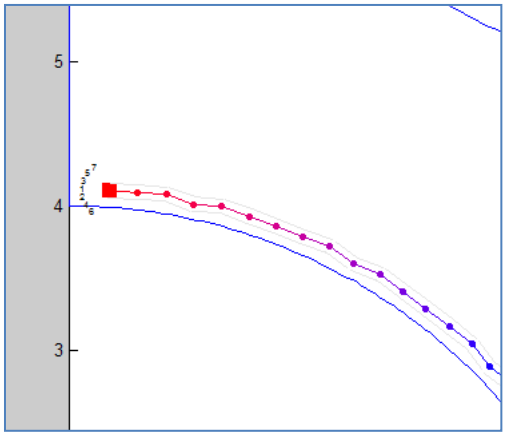

Figure 6.47 Last point before corner

Figure 6.47 shows the last point before a corner. The best method is to use the constrained packing region method to stay along the outer wall which is path option five. Path

option three leads to no future valid points and path option seven wastes space for the future adjacent layer.

The simulation packing configurations almost completely fills the enclosure. It must be realized that these body in tube packing configuration must be packed before inserting into tube so an outside-inward wrap pack may not be practical for physical packing. A z-pack may be easier to pack prior to insertion. If the tube has a hinge or is made up of two halves then some packing configurations may be easier to insert.

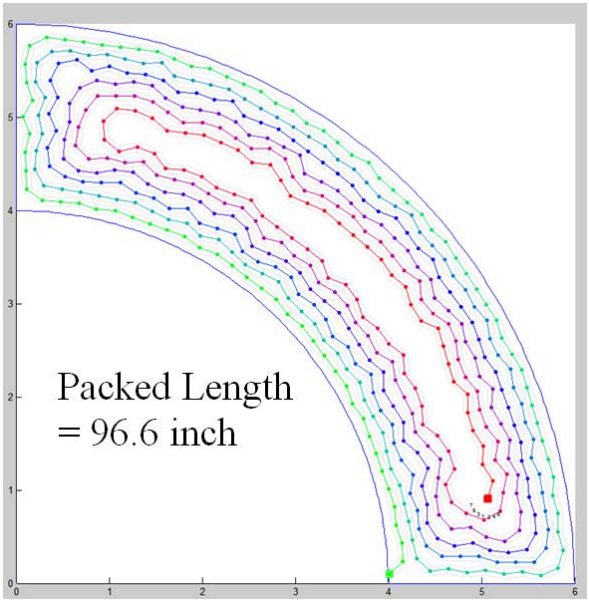

Figure 6.48 61.6% packed, enclosure area is 15.7 inches^2

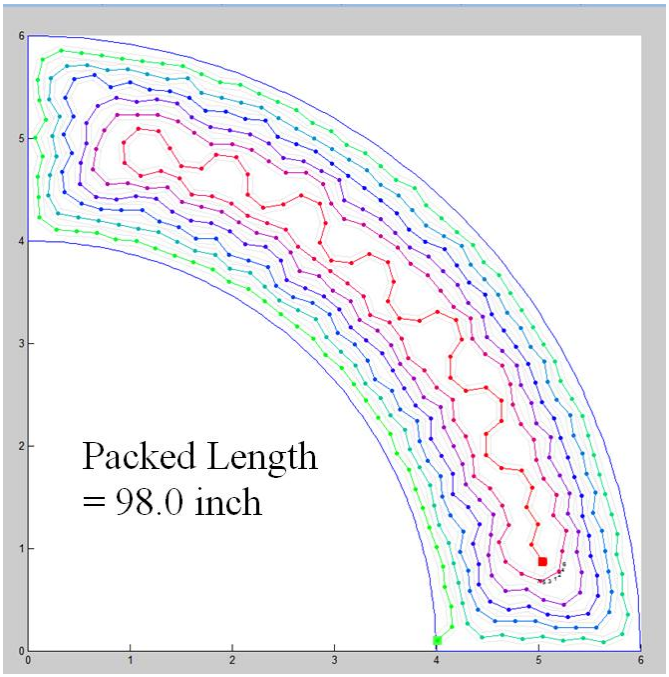

Figure 6.49 62.5% packed, utilized wave pack for inner most region

The simulation resulted in long packed length, but by inspection the inner most region could be packed better. A slight improvement in length is gained by using a wave-pack on the last wrap. This added 1.4 inches of wing material for a 1.45% increase in wing packed length. Using the enclosure's symmetry reduces simulation time, but does not allow for the best packing configurations. By reducing the area of the enclosure, this caused more 180 degree fold backs per given wrap. A full simulation with fuselage, two wings, and enclosure is not possible because only one wing can be simulated at a time. The best packing for a full simulation of Figure 6.49 is theorized to be both wings simultaneously wrapping around the fuselage which would result in adjacent layers alternating between each wing material, similar to a string trimmer head used for lawn care. The quarter symmetry enclosure was defined by two quarter circles with centers at the origin and radiuses of four and six inches. The code needs the segments of each enclosure line to be in continuous order. The start point for the inner radius was (4,0) to the end of (0,4). The vertical line was from (0,4.1) to (0,5.9). The outer radius

started at (0,6) and ended at (6,0). The last line segment was from (5.9,0) to (4.1,0). An enclosure of any closed polygon can be modeled with this two dimensional packing simulation code. The input text files used were bodyINtubeQuaterMaterialSmall.txt and bodyINtubeQuaterMaterial.txt.

A more refined packing could be simulated with a shorter addTo length and more path options. This is similar to the finite element analysis, FEA, strategy of refining a model's mesh. However with the "user trace" approach, the significant additional time is not worth the trade off.

Simulation 10: A Quick Wing Length Estimation

A quick "back of the envelope" calculation can be made if the minimum fold thickness and FRL are significantly small and neglected. The height, h, of the enclosure is divided by the thickness, t, of the deflated wing to determine the number of layers that will stack into an enclosure. The number of layers is multiplied by the length of the enclosure to estimate the theoretical maximum wing length inside of the enclosure.

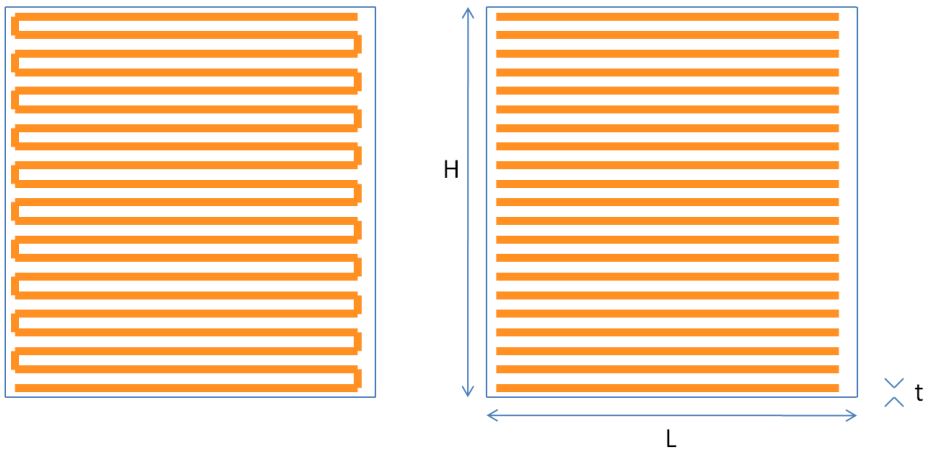

Figure 6.50 Quick wing length estimation

$$Wing\ Length = \frac{HL}{t} = \frac{A}{t}$$ Equation 6.4

Equation 6.4 works with any enclosure area, A. However it over estimates the wing length, but does provide a simple method to determine an upper bound. The minimum fold thickness, r, can be measured for a short wing segment as was part of the empirical packing study. The minimum fold thickness overlaps by one wing thickness as shown in Figure 6.51 Quick wing estimation with minium fold thickness

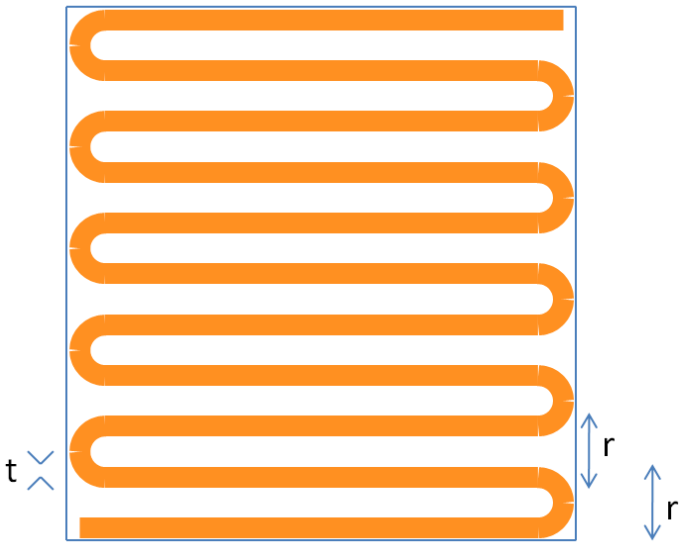

Figure 6.51 Quick wing estimation with minium fold thickness

Equation 6.5 utilizes the minimum fold thickness, r, to determine the number of layers that stack into the height of the enclosure. This provides a conservative lower bound for the wing length inside of the enclosure.

$$Wing\ Length = \frac{HL}{r} = \frac{A}{r}$$ Equation 6.5

Equation 6.6 yields a better approximation between the upper and lower equations by utilizing the wing thickness and the minimum fold thickness.

$$Wing\ Length = \frac{HL}{(r-t)} = \frac{A}{(r-t)}$$ Equation 6.6

Substituting in orange wing material properties with a thickness of 0.1" and a minimum fold thickness of 0.3" with enclosure area of 16 inch^2 gives a lower bond of 53", an upper bound of 160", and a conservative 80" estimate which corresponds well to the previous simulations in Chapter 6.

Chapter 7

7.1 Long Term Packing Study

Inflatable wing technology's primary benefit is the ability to pack into a small enclosure for transport. Certain missions could require a UAV to be packed for longer periods, even years before deployment. The main goal of this long term packing study was to determine if creases resulting from long-term storage caused loss of material strength. Other unforeseen long-duration pack problems were also identified.

Five wing materials, (including those tested previously [16]) were packed for 538 consecutive days. The materials were BBV orange wing, BBIII vectran wing, ILC Dover yellow-D, Seattle Fabrics red and blue. The five fabrics tested will be referred to by their color for the remainder of Chapter 7. The material thicknesses were measured with a Teclock Corporation SI-112. It uses spring force to apply a consistent clamp which gives accurate thickness measurements as shown in Table 7.1. Table 7.1 is a summary of the fabrics, their manufacture, and their general descriptions. The yellow material was part of Phase I testing only.

Table 7.1 Material thicknesses

Name	Thickness [in]	Mfg.	Notes
Orange	0.0165	ILC Dover	BIG BLUE V
Blue	0.0140	Seattle Fabrics	Single sidded coating
Vectran	0.0130	ILC Dover	BIG BLUE III
Yellow-D	0.0120	ILC Dover	Coating on both Sides
Yellow	0.0110	Seattle Fabrics	Single sidded coating
Red	0.0100	Seattle Fabrics	Single sidded coating

For each of the five materials, samples were cut with three orientations: warp, fill, and 45 degrees as seen in Figure 7.1. Two temperatures, 25^{o}C and -70^{o}C, three orientations, five materials with two samples of each were tested for a total of 60 tensile tests. Before packing, each material thickness was measured and corresponding thickness washers were obtained to

control the gap between precision-ground steel plates as seen in Figure 7.2. The five gaps were set to be twice the material thickness producing a strong crease. This test crease would be more severe than an inflatable wing would experience for most long term packing situations. All materials had orthogonal material properties, which were aligned with the warp and fill directions. Each material was creased across the warp, fill, and 45-degree directions. The clamping force was applied with several c-clamps Figure 7.3. The samples were stored on June 16, 2009.

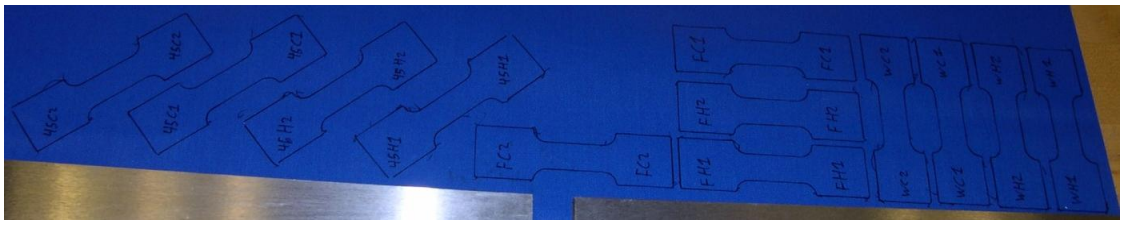

Figure 7.1 45-degree direction (left), fill direction (center), warp direction (right)

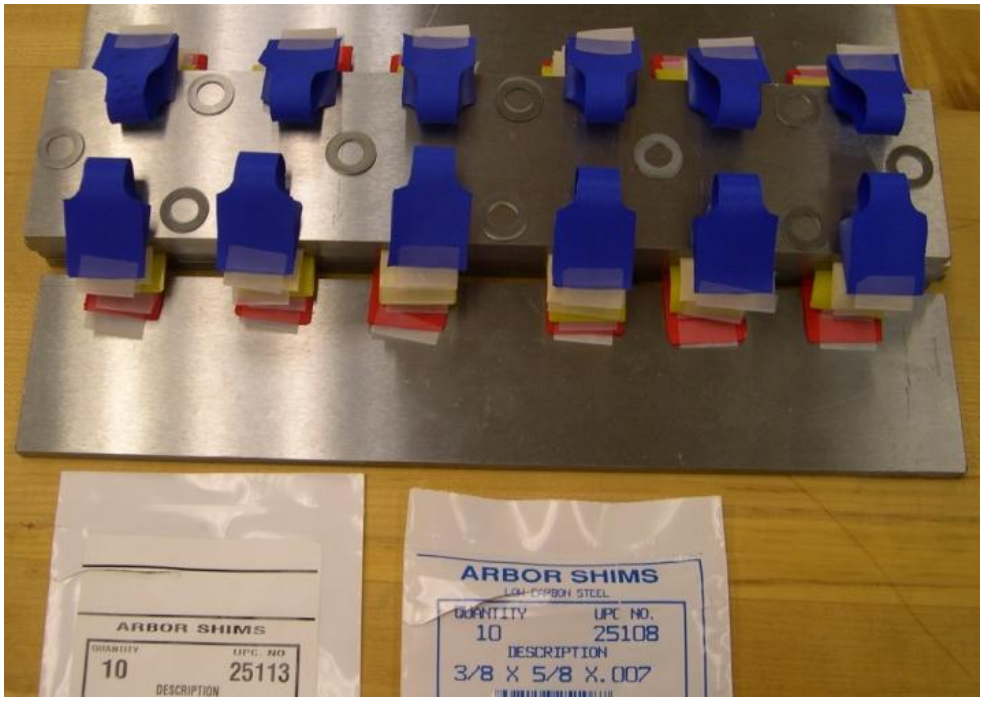

Figure 7.2 Folded samples with shims to control gap and fold crease

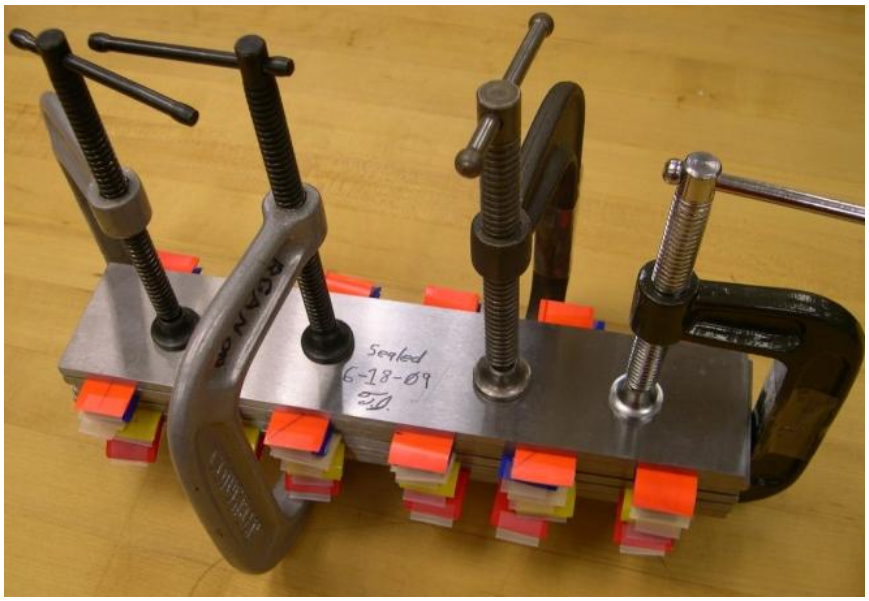

Figure 7.3 Packed samples for long term crease test

7.1.1 Unpacking Samples

The clamped samples were opened December 7, 2010. The first plate removed exposed the orange samples. The two sided coating on the orange sample adhered to the steel plate and caused slight rusting. The rust also lightly stained the samples. The orange sample did not adhere to itself and shows a sharp crease seen in Figure 7.6.

The blue samples were packed with the single sided polymer coating on the inside of the fold. Thus the coating did not contact the steel plates. The blue sample did not cause rust and did not stick to the steel plates. The Vectran sample did not stick or cause rust, but it did adhere to itself. The yellow-D sample also had double sided coating and stuck to the plate. It left a film on the metal plate that seemed to prevent rusting. The area under the yellow sample was shinier than the rest of the metal surface. The red samples were coated on one side and with the coating folded on the inside. There were no signs of rust on the plates and the samples did not stick.

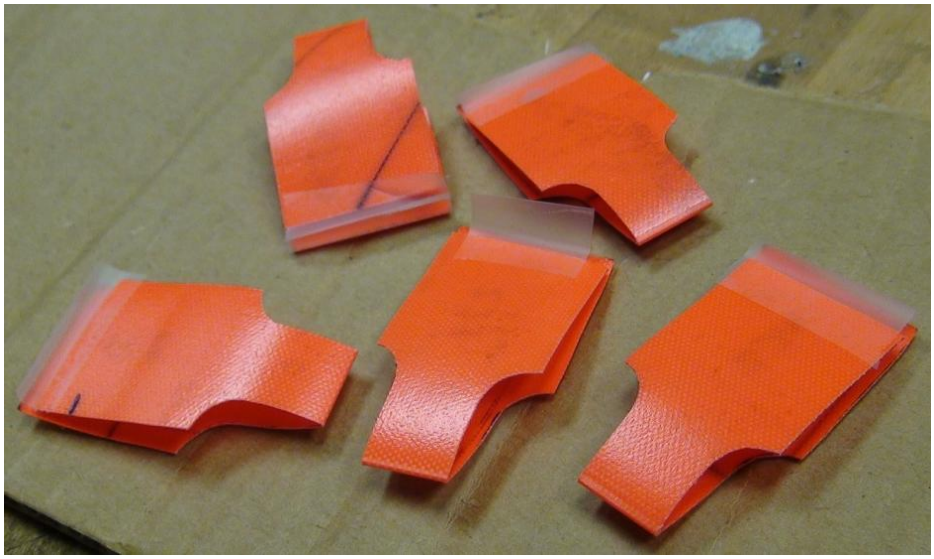

Figure 7.4 Rust staining on orange samples

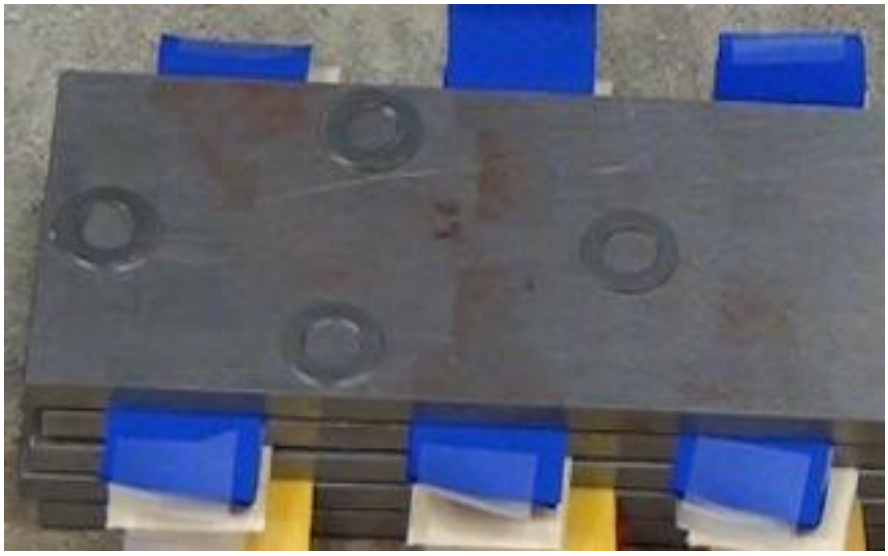

Figure 7.5 Rust on steel plates directly under orange samples

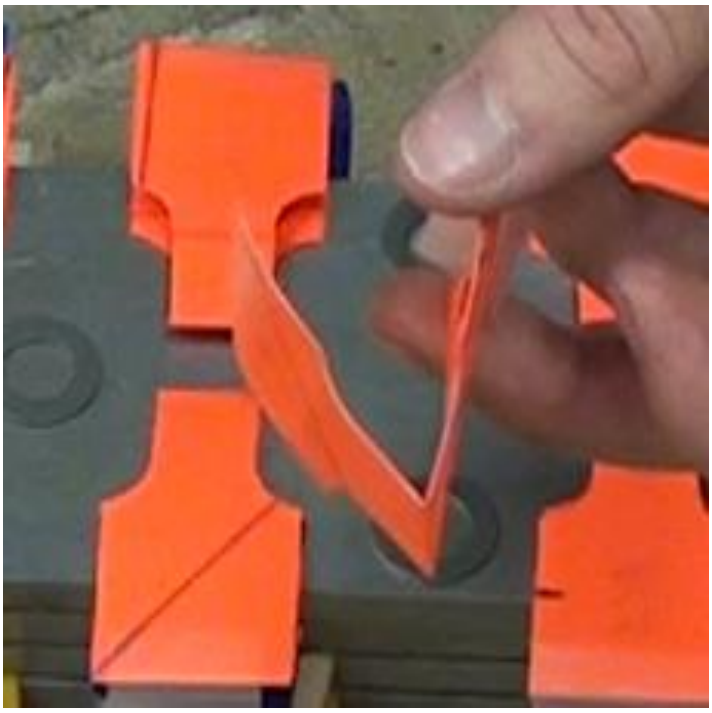

Figure 7.6 Free creased position immediately after unpacking

Figure 7.7 Free creased position of yellow-D material

7.1.2 Tensile Testing

The results of the long-term packing study were to be compared to results from a material study performed under the Phase I effort of NextGen Aeronautics SUAVE high-aspect ratio deployable wing program. These prior results were summarized in [16], but are adjusted and some aspects corrected, here for comparison to the results of the current study.

The previous study used sample strips with a width of 1.0 inch, tested at ambient temperature 25^{o}C, at -30^{o}C, and at -70^{o}C. Each sample was tensile tested following standard practice. The Phase II study used dog-bone samples with a 0.5 inch wide by 1.0 inch long midsection with ends of 1.0 inch by 1.0 wide for a total length of 3.0 inches.

7.1.3 Ambient Temperature Tensile Tests

Each sample was placed into the machine grips and tested with identical conditions. The head speed rate was 0.25 inch/minute. The grips were aligned using machinist parallels. In initial testing, four samples broke at the top gripper. Therefore, following tests used a modified tightening procedure. The bolts farthest from the sample were tightened first, but bolts near the sample were just snug, not extra tight. There may have been a sharp edge of the top grip that caused four of sixty samples to fail early. Each test combination had two samples that were averaged so that variability is reduced. Figure 7.8 shows a side view of the permanent crease and the resulting shape of the sample in loose grips.

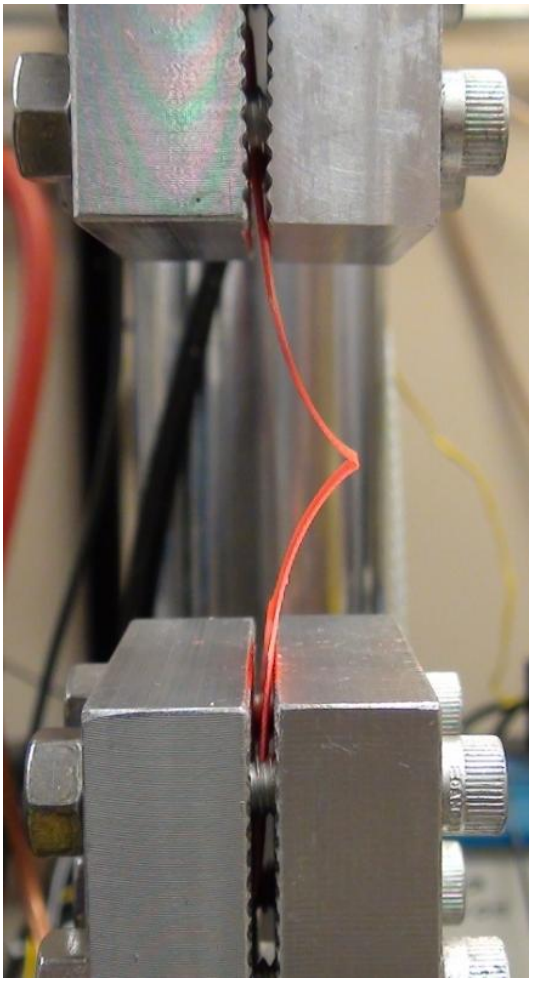

Figure 7.8 Permanent creased sample in loose grips

7.1.4 Low-Temperature (-70^{o}C) Tensile Tests

An insulated enclosure was built for the low-temperature test. It consisted of five plywood walls each with 2 1/8-inch thick Styrofoam liners and a 2-inch thick foam door. Liquid nitrogen was supplied to the top left back corner and a thermal couple probe was positioned 0.5 inch behind the sample as shown in Figure 7.9. A PID digital controller controlled an open/close valve for the liquid nitrogen. The PID controller's auto-tune feature was used to learn the system control characteristics. Despite several attempts to use the auto-tune feature, the cooling chamber had an unacceptable swing in temperature from -30 to -130^{o}C.

The digital PID controller struggled keeping the temperature inside of the insulated chamber consistent. Therefore, the tensile data was filtered to only include -70 +/- 2^{o}C for the low-temperature tests. This smaller set of filtered data was used to calculate an additional "filtered modulus" and "filtered ultimate strength" as shown in Figure 7.14 and Table 7.3

To help steady the temperature control a smaller volume was achieved by packing blocks of foam as shown in Figure 7.11. Also, the foam door was pressed deeper into the box to help seal the enclosure. These modifications, along with a five minute soak time, were used to keep the temperature at -70 +/- 10^{o} C. The modifications were incorporated after some samples were tested. The Young's modulus generally increases for cold temperature. The temperature fluctuation's effect can be seen in the cold temperature Stress-Strain Phase II plots. The Phase II long term packing tensile tests used dog bone samples. The Phase I tests used rectangular strips. This explained the discrepancies between Phase I and Phase II maximum tensile force. The data matched well after using stress to normalize the sample dimensions.

Several inconsistencies occurred during the test. The starting absolute zero displacement was not the same. The machine was zeroed relatively after each material was

placed into the grippers. This caused the stress-strain data to shift left and right on the x-axis. All Phase II data was adjusted so that the first time the stress reached 3.0 MPa occurred at 0.0 strain for each sample.

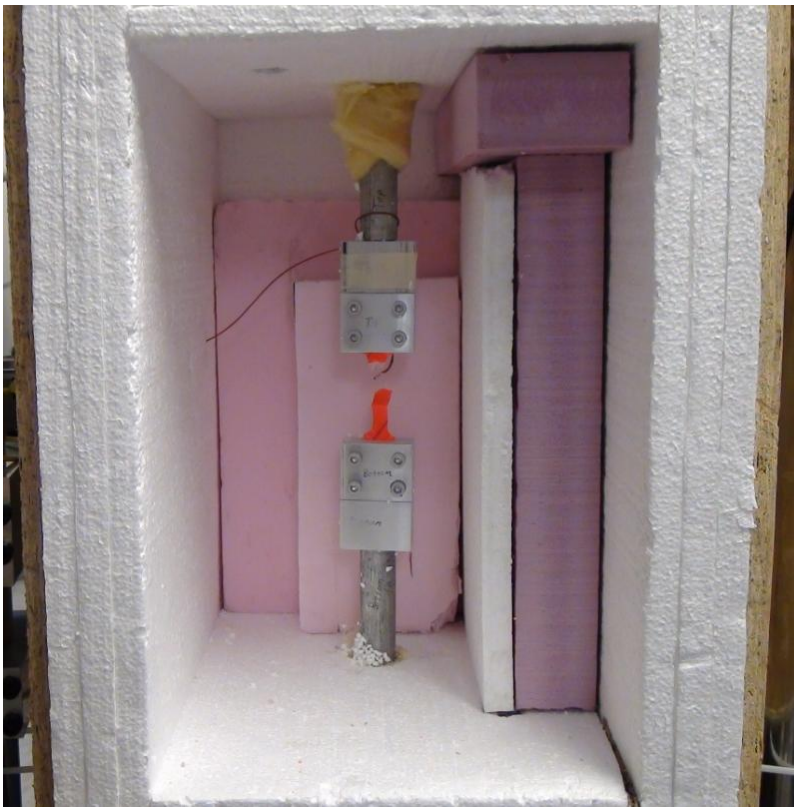

Figure 7.9 Low-temperature insulated enclosure

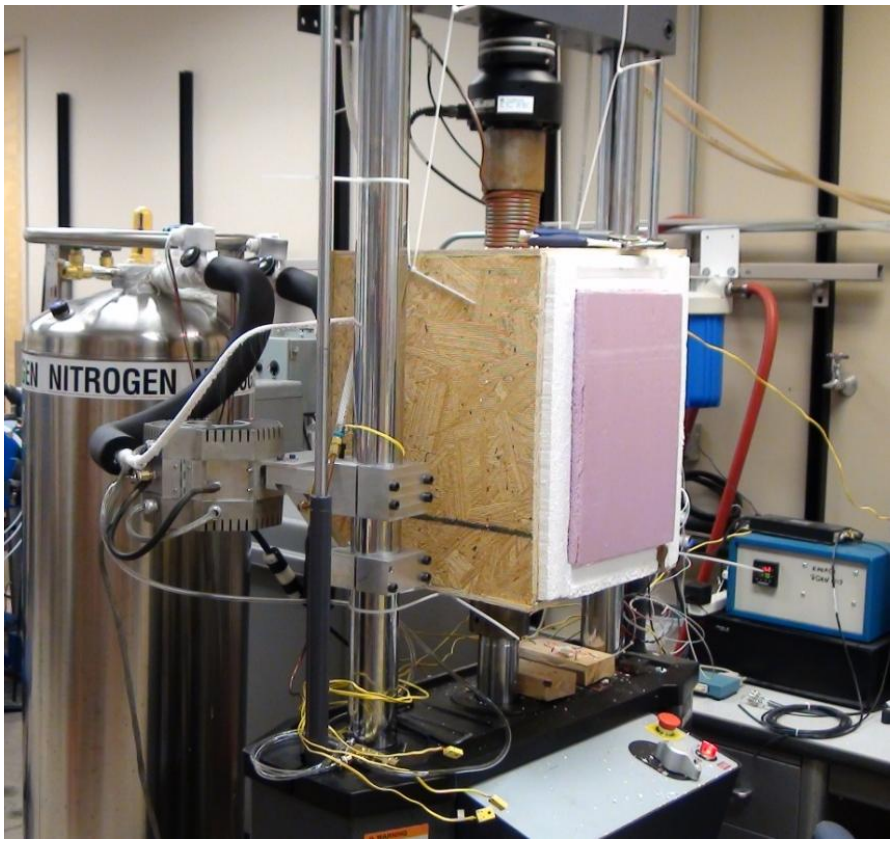

Figure 7.10 Low-temperature insulated enclosure with door

Figure 7.11 Foam blocks used to reduce total cooling chamber volume

7.2 Results

The samples did not break at the crease or at the grippers for 56 of 60 cases. This is the first indication that long-term packing does not significantly affect material strength. All ambient tested samples are shown in Figure 7.12. Figure 7.13 shows all low-temperature tested samples. The majority of the samples failed away from the long term crease for both temperatures, thus the long term pack did not reduce the ultimate strength of the samples.

Figure 7.12 Phase II 25^{o}C, tensile tested ambient samples

Figure 7.13 Phase II -70 deg C, tensile tested samples

The ambient data was used to determine the maximum ultimate strength and Young's modulus by averaging the two samples for each material and fold direction. Results are summarized in Table 7.2. The low-temperature tensile data showed a strong correspondence with temperature's effect on Young's modulus and maximum ultimate strength. The Young's modulus of ambient samples was consistently lower (35-50%) than the corresponding modulus of low-temperature samples. The maximum ultimate strength was consistently lower (20-55%) than the corresponding ultimate strength of low-temperature samples. Table 7.2 lists Phase II ambient temperature tensile results for the three fold directions, 45-degree, warp, and fill.

To correct low-temperature tensile test data for temperature swings the data was filtered to only include stress and strain data that occurred within +/- 2^{o}C of the target

temperature of -70^{o}C. A linear trend line was fit to these filtered data points so that a filtered ultimate strength and filtered modulus could be determined as shown in Figure 7.14 Tensile data and -70 filtered trend lineand Table 7.3.

Table 7.2 Phase II ambient samples tensile test data

Material	Direction	Ave. Ultimate [MPa]	Ave. Modulus [MPa]
Orange	45c1	106.6	209.8
	fc1	103.65	442.3
	wc1	142.9	511.1
Blue	45c1	61.25	119.95
	fc1	57.95	203.25
	wc1	80.4	327.95
Vectran	45c1	9.8	66.75
	Ac1	188.15	1880.8
	Bc1	194.15	1580.65
Yellow	45c1	53.2	77.7
	fc1	39.6	109
	wc1	51.7	162.8
Red	45c1	40.15	65.3
	fc1	45.5	181.05
	wc1	32.45	105

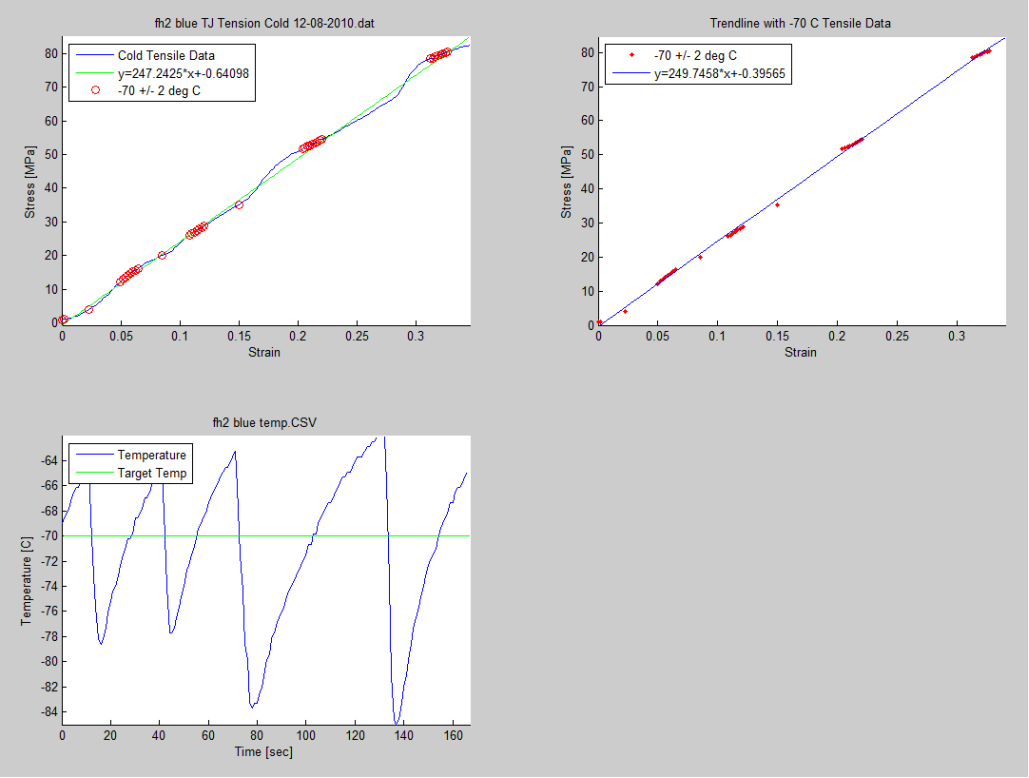

Figure 7.14 Tensile data and -70 filtered trend line

Table 7.3 Phase II Cold temperature tensile data and filtered low-temperature modulus and ultimate strength

		Ultimate [MPa]	-70 Filtered Ultimate [MPa]	Modulus [MPa]	-70 Theory Modulus [MPa]
Orange	45h1	134.4	129.0	289.7	303.0
	45h2	NA	NA	NA	NA
	fh1	NA	NA	NA	NA
	fh2	139.0	122.6	475.5	456.9
	wh1	151.6	151.5	611.6	618.0
	wh2	144.3	143.3	590.9	604.7
Blue	45h1	98.7	96.7	187.3	188.2
	45h2	93.0	92.6	207.7	206.2
	fh1	99.0	97.4	310.8	315.5
	fh2	99.9	101.7	300.7	304.6
	wh1	133.3	133.5	690.5	648.3
	wh2	115.4	124.3	612.6	618.8
Vectran	45h1	96.5	94.1	333.1	351.2
	45h2	119.3	110.9	361.2	375.6
	Ah1	171.2	166.6	1669.9	2044.2
	Ah2	331.9	294.3	2616.1	2989.6
	Bh1	347.6	324.9	2580.4	2667.8
	Bh2	NA	NA	NA	NA
Yellow-D	45h1	103.2	86.5	188.5	162.9
	45h2	84.7	72.9	185.7	172.6
	fh1	91.8	91.0	259.1	264.9
	fh2	89.1	89.3	265.0	295.0
	wh1	90.5	93.9	510.2	479.3
	wh2	107.1	106.6	454.3	388.0
Red	45h1	90.8	70.4	150.5	127.7
	45h2	NA	NA	NA	NA
	fh1	127.9	120.0	523.8	421.9
	fh2	116.5	124.0	577.8	636.2
	wh1	81.9	86.9	283.6	302.8
	wh2	83.9	86.6	311.8	299.9

7.2.2 Long Term Packing Phase I and Phase II Comparisons

Prior SUAVE Phase I testing data was rechecked. It was found prior modulus was calculated at the single maximum ultimate strength point instead of using a linear trend line to

determine Young's modulus. Material thickness, ultimate strength, and modulus were corrected for the comparison between Phase I and Phase II results. The corrected results are in Table 7.4.

Table 7.4 Phase I, tensile data with corrected sample thicknesses, modulus, and ultimate strength

Temp [C]	Material	Direction	Ave. Ultimate [MPa]	Ave. Modulus [MPa]
-70	orange	fill	138.2	358.3
-70	orange	warp	207.1	425.2
-30	orange	fill	134.8	350.6
-30	orange	warp	180.7	402.5
25	orange	fill	94.5	231.3
25	orange	warp	165.5	296.8
-70	yellow-D	fill	96.7	123.9
-70	yellow-D	warp	120.0	228.4
-30	yellow-D	fill	67.3	145.7
-30	yellow-D	warp	91.7	220.4
25	yellow-D	fill	54.4	73.7
25	yellow-D	warp	68.0	145.4
-30	blue	fill	87.4	182.9
-30	blue	warp	115.0	331.4
25	blue	fill	53.2	121.7
25	blue	warp	96.1	220.3

The Phase II tensile testing data from December 7, 2010 had to be zeroed for consistent displacement due to different gripper start locations. The zero method identified 3.0 MPa stress for each sample and set this as zero displacement and corresponding zero strain. This was applied to all long-term packed samples. It won't affect ultimate strength, but it does affect strain values. Initially, 1.0 MPa stress was used, but a single yellow sample required using the higher stress value. This zeroing can be seen in Figure 7.15; the y-axis does not start at 0.0 MPa.

Figure 7.15 shows the low-temperature swing effects and Figure 7.16 shows ambient tensile test on the same material. The bi-modulus results occur for some material samples at ambient temperature for the warp direction. This is not due to manufacturing defects or process differences, but is part of the fabric design (weave, fibers, etc.).

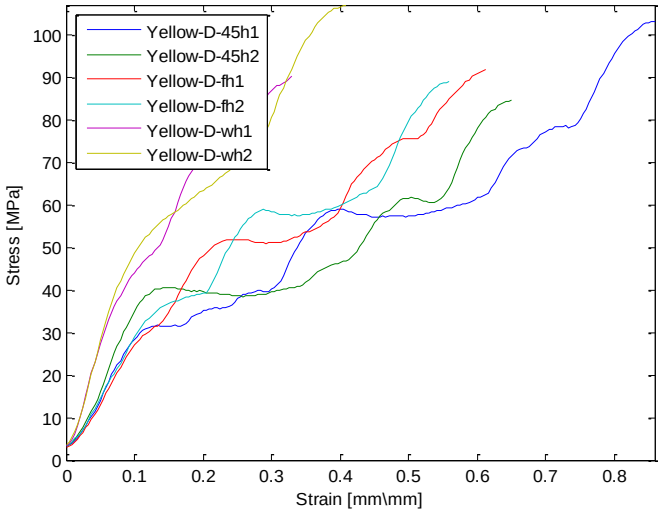

Figure 7.15 Phase II, -70^{o}C, Temperature swing effects on yellow-D sample

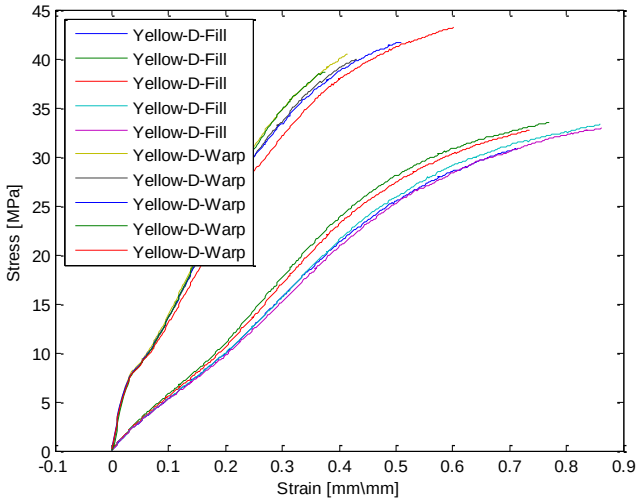

Figure 7.16 Phase I, Ambient tensile test results with orthotropic behavior, yellow-D fabric

To further illustrate that long duration storage does not affect material properties, Phase I and Phase II results are compared side by side for the wing materials. The ultimate strength for warp and fill directions as well as the modulus for both fill directions are compared for orange and yellow-D in Figure 7.17 and Figure 7.18 respectively. Note that both figures have sub plots with the same scale for visual comparisons.

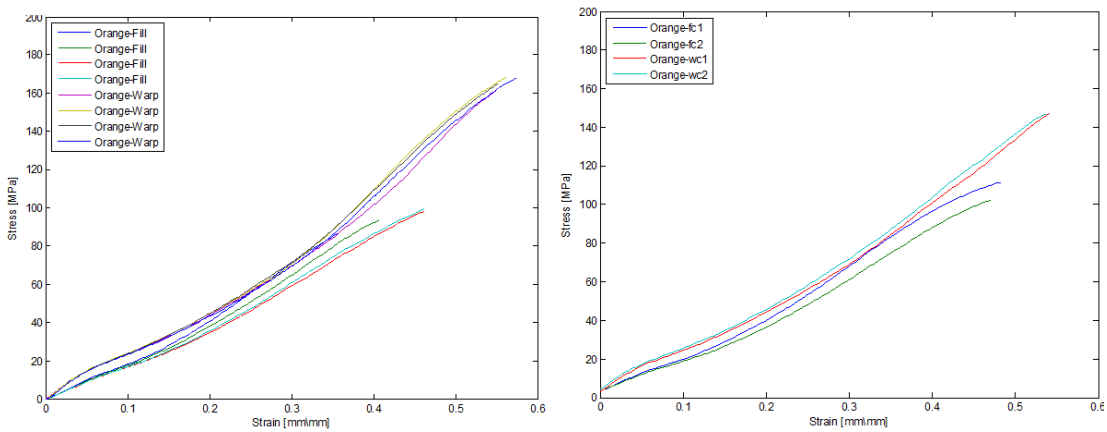

Figure 7.17 Phase I 25°C orange (left), Phase II long term pack 25°C orange (right)

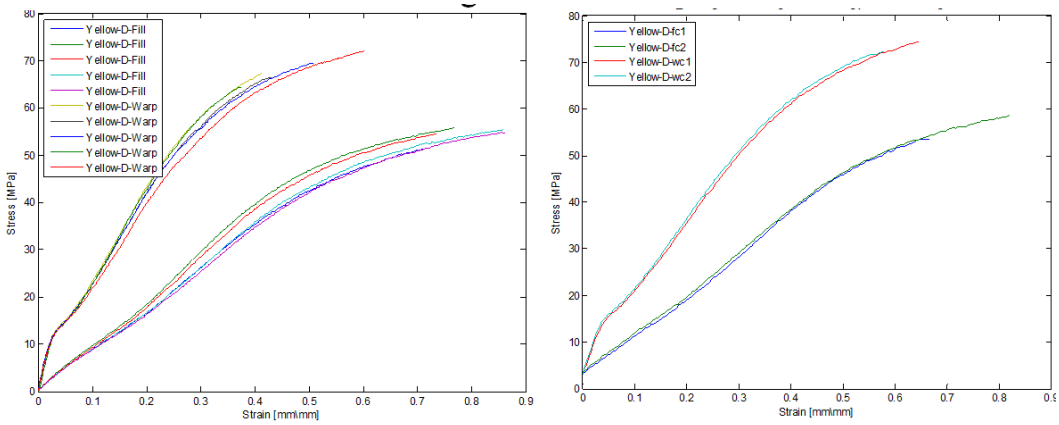

Figure 7.18 Phase I yellow-D 25°C (left), Phasae II long term pack 25°C yellow-D (right)

A similar comparison of Phase I and Phase II for low temperature is shown in Figure 7.19. Note that the combination of cooling chamber along with the PID controller used in Phase II caused temperature swings that can be seen in the right subplot. The Phase II also had an orange sample with invalid test data thus there is only one fill direction sample. Despite the temperature effects, the modulus and ultimate strength are similar to Phase I.

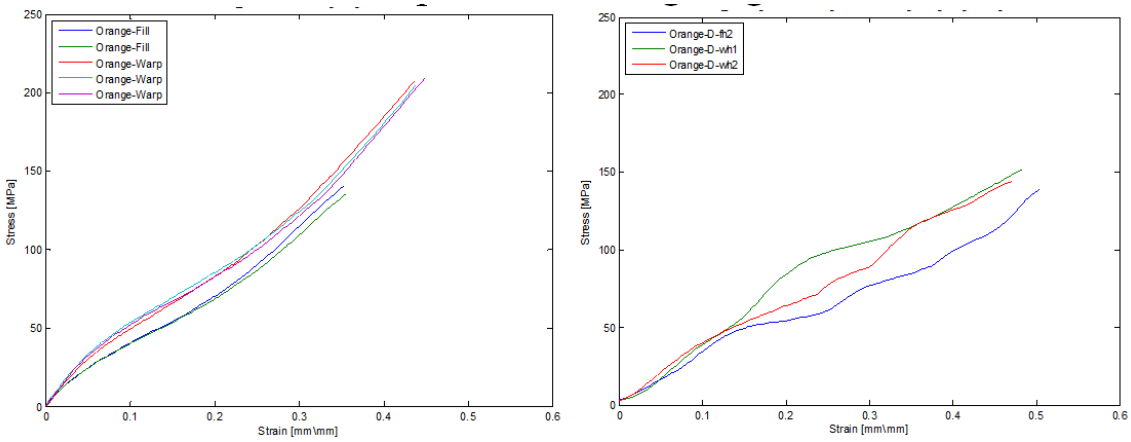

Figure 7.19 Phase I orange -70°C (left), Phase II orange -70°C with temperature swings (right)

Phase II tensile test results are only presented for three materials for comparison. The Seattle Fabrics red and yellow were not part of Phase I, thus cannot be compared. The blue material was not tested at low-temperature in Phase I. Two samples of each material and orientation direction were averaged for ultimate strength and modulus as shown in Table 7.5. Table 7.6 used the low-temperature filtered stress and strain data to determine ultimate strength and modulus. The unfiltered low-temperature data is not presented to avoid confusion.

Table 7.5 Phase II, long term pack ambient 25°C temperature

Material	Direction	Ave. Ultimate [MPa]	Ave. Modulus [MPa]
orange	fill	106.8	220.25
orange	warp	147.2	260.8
yellow-D	fill	56.05	69.55
yellow-D	warp	73.25	107.95
blue	fill	70.3	121.4
blue	warp	97.65	202

Table 7.6 Phase II, long term pack filtered (+/-2°C) -70°C tensile data

Material	Direction	Ave. -70 Filtered Ultimate [MPa]	Ave. -70 Filtered Modulus [MPa]
orange	fill	122.6	456.9
orange	warp	147.4	611.35
yellow-D	fill	90.15	279.95
yellow-D	warp	100.25	433.65

The Phase II long term storage test used materials left over from Phase I and BIG BLUE projects. Because a comparison was desired to determine long duration crease influences, the orange and yellow-D material were checked for percent differences of ultimate strength and Young's modulus at ambient and low-temperature. The ultimate strength largest percent difference, 27.8%, at ambient temperature occurred in the blue material fill direction. The lowest percent difference, -11.7%, at ambient temperature occurred in the orange material warp direction Figure 7.20. The other materials are inside this range of values. These ultimate strength percent differences are the extremes and are considered reasonable for a small sample size, two, of each test combination.

The ultimate strength percent difference comparison of low-temperature for Phase I and Phase II reviled a reduction in ultimate strength of -7.1% to -33.7%. The Phase II data is filtered for temperature swings and to normalize the absolute displacement values. Figure 7.21 shows that the low-temperature ultimate strength was reduced for both materials. The

reduction in ultimate strength did not occur for the ambient temperature. Thus, the reduction in strength is due to a combination of permanent crease and low temperature or due to the filtering and linear trend line. Figure 7.17 shows the stress-strain curve is not truly linear. Using a linear trend line could be why there is an indication of reduction in ultimate strength.

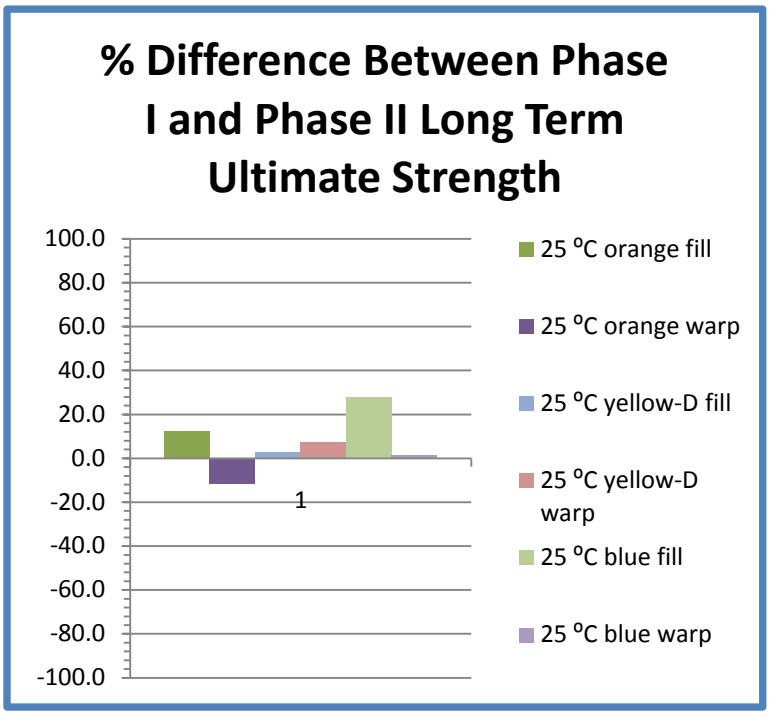

Figure 7.20 Phase I and Phase II ambient temperature

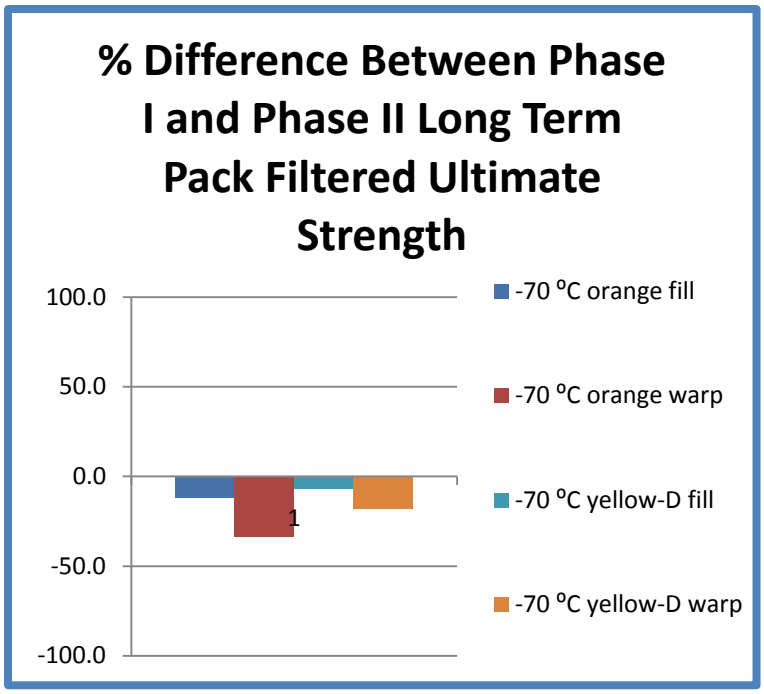

Figure 7.21 Phase I and Phase II -70°C

The long term crease did not reduce the strength of the samples based on two aspects of the test results. The first aspect is that the samples failed at the crease only two out of 75 tension tests. Most samples failed in the material between the grip and the crease. The second supporting test result is shown in Figure 7.20 with the percent difference for three ambient temperatures of three material samples. Most samples failed within +/- 15% of the Phase I samples.

The affect of long term packing on modulus is less conclusive. The data trend is for low-temperature that the modulus increased 25-70% and for ambient temperatures that the modulus decreased 5-25% as shown in Figure 7.22 and Figure 7.23, respectively. The long term results should have affected all samples in a similar way, either increase or decrease. It is possible the liquid nitrogen swings caused the samples to cool too much during the temperature swings and thus the sample was tested at lower temperatures than the thermal couple reading

indicated. This would explain the increase in modulus for low-temperature testing. If only considering ambient testing, then it appears there is a slight decrease in modulus due to long term storage.

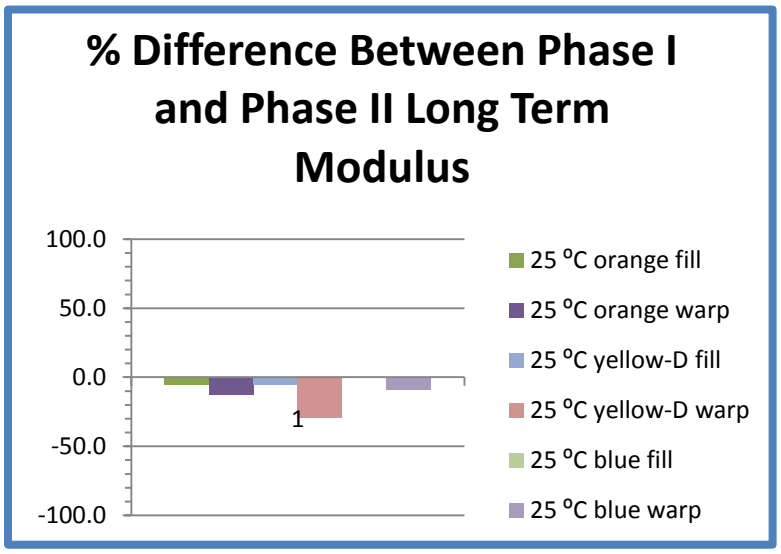

Figure 7.22 Phase I and Phase II ambient temperature

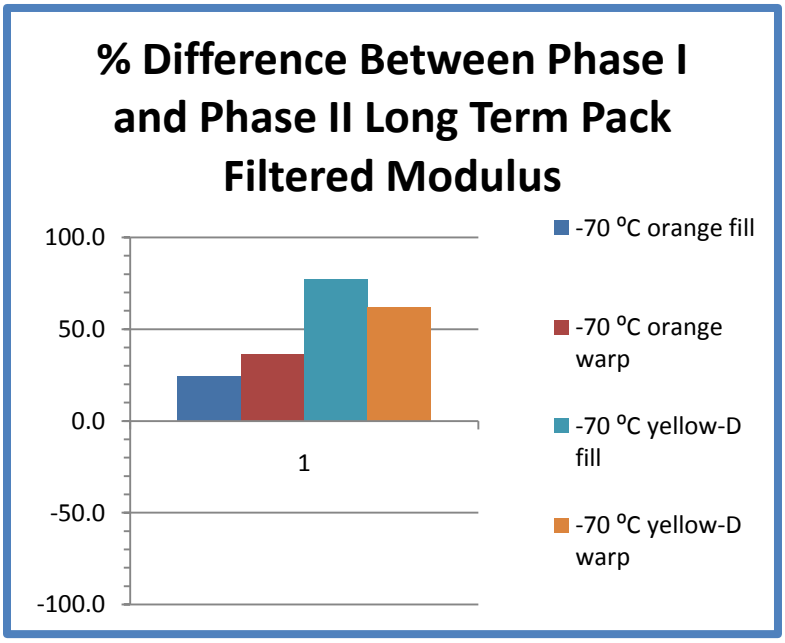

Figure 7.23 Phase I and Phase II -70°C

A method to filter the temperature swing affects used the tensile data that occurred when the environment was within +/- 2^{o}C. These data points were then linear fit and a theoretical -70^{o}C ultimate and modulus were calculated. The theoretical ultimate for long term crease was 7-33% lower than non long term tensile tests. The theoretical modulus is shown in Figure 7.23. The filtered trend line values are more consistent and expected results for both ultimate and modulus. A better testing environment and digital temperature control would eliminate the need for this method.

7.2.1 Long Term Pack Summary

The majority of the samples failed away from the long term crease for both test temperatures, thus the long term pack did not reduce the strength of the samples. This result reduces uncertainty and builds on the reported durability of inflatable wing technology [3]. The unexpected adhesion between coated samples and the steel plates as well as the adhesion of some folded samples to themselves should bring further considerations when designing packable UAV wings.

A future test might have a sample under different levels of constant tension in the cold chamber with fluctuating temperatures. The tensile data would show fluctuating stress with constant strain due to the temperature swings. The test would allow for a temperature correction factor to be determined. This temperature correction factor could be used in FEA analysis for high altitude simulations and it could be used to adjust low-temperature tensile data results.

Chapter 8

8.1 Summary

The deployable wings at the University of Kentucky were of great assistance in researching this thesis. Without the physical wings in hand, the packing heuristics would not have been discovered. The deployable packing study with Figure 3.4 provides a significant aid for designers by demonstrating the design space.

The inflatable wing packing simulation gives a method to estimate wing length that will fit into an enclosure before prototypes are built. By developing a packing simulation, critical packing details were discovered. The simulated pack shows details to help understand real world packing situation. This exercise brought common sense concepts to the surface so that had to be considered and contemplated. Many times drawing out the geometry also made the overlooked math standout to be coded. The end of Chapter 6 provides an equation to quickly do a back of the envelope calculation to estimate wing length inside of an enclosure without a computer simulation.

The simulation verifies if a packing configuration is valid, inside of enclosure and is physically possible with the given material properties. The code does allow comparison between different wing materials and designs. The packing simulation problem is difficult because early choices of packing starting from the attachment point significantly influence the final packing configuration. Also, the random and genetic algorithm simulations produced complex packing arrangements that are not suitable for actual applications. They do not accurately represent a physical, randomly stuffed pack, because the simulation uses fixed coordinates.

A simulation that could use a transferable packing coordinates needs to be developed. The difficulty arises when shifting one material coordinate point, then the next point must be

checked against all criteria as well as the next point until the entire wing's points have been verified. Perhaps the best method for simulation would be a person tracing a packing configuration one point at a time and the code will give valid options for the next possible paths. Assuming a person would make a simple packing configuration and could explore many high quality configurations quickly. The trace interface could be with a touch screen, mouse, or a simple numeric keypad.

A packing simulation would help a designer determine initial wing sizing constraints to help determine overall UAV size, payload, propulsion, endurance, and cost. Before the prototype stage and after wing design has been decided, further simulations could be run with a well defined enclosure. The longest simulated wing that fits could be built along with a second wing that is 10-20% longer. The simulation does not account for transferable packing coordinates and thus conservatively estimates total wing length. These two wings and prototype would be packed into the enclosure and with packing experience a final wing length could be decided. A more thorough simulation is not necessary after an initial wing length has been packed into enclosure. Initial path selection affects all future choices. It also voids many possible solutions. Any second choice also affects remaining future choices possibly revalidating old solutions. The ability to back up and reverse the packing direction is very important.

The difference between packing a wing in real life and the simulation is the simulation is a static pack meaning once material has been assigned a coordinate or a location it will remain throughout the rest of the simulation. Packing in the physical world is a dynamic situation. A material can be rolled up then squeezed under pressure or rolled up and placed inside the enclosure. The physical rolled pack self aligns and self centers inside of any shaped enclosure as

long as the friction isn't too large. To get similar results in simulation prior calculations must occur such as MCD shift.

Deployable wing designs need to consider the entire system to arrive at a balanced design. Each wing design has several optimal packing configurations. There is an optimal wing pack when only considering the wing. There is an optimal pack when considering the wing with attachment methods, and wing with fuselage interaction. Additionally, there is an optimal pack when considering wing, fuselage, and the enclosure together as a system.

Figure 8.1 Wing rolled across span-direction without attachment

Figure 8.2 Wing packed with tape attachment

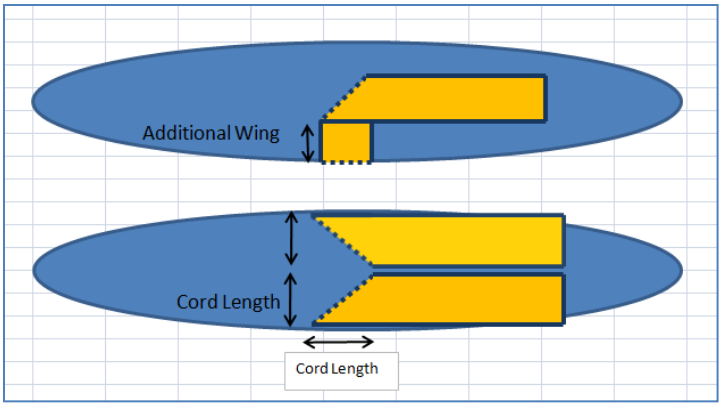

Figure 8.3 Wing packed with fuselage

8.2 Future Work

The packing simulations could be improved to include multiple-direction packing in three dimensional space. The move to three dimensions is difficult. A proposed method for two dimensional packing that is upgradable to the third dimension is presented. For two-dimension simulations, a square matrix could be used to represent the enclosure area. Each matrix index, (m,n), would represent a portion of a physical grid. A place holder in the matrix would be equal to a square area. The matrix will be stored in a computer's RAM. If the matrix's index is used, then material is packed into that matrix. A simple 5x5 matrix could have points (5,1),(5,2),(5,3),(5,4),(4,4),(3,4),(2,4),(1,4),(1,4),(1,2),(2,2),(2,3),(3,3),(2,3). A bigger and more complex example is shown in Figure 8.4 Attachment/start point centered at (10,10) plot of matrix index storage method.

This is a simple roll pack. It can be drawn in a spreadsheet program. Using matrix index to store the packing configuration would significantly reduce the extra calculations needed for my simulation packing method. Some simple matrix math operations would verify valid packing configurations. This concept could be extended to 3D space as well, where each matrix index

represents a regular cube of given length. The enclosure and fuselage could be defined by using NAN to block out matrix indexes.

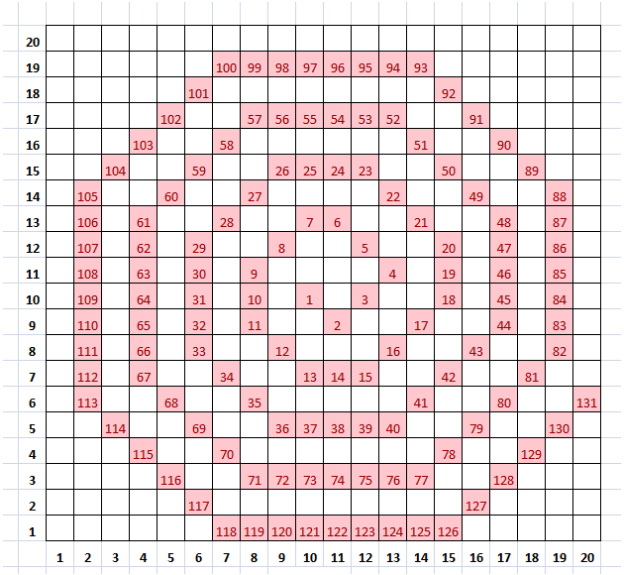

	1	2	3	4	5	6	7	8	9	10	11	12	13	14	15	16	17	18	19	20
20																				
19							100	99	98	97	96	95	94	93						
18						101									92					
17					102			57	56	55	54	53	52			91				
16				103			58							51			90			
15			104			59			26	25	24	23			50			89		
14		105			60			27					22			49			88	
13		106		61			28			7	6			21			48		87	
12		107		62		29			8			5			20		47		86	
11		108		63		30		9					4		19		46		85	
10		109		64		31		10		1		3			18		45		84	
9		110		65		32		11			2			17			44		83	
8		111		66		33			12				16			43			82	
7		112		67			34			13	14	15			42			81		
6		113			68			35						41			80			131
5			114			69			36	37	38	39	40			79			130	
4				115			70								78			129		
3					116			71	72	73	74	75	76	77			128			
2						117										127				
1							118	119	120	121	122	123	124	125	126					

Figure 8.4 Attachment/start point centered at (10,10) plot of matrix index storage method

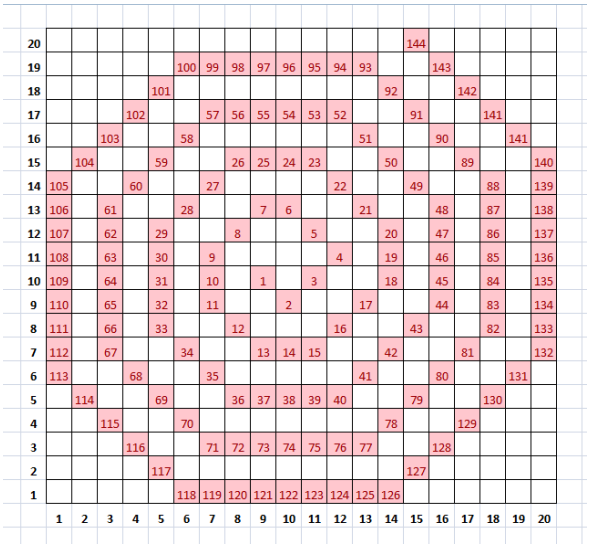

	1	2	3	4	5	6	7	8	9	10	11	12	13	14	15	16	17	18	19	20
20														144						
19						100	99	98	97	96	95	94	93			143				
18					101									92			142			
17				102			57	56	55	54	53	52			91			141		
16			103			58							51			90			141	
15		104			59			26	25	24	23			50			89			140
14	105			60			27					22			49			88		139
13	106		61			28			7	6			21			48		87		138
12	107		62		29			8			5			20		47		86		137
11	108		63		30		9					4		19		46		85		136
10	109		64		31		10		1		3			18		45		84		135
9	110		65		32		11			2			17			44		83		134
8	111		66		33			12				16			43			82		133
7	112		67			34			13	14	15			42			81			132
6	113			68			35						41			80			131	
5		114			69			36	37	38	39	40			79			130		
4			115			70								78			129			
3				116			71	72	73	74	75	76	77			128				
2					117										127					
1						118	119	120	121	122	123	124	125	126						

Figure 8.5 MCD centered at (9,10), i.e. shift left one inch, 10% improvement

This method of using matrix index to store the material coordinates can be extended to three dimensional enclosures. The matrix method allows for fast computational speed by using

RAM memory with vectorized code for larger problems. There are reductions in calculations for each line segment such as: eliminate inside of polygon check, eliminate distance checks between material layers, eliminate wastefully generating candidate points, and the many coordinate calculations for each point is handled by the matrix index. The matrix method would also allow for three-dimensional plots of packed wing configurations with fuselage and enclosure. Radical enclosure shapes can be defined by filling voided space with NANs or zeros.

An interesting note is that the top layer of each wrap is one unit longer than the other three sides. Similarly, the lower left diagonal is one unit less than the other three diagonals. There are more packing details to learn with this matrix index method.

A second future simulation method might be possible with matrix rotations of a series of end to end line segments in a straight line. To use matrix rotations, start with a segmented straight wing of known length. Initially, only the first segment must be valid. Next, rotate and check second segment. The remaining segments follow the second segment to remain in a straight line. The process is repeated until the wing tip is reached or until the simulation is complete.

The wings in the Empirical packing study are resilient to damage and reliable. However, improvements could be made to these wings to adapt them to the smaller class of micro UAVs. A PTFE coated wing or a wing made from silk should pack more effectively when packing pressure is applied. The theoretical ideal wing material would be a thin silk-like fabric with outer polymer coating for pressurizing and a PTFE coating on the inside and outside. These wing properties would improve packing characteristics.

Distant future work could investigate balloon type inflatable wings with stretchy textile materials. Future simulations should utilize two wings so that symmetry problems can be

handled properly. Additionally, a packing simulation with different material properties at root than at the tip is needed for hybrid wings.

The packing simulation heavily depends on enclosure, wing material, and each packing path chose. All path choices, first to the last, influence the finial packed wing length. The difficultly of solving this packing simulation problem can be useful for digital security encryption. The enclosure with fuselage problem with specific wing properties and start location would be the hidden lock. Only a few "keys", the packing configuration path vector that completely fills the enclosure, would be valid to solve the problem. The benefit is a simple problem that requires a significant amount of computations and effort to solve. There could be more than one valid vector key depending on how the lock is defined.

Appendix A: Nomenclature and Definitions

Fill: The cross direction of a manufactured roll of material. The short yarns which run crosswise to the roll direction.

Fold Radius Length: The length of wing material used in each fold. It is used to increase accuracy of predicted wing length and to calculate z-packs without excess wing overhang.

Deployed Boxed Volume: The volume of the smallest box that will contain a wing without deformation.

Minimum Circle Diameter: The smallest diameter that a wing can roll into. The first layer of a pack wrap/roll configuration.

One Wrap Intersection: A conditional packing simulation where a wing is flexible enough to roll-pack inside of the first roll layer.

Packed efficiency: The percent of an enclosure filled. 10% is a barely filled enclosure.

Packed percentage: The packed box volume divided by the deployed box volume of a wing.

Pleat: A part of the one-direction z-folding. It is a group of folds.

Rotation/start angle: Used in wing packing simulation to change the index location of candidate points.

Warp: The direction of a manufactured roll of material. It is continuous for the entire length of the roll.

Appendix B: Code

The simulations presented in this thesis were produced from written code. M-files are written for MATLAB of MathWorks and are hyperlinked in the list of files.

List of Matlab Files			2389
File Name	**Description**	**Called By**	**Lines**
adjHingeRigidWingPackVolFunc.m	takes inputs and calculates percent packed	RunRigidWingPackingVolTEN.m	48
bodyIntubeQuater.txt	round fuselage in side of tube quarter symmetry.	RunRandPacking5Oct.m	24
box.txt	enclosure points	RunRandPacking5Oct.m	4
boxPE.txt	enclosure points and potential energy points	RunRandPacking5Oct.m	4
closenessFunc.m	determines if point is near and should be checked	PackingCodeQuickLaunchAngle.m	10
closenessFunc2.m	determines if point is near and should be checked	PackingCodeQuickLaunchAngle.m	16
colorPlotFunc.m	plots wing packed configuration	PackingCodeQuickLaunchAngle.m	110
confinementAreaFunc.m	makes confinement area	RunRandPacking5Oct.m	86
cross2Func.m	checks if two line segments cross	PackingCodeQuickLaunchAngle.m	45
FadiDataReadIn.m	reads in phase 1 data		57
importfileTJ.m	imports excel spread sheet		9
inpoly.m	Darren Engwirda 2005-2007, check point inside polygon	PackingCodeQuickLaunchAngle.m	210
LongTermDataReadInAMBII.m	reads in phase 2 long term pack AMBI data		103
LongTermDataReadInCOLD.m	reads in phase 2 long term pack COLD data		103
orange.txt	material properties	RunRandPacking5Oct.m	3
orangeLeftWall.txt	material properties with left wall attachment	RunRandPacking5Oct.m	3
PackingCodeQuickLaunchAngle.m	body of simulation with validation checks	RunRandPacking5Oct.m	532
pePlotsPointsFunc.m	plots potential energy plot and potential energy points	PackingCodeQuickLaunchAngle.m	56
pointOnLineSegmentFunc.m	check if point is on line segment	PackingCodeQuickLaunchAngle.m	96
quadrentSlopeFunc.m	determine quadrant,so inverse trig used to represent slope	PackingCodeQuickLaunchAngle.m	102
LongTermTensileCold.m	reads in phase 2 long term data and filters data		143
rot2dFunc.m	used to handle vertical slope with slight rotation	PackingCodeQuickLaunchAngle.m	10
RunRandomPacking5Oct.m	user inputs and runs simulation		340
RunRigidWingPackingVolTEN.m	10 runs		48
calcPleatExcessLength.m	Calculates pleat and excess wing length		79
slopeFunc.m	determines slope of line segment	PackingCodeQuickLaunchAngle.m	18
thicknessCheckFunc.m	checks points if close to material coordinates	PackingCodeQuickLaunchAngle.m	80
traceOptPlotTextFunc.m	creates text numbers on plot to show temporary points	PackingCodeQuickLaunchAngle.m	15
validStartPointFunc.m	checks if start point is inside of enclosure	RunRandPacking5Oct.m	23

Summary of simulation files and the functions that call them

References

1. **Levine, Joel S.** [Online] Jan 14, 2010. [Cited: Feb 20, 2011.] http://marsairplane.larc.nasa.gov/platform.html.

2. **DARPA.** *Rapid Response, Long Endurance Unmanned Aircraft System Program.* Arlington : Defense Advanced Research Project Agency, 2007.

3. **Simpson, Andrew D.** *Design and Performance of UAVs with Inflatable Wings.* Mechanical Engineering, University of Kentucky. 2008. Dissertation.

4. *Recent development and testing of inflatable wings.* **D.P. Cadogan, S.E. Scarborough, D. Gleeson, A. Dixit, J.D. Jacob, A.D. Simpson.** Newport : s.n., 2006. 47th AIAA/ASME/ASCE/AHS/ASC Structures, Structural Dynamics, and Materials Conference. AIAA 2006-2139.

5. **Landon, Steven D.** *Development of Deployable Wings for Small Unmanned Aerial Vehicles Using Compliant Mechanisms.* Mechanical Engineering, Brigham Young University. 2007. Thesis.

6. *Inflatable and Rigidizable Wing Components for Unmanned Aerial Vehicles.* **David Cadogan, Tim smith, Ryan Lee, Stephen Scarborough, David Graziosi.** Norfolk : American Institute of Aeronautics and Astronautics, Inc., 2003. 44th AIAA/ASME/ASCE/AHS Structures, Structural Dynamics, and Materials Conference. AIAA-2003-1801-147.

7. **Suzanne Weaver Smith, Jamey D. Jacob.** *Summary Report on High Altitude Testing of Inflatable Wing Technologies.* 2008. BIG BLUE Report 2008-001.

8. *Morphing Inflatable Wing Development for Compact Package Unmanned Aerial Vehicles.* **David Cadogan, Tim Smith, Frank Uhelsky, Matt MacKusick.** Palm Springs : s.n., 2004.

45th AIAA/ASME/ASCE/ASC Structures, Structural Dynamics & Materials Conference. AIAA-2004-1807-170.

9. *Alternative Packaging Study.* **Eichstadt, Frank.** s.l. : NASA, 2009. Lunar Surface Systems BAA Collaborative Technical Exchange. 315876.

10. **Alfram V. Bright, Luisa Chiesa, Richard Wlezien.** Orlando : s.n., 2010. 48th AIAA Aerospace Sciences Meeting Including the New Horizons Forum and Aerospace Exposition.

11. *Adapted Concept Generation and Computational Techniqques for the Application of a Transformer Design Theory.* **Stewart M. Skiles, Vikramjit Singh, Jarden Krager, Carolyn Conner Seepersad, Kristin L. Wood, Dan Jensend.** Philadelphia : s.n., 2006. ASME 2006 International Design Engineering Technical Conferences & Computers and Information in Engineering Conference. DETC 2006-99584.

12. *Parachute Deployment Process Testing Technique.* **III, Ralph J. Speelman.** 4, 1977, J. Aircraft, Vol. 14, pp. 401-402. AIAA-58791-264.

13. **Alioto, V., Buttitta, J., Epps, A., Nguyen, D-B., Yahaghi, A., Mourtos, N.J.** *Design of a Micro-Scale Deployable Unmanned Aerial Vehicle.* Aerospace Engineering, San Jose State University. 2010.

14. *NRL's XFC UAS Achieves Flight Endurance Milestone.* Office of Naval Research, Department of Defense's Rapid Reaction Technology Office, Office of Technology Transition. s.l. : Naval Research Labratory, 2009.

15. **Engwirda, Darren.** Fast Points-In-Polygon Test. [m-file]. 2007.

16. **Suzanne Weaver Smith, Abu Farha Fadi.** *Materials for High Altitude Deployable Wings.* Mechanical Engineering, University of Kentucky. 2009.

17. *Strategies for Constrained Volume Packing of Deployable UAV Wings.* **Turner John Harris, Suzanne Weaver Smith.** 2010.

18. **Smith, Suzanne Weaver.** *Research Overview: University of Kentucky Deployable UAVs Research and Development.* Lexington : s.n., 2010. DINA Planning Meeting.

19. *Bioinspired UAV Wing.* **Alfram V. Bright, Luisa Chiesa, Richard Wlezien.** Orlando : American Institute of Aeronautics and Astronautics, Inc., 2010. 48th AIAA Aerospace Sciences Meeting Including the New Horizons Forum and Aerospace Exposition. AIAA-2010-485-523.

20. *Design of a Micro-Scale Deployable Unmanned Aerial Vehicle.* **Alioto, Vinvent, Josh Buttita, Autin Epps, Duy-Bao, and Amir Yahaghi.** 2009. AIAA Region VI Student Conference.

21. *Design Limitations of Deployable Wings for Small Low Altitude UAVs.* **Jamey D. Jacob, Suzanne W. Smith.** Orlando : American Institute of Aeronautics and Astronautics, Inc., 2009. 47th AIAA Aerospace Sciences Meeting Including the New Horizons Forum and Aerospace Exposition. AIAA-2009-745-323.

22. *Testing of Compact Inflatable Wings for Small Autonomous Aircraft.* **Suzanne Weaver Smith, Raymond P. LeBeau, T. Michael Seigler.** Schaumburg : American Institute of Aeronautics and Astronautics, Inc., 2008. 49th AIAA/ASME/ASCE/AHS/ASC Structures, Structural Dynamics, and Materials Conference. AIAA-2008-2216-451.

23. *Design of HALE Aircraft Using Inflatable Wings.* **Jamey D. Jacob, Suzanne W. Smith.** Reno : American Institute of Aeronautics and Astronautics, Inc., 2008. 46th AIAA Aerospace Sciences Meeting and Exhibit. AIAA-2008-167-143.

24. *Flight Testing and Simulation of a Mars Aircraft Design Using Inflatable Wings.* **Daniel A. Reasor, Raymond P. Lebeau, Suzanne W. Smith.** Reno : American Institute of Aeronautics and Astronautics, 2007. AIAA-2007-243-680.

25. **Rowe, Johnathan Michael.** *Finite Element Modeling of an Inflatable Wing.* Mechanical Engineering. Lexington : University of Kentucky, 2007. Thesis.

26. *Development of a Composite Bendable-Wing Micro Air Vehicle.* **Baron Johnson, Daniel Claxton, Bret Stanford, Vijay Jagdale, Peter Ifju.** Reno : American Institute of Aeronautics and Astronautics, 2007. 45th AIAA Aerospace Sciences Meeting and Exhibit. AIAA-2007-1044-589.

27. *Challenges of Modeling Inflatable Wings.* **Johnathan M. Rowe, Suzanne W. Smith.** Honolulu : American Institute of Aeronautics and Astronautics, Inc., 2007. 48th AIAA/ASME/ASCE/AHS/ASC Structures, Structural Dynamics, and Materials Conference. AIAA-2007-1848-485.

28. *Advanced Self-Deployable Structures for Space Applications.* **Witold M. Sokolowski, Seng C. Tan.** 4, 2007, Journal of Spacecraft and Rockets, Vol. 44. AIAA-22854-941.

29. **Soykasap, Omer.** Folding Design of Composite Structures. *Science Direct.* 2006.

30. *Inflatable and Warpable Wings for Meso-scale UAVs.* **Andrew Simpson, Jamey Jacob, Suzanne Smith.** DC : American Institue of Aeronautics and Astronautics, 2005. AIAA Infotech@Aerospace. 10.1.1.113.9830.

31. **Veldman, S.L.** *Design and Analysis Methodologies for Inflated Beams.* s.l. : DUP Science, 2005. ISBN: 90-407-2586.

32. *Morphing Inflatable Wing Development for Compact Package Unmanned Aerial Vehicles.* **David Cadogan, Tim Smith, Frank Uhelsky, Matt MacKusick.** 2004. AIAA SDM Adaptive Structures Forum. 10.1.1.124.6746.

33. **Boroczky, K.** *Finite Packing and Covering.* Cambridge : Cambridge UP, 2004.

34. **ASTM.** *Standard Test Method for Breaking Force and Elongation of Textile Fabrics (Strip Method).* West Conshohocken : ASTM International, 2003. D 5035-95.

35. **E.C. Aldridge Jr., John P. Stenbit.** *Unmanned Aerial Vehicles Roadmap 2002-2027.* Acquisition, Technology, & Logistics, Air Warfare, Office of the Secretary of Defense. 2002.

36. **Koryo Miura, Sergio Pellegrino.** *Structural Concepts and Their Theoretical Foundations.* 2001. Unpublished.

37. **Haggard G. Brown, B. R. Brown.** *Inflatable Structures for Deployable Wings.* 2001. AIAA-2001-2068.

38. **Gantes, Charis J.** *Deployable Structures: Analysis and Design.* Southampton : WIP, 2001.

39. **Conway, John Horton.** *Sphere Packings, Lattices, and Groups.* New York : Springer, 1999.

40. **Coffman, E.G.** *Probabilistic Analysis of Packing and Partitioning Algorithms.* New York : Wiley, 1991.

41. **Durst, Martin J.** *Preclassification and Delayed Classification of Boundary Entities in Arbitrary Dimensions.* s.l. : Springer-Verlag Berlin Heidelberg, 1991.

42. **Salvador Dominguez, Oliver Gunther.** *Performance Analysis of Three Curce Representation Schemes.* s.l. : Springer-Verlag Berlin Heidelberg, 1991. Paper.

43. *Parachute Mortar Design.* **Pleasants, James E.** 4, 1974, J. Aircraft, Vol. 11. AIAA-62051-807.

44. **Glen Brown, Roy Haggard, Brook Norton.** *Inflatable Structures for Deployable Wings.* s.l. : American Institute of Aeronautics and Astronautics, Inc. AIAA-2001-2068.

45. **Joep Breuer, Wubbo Ockels, Rolf, H. Luchsinger.** *An Inflatable Wing Using the Principle of Tensairity.*

46. *NRL Research Aircraft Tactical Vehicles.* Navy Research Labratory, 2006. NRL 5712 AUVSI 2006.

47. **Eugenio Onate, Bernard Kroplin.** *Textile Composites and Inflatable Structures II.* Dordrecht : Springer, 2008.

48. Naval Research Labratory. [Online] 2002. http://tid-www.nrl.navy.mil/Exhibits/pdfs/Info%20Sheet%20pdfs/UAV%20Info%20Sheets/DragonEye2002.pdf.

49. **Matthew J. Scott, Jamey D. Jacob, Suzanne W. Smith, Laila T. Asheghian, Jayanth N. Kudva.** *Development of a Novel Low Stored Volume High-Altitude Wing Design.* s.l. : American Institute of Aeronautics and Astronautics.

Vita

Author's name: Turner John Harris

Birth place: Concordia, Kansas

Birth date: July 28, 1984

Education: Bachelor of Science in Mechanical Engineering, University of Kentucky May 2008

Research Experience:

University of Kentucky, Lexington Kentucky, August 2008 to present, Research Assistant

Honors, Awards, and Activities:

NCAA University of Kentucky Rifle Team, VP Outreach for UK Athletics, Catspys Community Service Award, NCAA Honorable Mention, State Farm Student Athlete of the Month, American Society of Mechanical Engineers